ABNORMAL VENTILATION PRIOR TO LUNG CANCER RESECTION

PREVALENCE AND CLINICAL RELEVANCE OF ABNORMAL VENTILATION IN LUNG CANCER PATIENTS PRIOR TO LUNG RESECTION

By NISARG RADADIA, BSC (HONS)

A Thesis Submitted to the School of Graduate Studies in Partial Fulfilment of the Requirements for the Degree Master of Sciences

Descriptive Note

McMaster University MASTER OF SCIENCE (2024) Hamilton, Ontario (Medical Sciences)

TITLE: Prevalence and Clinical Relevance of Abnormal Ventilation in Lung Cancer Patients prior to Lung Resection

AUTHOR: Nisarg Radadia, Honours B.Sc

SUPERVISOR: Dr. Sarah Svenningsen, PhD

NUMBER OF PAGES: 106

Lay Abstract

Post-operative complications are frequent adverse events following lung cancer resection, resulting in substantial patient morbidity and mortality that have a significant clinical and economic impact. Despite this, post-operative complications remain inadequately predicted, and limited research has been dedicated to reducing the risk of pulmonary complications after lung cancer resection. Standard clinical screening tools, such as pulmonary function tests, are used for patient selection in lung cancer resection surgery; however, they provide a global estimate of a complex multicompartment organ and may lack the sensitivity to detect subclinical lung pathology that influences post-operative outcomes. Thus, using high-resolution medical imaging modalities such as single photon emission computed tomography (SPECT) and magnetic resonance imaging (MRI), we investigated the prevalence and clinical relevance of abnormal ventilation, a functional consequence of airway and/or parenchymal disease. One hundred and three participants were enrolled in a six-week prospective, proof-of-concept observational study. Participants performed pre-operative imaging and were followed for four weeks post-operatively to document post-operative complications and relevant clinical outcomes. Pre-operative SPECT and MRI revealed a high prevalence of abnormal ventilation. The pre-operative ventilation defect burden was greater in participants who developed one or more complications during the four-week post-operative period and was an independent predictor of both the incidence of post-operative complications and the length of hospital stay. These observations provide proof-of-concept evidence that abnormal ventilation, assessed by two ventilation imaging modalities, is prevalent and clinically relevant prior to lung cancer resection. Taken together, this thesis establishes that ventilation imaging may have implications for risk stratification and risk modification in patients scheduled to undergo lung cancer resection.

Abstract

INTRODUCTION: Despite the use of modern minimally invasive surgical techniques, post-operative complications following lung cancer resection remain common and challenging to predict. Pulmonary ventilation imaging modalities offer detailed regional assessment of airflow obstruction and are highly sensitive to subclinical airway and/or parenchymal disease. Nevertheless, ventilation imaging is seldom integrated into pre-operative lung function assessment and risk stratification procedures. Therefore, the objective of this thesis was to quantify the burden of ventilation defects observed by Technegas SPECT and ^{129}Xe MRI before lung cancer resection and establish their association with the occurrence and clinical impact of post-operative complications.

METHODS: Patients undergoing lung cancer resection at St. Joseph's Healthcare Hamilton were recruited into a prospective, proof-of-concept, six-week observational study. Participants were evaluated prior to resection surgery to document baseline demographics and clinical characteristics, performed standard pulmonary function tests and sputum induction, and underwent Technegas SPECT and ^{129}Xe MRI to assess ventilation. Abnormal ventilation was quantified as the ventilation defect percent (VDP) and was considered abnormal if VDP was ≥mean+2 standard deviations of a healthy population. Following surgery, participants were followed for 4 weeks to document the incidence of post-operative complications, as specified by the Ottawa TM&M categorization system, and the length of hospital stay.

RESULTS: One hundred and twenty-three participants were enrolled, of whom 103 were evaluated pre-operatively and followed for post-operative outcomes. Of the 103 participants (69±8 years, 58% female), 89% (92/103) underwent minimally invasive surgery, and 74% (76/103)

underwent lobectomy. Abnormal ventilation was observed pre-operatively by Technegas SPECT and ^{129}Xe MRI for 59% (58/99) and 84% (82/98) of participants, respectively. In a subset of 69 participants in whom sputum was collected, 51% (35/69) had intraluminal inflammation. A total of 64 post-operative complications occurred; 16 (25%) were pulmonary, and 48 (75%) were pleural complications. A post-operative complication occurred in 42% (41/103) of participants. Pre-operative Technegas SPECT and ^{129}Xe MRI VDP were higher for participants with post-operative complications compared to those without (Technegas SPECT: 26±17% vs 19±7%, p=0.02; ^{129}Xe MRI: 13±12% vs 7±6% p=0.003) and were positively correlated with post-operative length of hospital stay (Technegas SPECT: r=0.43, p<0.0001; ^{129}Xe MRI: r=0.49, p<0.0001). Multivariable regression models revealed that preoperative Technegas SPECT and ^{129}Xe MRI VDP were predictors of post-operative complications (Technegas SPECT: Odds ratio=1.08, p=0.005; ^{129}Xe MRI: Odds ratio=1.16, p=0.002) and post-operative length of hospital stay (Technegas SPECT: unstandardized β=0.13, p<0.001; ^{129}Xe MRI: unstandardized β=0.24, p<0.001).

CONCLUSIONS: Abnormal ventilation, quantified by Technegas SPECT and ^{129}Xe MRI VDP, is prevalent prior to lung cancer resection and a predictor of post-operative complications and length of hospital stay.

कर्मण्येवाधिकारस्ते मा फलेषु कदाचन।
मा कर्मफलहेतुर्भूर्मा ते सङ्गोऽस्त्वकर्मणि॥

- Bhagavat Geeta, Adhyay 2, Shloka 46

Translation:

Focus on your actions, not the results.

Acknowledgments

This multidisciplinary project would not have been possible without the collective support from the various departments, every individual involved, and most importantly, the participants who generously gave their invaluable time at such a difficult moment in their lives. Over the past two years, my involvement in this project has truly influenced my personal and professional growth. It truly takes a village to raise a researcher.

First and foremost, I would like to express my gratitude to my supervisor Dr. Sarah Svenningsen, who made this work possible. I am truly thankful for the opportunity you provided by entrusting me with this project, pushing me beyond my boundaries, granting me intellectual freedom, and supporting my participation in international conferences and presentations. Your dedication to research is truly inspirational, and seeing you work hard made me want to put in even more effort. Yes, I made many mistakes and repeated mistakes, but I thank you for being patient. Your commitment to high-quality research and unwavering demand for excellence has shaped my outlook on academia. Lastly, I am indebted to your guidance and support for my aspirations of becoming a clinician.

I am extremely grateful to my committee members, Dr. Yaron Shargall, Dr. Parameswaran Nair, and Dr. Noseworthy. The keen scientific insight and constant guidance from the committee have provided me a crucial direction to the project. Dr. Yaron Shargall, your support, from participant recruitment to sharing clinical insights amidst your busy clinic schedule, has been crucial. I have witnessed firsthand how hectic clinics can get, and despite this, you took the time from your busy schedule to help with the study recruitment. To Dr. Parameswaran Nair, thank you

for not only contributing to the project but also sharing life advice and supporting my academic endeavors.

I would like to express my deepest appreciation to Dr. Eldar Priel and Dr. Carmen Venegas for answering my questions, engaging in insightful discussions, and being available when I needed assistance with the project.

Words cannot express my gratitude to Melanie Kjarsgaard, Chynna Huang, and Katherine Radford for providing the training to make this research successful. You took the time to train me on performing breathing tests, and the day-to-day activities of the lab. Thank you for being patient with us when we repeatedly asked the same questions. Thank you for taking care of us and creating a friendly environment for the students to feel comfortable and at home.

I am grateful for the lab members and new friends I have made on this journey. To our research team: Ashutosh Thakar, Nandhitha Ragunayakam, Dr. Yonni Friedlander, and Anusha Mappanasingam – thank you. I have cherished every moment in the lab. I truly enjoyed working with you all, the dinners, talking about life, and having meaningful and insightful discussions on various lung diseases – I will miss this. Special thanks to Dr. Yonni Friedlander for always taking my calls when I have burning questions, teaching me the basics of MRI, and assisting with MATLAB. Your expertise is truly invaluable. I am glad and grateful for all the trainees I met along my journey, Kayla Zhang, Nadia Tan, Kate Miyazaki, and Zil Patel. I enjoyed attending conferences and having life discussions with you all. Special thanks to Kayla Zhang and Ying Lan Xie for their assistance in processing sputum samples.

Many thanks to Dr. John Agzarian and Dr. Christian Finely for assisting with participant recruitment and showing support for research. Thank you, Dr. Troy Francombe, and Dr. Christopher Marriott for assisting with questions related to nuclear medicine.

This project would not have been a success without the support from the surgery administrators, nuclear medicine, and MRI technologists. Thank you, Leah Morrison, Elizabeth DeCosta, and Fidous Haseeb for taking the time to provide the OR schedules and surgery dates and providing participant names for recruitment. You truly made the process of recruitment easier. To the nuclear medicine technologists – Laura Speziale, Meher Jamal, Susan Fitzgerald, Joon, and Karen Fraser – and MRI techs – Julie Lecomte, Carol Awde, Suzanne Weir, and Shannon Faseruk – thank you for accommodating study visits in your busy schedules and making participants feel comfortable before their surgeries.

To my family – Mom, Dad, and Sister – your constant support and love have been pillars for success in my academic career. Thank you for being there in the most difficult of times. To my sister Hetavi, thank you for being there for emotional support, and providing a listening ear. Of course, special thanks to Moksh, Parth, Priyanshu, Tarpan, and Tanmay. You all have been there for me in the most difficult moments in my life. It is good to have friends like you in life. Jaineel and Tapan, the 2:00 AM drives and our conversations about life aspirations have motivated me through and through.

Finally, I am grateful to the funding sources that have supported this project and my research over the past two years. This was an investigator-initiated study funded by Cyclomedica Australia Pty Ltd and The Lung Association. I acknowledge and am thankful for the funding support from the Canadian Institutes of Health Research.

Table of Contents

List of Figures

List of Tables

List of Abbreviations and Symbols

ACCP	American College of Chest Physicians
ANOVA	Analysis of Variance
ARDS	Acute Respiratory Distress Syndrome
ASA	American Society of Anesthesiologists
ATS	American Thoracic Society
BMI	Body Mass Index
BTS	British Thoracic Society
CCI	Charlson Comorbidity Index
COPD	Chronic Obstructive Pulmonary Disease
CT	Computed Tomography
DLco	Diffusion Capacity of the Lungs for Carbon Monoxide
FEV_1	Forced Expiratory Volume in One Second
FRC	Functional Residual Capacity
FVC	Forced Vital Capacity
HU	Hounsfield Unit
MIS	Minimally Invasive Surgery
MRI	Magnetic Resonance Imaging
NSCLC	Non-Small Cell Lung Cancer
OR	Odds Ratio
PET	Positron Emission Tomography
RATS	Robot-Assisted Thoracoscopic Surgery
RV	Residual Volume
SCLC	Small Cell Lung Cancer
SD	Standard Deviation
SPECT	Single Photon Emission Computed Tomography
VATS	Video-Assisted Thoracoscopic Surgery
VDP	Ventilation Defect Percent
^{99m}Tc	Technetium-99m
^{129}Xe	Xenon-129

Declaration of Academic Achievement

I declare that the research presented in this thesis is original content and is my work. I significantly contributed to all aspects of this thesis, including recruitment of study participants, conducting study visits, data acquisition, analysis, and interpretation.

The research presented in this thesis has been prepared for two publications. The first, titled "Comparison of Ventilation Defects Quantified by Technegas SPECT and ^{129}Xe MRI" has been published in *Frontiers in Physiology*. Sarah Svenningsen, Yaron Shargall, and Parameswaran Nair were responsible for the study conception and study design. Yaron Shargall, Eldar Priel, Christian Finley, John Agzarian, and Parameswaran Nair were responsible for identifying and characterizing the patients, and for clinical interpretation of the data. Nisarg Radadia, Mobin Jamal, and Chynna Huang were responsible for recruiting study participants. Christopher Marriott, Troy Farncombe and Mike Noseworthy were responsible for VQ SPECT-CT acquisition and/or interpretation. Norm B Konyer and Mike Noseworthy were responsible for MRI acquisition and/or interpretation. Nisarg Radadia, Yonni Friedlander, and Sarah Svenningsen were responsible for data acquisition, analysis, and interpretation, and for preparing the first draft of the manuscript.

The second original article titled "Prevalence and Clinical Relevance of Abnormal Ventilation in Lung Cancer Patients prior to Lung Resection" is being prepared for submission. In addition to the contributions of the aforementioned co-authors to the thesis, Nicola LaVigne and Katherine Radford were responsible for performing sputum cell cytology. Katherine Radford, Kalya Zhang, and Yinglan Xie were responsible for processing sputum samples.

Chapter 1: Introduction

1.1 Overview and Motivation

In Canada, lung cancer is the leading cause of cancer-related death for both males and females and accounts for more deaths than colorectal, pancreatic, and breast cancers combined.[1] In 2022 alone, approximately 21,000 Canadians died of lung cancer (with an additional 29,600 being diagnosed), accounting for approximately 25% of all cancer-related deaths.[1] Despite the five-year net survival for all cancers increasing from 55% to 64%, lung cancer has one of the lowest 5-year net survival rates (22%).[1]

Curative-intent lung resection surgery is considered the first-line treatment option for patients with early-stage lung cancer. However, post-operative pulmonary and pleural complications are frequent adverse events following lung resection surgery, with an overall incidence of 15-40%,[2-6] which are often associated with substantial patient morbidity and mortality.[7] The clinical and economic impact of post-operative complications is significant, with prolonged post-operative hospital stays, high frequency of emergency room visits, and increased mortality.[4,5] Approximately 14-30% of patients who have a post-operative pulmonary complication (PPC) following a curative-intent lung resection will die within 30 days of surgery, compared to 0.2-3% without a PPC.[8] Despite the clinical and economic burden, post-operative complications remain inadequately predicted and little effort is being directed towards identifying risk factors that can be modified prior to surgery to prevent their development. Clinical studies have identified older age, poor pre-operative lung function, extensive smoking history, and chronic obstructive pulmonary disease (COPD) as risk factors for developing post-operative complications.[2-5,9] From a clinical perspective, it is important to note that aside from smoking

cessation,[10-12] very few of the above-mentioned risk factors are modifiable prior to lung cancer resection.

Functional lung imaging modalities, such as ventilation single photon emission computed tomography (SPECT) and inhaled hyperpolarized gas magnetic resonance imaging (MRI), can be used to visualize and quantify regions of the lung that are not ventilated, known as "ventilation defects."[13,14] While ventilation SPECT is widely employed in clinical practice, its application in pre-operative ventilation imaging is rare, except in cases where the patient is scheduled to undergo a pneumonectomy – a complete removal of a lung. Functional MRI using inhaled helium-3 (^{3}He) and xenon-129 (^{129}Xe) gas, has been extensively studied in obstructive lung diseases such as asthma and COPD, however, its use is currently limited to specialized academic centers.

In patients without lung cancer, older age, poor lung function, extensive smoking history, and COPD have all been associated with abnormal ventilation, which is the functional consequence of airway and/or parenchymal disease. Abnormal ventilation has been observed in ex-smokers without airflow limitation,[15] healthy elderly,[16] asthmatics, COPD,[17-19], and lung cancer patients.[20-24] A common and modifiable component of airway disease that may contribute to abnormal ventilation is intraluminal cellular inflammation. Eosinophilic and neutrophilic airway inflammation can be evaluated using the cytology of spontaneous or induced sputum.[25] As such, it is possible that pre-operative identification of abnormal ventilation and airway inflammation, and active management to improve it prior to lung resection, may decrease the risk of post-operative complications.

Thus, in pursuit of two goals – risk stratification and risk modification for patients scheduled to undergo lung resection, and identification of modifiable risk factors for post-operative

complications – it is pertinent to identify the prevalence and clinical relevance of abnormal ventilation in lung cancer patients before lung resection surgery.

This chapter will provide an overview of the necessary background information needed to understand the original research presented in Chapters 2 to 4. First, the anatomy of the respiratory system (1.3) and the lymphatic system are described (1.3). Subsequently, the types of lung cancer (1.4) and the operability and resectability of lung cancer (1.5) will be discussed. There will then be a brief discussion on post-operative care (1.6). Next, imaging modalities available to assess ventilation will be discussed in detail (1.7), followed by a summary of the literature on the risk factors for predicting post-operative complications (1.8). Finally, the specific hypotheses and objectives of this thesis are presented (1.9).

1.2 Anatomy of the Respiratory System

The lungs are made up of branching airways, parenchyma, and vasculature that serve two essential functions: 1) ventilation-perfusion matching to supply oxygen to the body and remove carbon dioxide produced as a metabolic byproduct, and 2) provide host defense against airborne pathogens, air particulates, and chemicals.

1.2.1 *The Bronchopulmonary Tree*

The respiratory system comprises of two distinct zones: the conducting zone and the respiratory zone, each serving a specific function in the process of respiration (**Figure 1-1A**).[26,27] In the conducting zone, which begins at the mouth and nose, inhaled air from the environment travels down the trachea which bifurcates into the right and left main bronchi. These bronchi further divide into lobar and segmental bronchi, creating a complex branching system that eventually leads to the formation of the terminal bronchioles. The conducting airways, consisting of the trachea, bronchi, and terminal bronchioles, are structurally supported by cartilage. The

conducting airways do not participate in respiratory gas exchange; thus, this region is referred to as the “anatomic dead space”. The term "dead space," totaling around 150 milliliters (ml), describes lung regions that receive ventilation but do not participate in the transfer of gases (both oxygen and carbon dioxide) with the bloodstream.

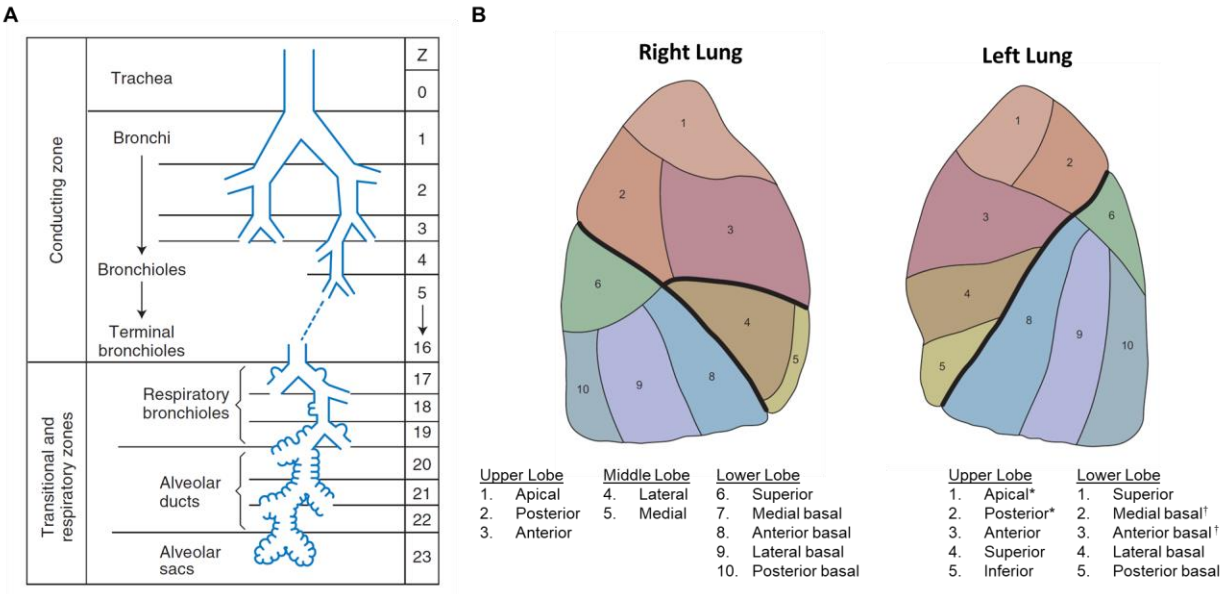

Figure 1-1 The Respiratory System

A. The conducting and respiratory zones of the respiratory system.
B. The bronchopulmonary segments of the right and left lung are shown in lateral view.
*Apical and posterior segments of the left lung are frequently considered single segment.
†Medial basal and anterior basal segments of the left lung are frequently considered single segment.

Adapted from Respiratory Physiology The Essentials by John West[26] and Anatomy A Regional Atlas Of the Human Body – 6th Edition by Carmine D. Clement.[27]

The respiratory zone begins with the respiratory bronchioles, noted for having alveoli on their walls. Respiratory bronchioles perform a dual role, acting both as airways and as a component of alveolar volume that participates in gas exchange. These respiratory bronchioles, along with alveolar ducts and alveoli, are collectively responsible for the exchange of gases. This region is where oxygen is taken up into the bloodstream and carbon dioxide is released from the bloodstream into the alveoli to be exhaled.

The Boyden classification method is used to categorize the bronchopulmonary segments according to their anatomical location (**Figure 1-1B**). In essence, each bronchopulmonary segment is a separate, independently functioning region of the lung with its own air, blood supply, and lymphatic return.[28] As illustrated in **Figure 1-1B**, the right lung is divided into three lobes-upper, middle, and lower, each comprising specific segments, while the left lung consists of two lobes-upper and lower – with distinct segments.

1.2.2 *Lung Parenchyma*

The primary function of lung parenchyma is to facilitate gas exchange. The parenchyma is comprised of approximately 480 million thin-walled alveoli (range: 274-790 million), with mean size of a single alveolus being 4.2×10^6 μm^3 (range: 3.3-4.8 $\times 10^6$ μm^3).[29] The blood-gas barrier, also known as the alveolar-capillary membrane, is a thin structure within the parenchyma that plays a central role in the exchange of gases, predominantly oxygen and carbon dioxide. The barrier is comprised of two primary layers: the alveolar epithelium, which is a single layer of flat epithelial cells that line the walls of the alveoli, and the capillary endothelium, consisting of endothelial cells comprising the walls of the adjacent pulmonary capillaries. The blood-gas barrier is measured at approximately 0.2-0.3 μm in thickness with a large surface area ranging from 50-100 m^2. This allows for rapid diffusion of oxygen from the alveoli into the capillaries and, conversely, for the transfer of carbon dioxide from the capillaries into the alveoli.

For diffusion to occur and maintain proper gas exchange, sufficient ventilation and perfusion to the lungs are essential. Perfusion refers to the blood flow to the dense network of capillaries surrounding the alveoli. Deoxygenated blood from the body is pumped from the heart to the pulmonary artery, subsequently reaching the alveolar capillaries. Here, carbon dioxide is removed from bloodstream and oxygen is picked up from alveoli. The ventilation/perfusion (V/Q)

ratio is a measurement of air entering the alveoli compared to the blood flow to the alveoli. It should be noted that there is variation in ventilation and perfusion in the lungs, with perfusion compared to ventilation being proportionally higher at the base than at the apex of the lung.[26]

1.3 Lymphatic System

The lymphatic system is a circulatory system comprised of lymph vessels, which serve a vital role in the maintenance of the body's fluid balance and providing defense against foreign invaders.[30] Central to this system are lymph nodes, which are small, bean-shaped masses of lymphatic tissue distributed throughout the body.[30] Lymph nodes serve as key sentinels for the immune system, detecting and responding to foreign pathogens such as bacteria, viruses, and most importantly cancer cells. As per the International Association for the Study of Lung Cancer (IASLC) lymph node map, the 14 lymph node stations are based on the anatomical location in the thoracic cavity and are further divided into 7 zones.[31] The zones are as follows: supraclavicular, upper, aortopulmonary, subcarinal, lower, hilar, and peripheral zones.[31] Cancer cells from a tumor can, on occasion, detach and travel through the bloodstream or nearby lymph vessels to distant parts of the body. This process is referred to as metastasis. The role of lymph nodes in lung cancer disease progression, staging, and planning of surgical and treatment strategy will be further discussed in Chapter 1.5.

1.4 Type of Lung Cancers

Lung cancer arises from the cells of the respiratory epithelium with the two most prevalent forms being non-small cell lung cancer (NSCLC) and small cell lung cancer (SCLC).[32] It is important to note that the terms "non-small" and "small" refer to the size of the cells present in the tumor when viewed under a microscope, not the size of the tumor itself. For both NSCLC and SCLC, smoking stands as the primary cause of lung cancer, and accounts for 85% of cases.[32]

Additional risk factors include second-hand smoke, asbestos exposure, radon exposure, and genetic predispositions.[33]

Non-small cell lung cancer (NSCLC) accounts for most lung cancer cases, roughly 80% to 85%.[34] This category comprises of three primary pathogenic subtypes:

I. *Adenocarcinoma* typically originates in mucus-producing glands, primarily within the outer regions of the lungs.[34] It ranks as the most common lung cancer overall, particularly amongst non-smokers.[35]

II. *Squamous cell carcinoma (SCC)* originates from the squamous cells (thin and flat cells) lining the bronchi and larger bronchioles, frequently within the central regions of the lungs.[36] It is more prevalent among smokers.[36]

III. *Large cell carcinoma (LCC)* may appear in various lung locations, are characterized by rapid growth, and may reach a considerable size before causing noticeable symptoms.[34]

Small cell lung cancers (SCLC) are highly malignant tumors derived from neuroendocrine cells, which are nerve cells or hormone-producing cells of the lung and account for approximately 15% of all lung cancers.[37,38] SCLC typically originate near the center of the lungs within the bronchi and have a propensity to invade nearby tissues and lymph nodes.[38] SCLC display distinct behavior compared to NSCLC; they are more aggressive, with cancer cells dividing rapidly to form large tumors that can metastasize throughout the body before becoming detectable.[38]

1.5 Operability and Resectability of Lung Cancer

The Lung Diagnosis Assessment Program (LDAP) is a collaborative effort involving the Niagara Health System, the Juravinski Cancer Centre, and St. Joseph's Healthcare Hamilton. Patients who are referred to the LDAP typically have a clinical suspicion of lung cancer based on chest x-ray and/or computed tomography (CT) scans. Following enrollment in the LDAP program,

the patient will undergo a clinical workup to determine the most suitable treatment approach, considering options such as surgery, radiation therapy, or chemotherapy. Surgical candidacy for suspected lung cancer is based on operability and resectability, which are detailed in sections 1.5.1 and 1.5.2 below.

1.5.1 *Operability*

Operability refers to whether a patient is fit enough to tolerate surgery and recover with minimal post-operative complications. As part of the clinical workup to assess the patients' operability, a detailed clinical history is taken, and pulmonary function tests are performed to determine adequate pulmonary function. In addition, echocardiogram or non-invasive stress tests are performed to evaluate cardiac function, and in select cases, cardiopulmonary exercising testing may be performed.

1.5.1.1 Clinical History and Physical Examination

During a detailed history and physical examination, risk factors such as age, body mass index, smoking history, occupational exposures to carcinogens, family history of lung cancer, previous surgeries, respiratory co-morbidities such as COPD, cardiovascular co-morbidities, and overall exercise capacity are recorded. This assists the surgeon in determining the patient's general health status and determining if the patient will be a good surgical candidate, which means whether they will tolerate the operation and have a low risk of developing complications following surgery.

The American Society of Anesthesiologists (ASA) physical status classification is a subjective grading system based on six classes (I to VI) used to assess the preoperative health of patients scheduled to undergo surgery (**Table 1-1**).[39] However, due to the subjective nature of ASA classification and low interobserver reliability, it has limited use in clinical practice for the assessment of pre-operative health.[40]

Table 1-1 The American Society of Anesthesiologists (ASA) physical status classification system

ASA Classification	Definition of Patient Status	Examples
I	A normal healthy patient	Healthy, non-smoker, non-obese (BMI<30) with good exercise tolerance
II	A patient with mild systemic disease with no functional limitations	Current smoker, social drinker, obesity (30<BMI<40), well-controlled hypertension and/or diabetes
III	A patient with severe systemic disease with substantive functional limitations	Poorly controlled hypertension, diabetes, or COPD, morbid obesity (BMI>40), history of (>3 months) myocardial infarction, transient ischemic attack, cerebrovascular accident, active hepatitis, alcohol dependence of abuse.
IV	A patient with a severe systemic disease that is a constant threat to life	Examples include recent history of (<3 months) myocardial infarction, transient ischemic attack, cerebrovascular accident. End-stage renal disease, severe reduction of ejection fraction
V	A moribund patient who is not expected to survive without the operation	Ruptured abdominal aortic aneurysm, massive trauma, and extensive intracranial hemorrhage with mass effect
VI	A declared brain-dead patient whose organs are being removed for donor purposes	

1.5.1.2 Pulmonary Function Tests

Pulmonary function tests are performed to assess lung function and serve a pivotal role in diagnosing respiratory diseases and monitoring disease progression. The current guidelines by the British Thoracic Society (BTS),[41] the American College of Chest Physician (ACCP), and the European Respiratory Society (ERS)[42] recommend using spirometry and diffusion capacity for the selection of patients suitable for lung resection surgery. Determining the patients' respiratory reserve is important for assessing the eligibility of patients for lung cancer resection.

Spirometry is a maneuver used to assess airflow obstruction.[43] Performed with the patient in an upright sitting position, the procedure comprises two distinct phases: maximal inspiration followed by a rapid and forceful exhalation phase, until the patient cannot expel anymore air. Key spirometry parameters include forced expiratory volume in one second (FEV_1), the forced vital capacity (FVC), and the FEV_1/FVC ratio. FEV_1 measures the volume of air expelled in the first

second of exhalation and FVC measures the total air volume expelled during the entire exhalation maneuver. These measurements are expressed in liters and as a percentage of the reference value according to factors such as patient's age, sex, height, and ethnicity.[43] A reduction in FEV_1 indicates airway obstruction and luminal narrowing and is associated with COPD.

The diffusing capacity of the lungs for carbon monoxide (DL_{CO}) assesses the lungs' ability to transfer carbon monoxide from inspired air to the bloodstream. For a single-breath maneuver, the procedure begins with the patient taking normal resting breaths, followed by a complete exhalation to residual volume. Subsequently, the patient is coached to take a full inspiration of a gas mixture (CO=0.31%, CH_4=0.29%, O_2=20.7%, N_2= balanced) and is instructed to hold their breath at total lung capacity for approximately 10 seconds, then exhale out completely. DL_{CO} is calculated from the maneuver based on factors including initial and final CO concentration, total lung volume, and the breath-holding duration. A reduction in DL_{CO} indicates impaired gas exchange, which may be attributed to decreased surface area of the alveolar-capillary membrane.

From the pre-operative FEV_1 and DL_{CO} the predicted post-operative pulmonary values of FEV_1 ($ppoFEV_1$) and DL_{CO} ($ppoDL_{CO}$) can be calculated using either simple anatomic calculations (Equation 1) or planar/three-dimensional lobar quantification with SPECT-CT (Equation 2).[41] These calculations provide an estimate of the patient's expected lung function after a planned lung resection surgery and is utilized to determine whether the patient will have sufficient post-operative lung function. Reduced FEV_1 and DL_{CO} are associated with higher rates of post-operative complications.

$$ppoFEV1 = preFEV1 \times \left(\frac{19 - segements\ to\ be\ removed}{19}\right) \quad \textbf{(1)}$$

$$ppoFEV1 = preFEV1 \times (1 - proportion\ of\ lung\ to\ be\ resected) \quad \textbf{(2)}$$

If the patient is scheduled for pneumonectomy with FEV_1 less than 2L, the BTS guidelines recommend that post-operative residual lung function be determined based on imaging-based calculations (Equation 2).[41] Similarly, the newer ERJ and ACCP guidelines recommend that all patients with FEV_1 or DL_{CO} less than 80% and scheduled for lobectomy or pneumonectomy undergo perfusion scintigraphy for the calculation of $ppoFEV_1$ and $ppoDL_{CO}$.[42]

1.5.2 *Resectability of Tumor*

Resectability refers to whether the tumor can be surgically excised with negative margins. Negative margins signify the absence of cancer cells in the surrounding healthy tissue of the surgically excised tumor. To determine tumor classification based on histology, patients may undergo tissue sampling using CT-guided transthoracic needle biopsy. To determine the extent and stage of disease, which entails assessing tumor location and size, the extent of involvement of mediastinal lymph nodes, and the presence of metastases, patients commonly undergo the following tests: CT of the chest and abdomen to evaluate staging, PET to evaluate spread of cancer to lymph nodes and liver, MRI to evaluate metastasis to the brain, and Endobronchial Ultrasound (EBUS) to evaluate staging.

1.5.2.1 Staging of Lung Cancer

Accurate staging is important in the assessment of patients with lung cancer, as it aids in determining the most suitable treatment approach, which may be surgery, radiation therapy, or chemotherapy. The tumor, node, and metastasis (TNM) 8th edition of staging is used to categorically describe the anatomic extent of cancer and consists of three components: the extent of the primary tumor (T), involvement of lymph nodes (N), and the presence or absence of distance

metastasis (M) (**Figure 1-2**).[44] The TNM system is mainly used to stage NSCLC. In the case of SCLC, it is typically classified as limited (localized within one hemithorax) or extensive (beyond the limits of one hemithorax). However, recently the American Joint Committee on Cancer (AJCC) recommended using the TNM system to stage SCLC as well.[45]

T (Primary Tumor)	
T0	No primary tumor
Tis	Carcinoma in situ (squamous or adenocarcinoma)
T1	Tumor ≤3 cm
T1(mi)	Minimally invasive adenocarcinoma
T1a	Superficial spreading tumor in central airways
T1a	Tumor ≤1 cm
T1b	Tumor >1 but ≤2 cm
T1c	Tumor >2 but ≤3 cm
T2	Tumor >3 but ≤5 cm or tumor involving: visceral pleura, main bronchus (not carina), atelectasis to hilum
T2a	Tumor >3 but ≤4 cm
T2b	Tumor >4 but ≤5 cm
T3	Tumor >5 but ≤7 cm or invading chest wall, pericardium, phrenic nerve or separate tumor nodule(s) in the same lobe
T4	Tumor >7 cm or tumor invading: mediastinum, diaphragm, heart, great vessels, recurrent laryngeal nerve, carina, trachea, esophagus, spine or tumor nodule(s) in a different ipsilateral lobe
N (Regional Lymph Nodes)	
N0	No regional node metastasis
N1	Metastasis in ipsilateral pulmonary or hilar nodes
N2	Metastasis in ipsilateral mediastinal/subcarinal nodes
N3	Metastasis in contralateral mediastinal hilar or supraclavicular nodes
M (Distant Metastasis)	
M0	No distant metastasis
M1a	Malignant pleural/pericardial effusion ‡ or pleural/pericardial nodules or separate tumor nodule (s) in a contralateral lobe
M1b	Single extrathoracic metastasis
M1c	Multiple extrathoracic metastases (1 or >1 organ)

Staging	**N0**	**N1**	**N2**	**N3**
T1	IA	IIB	IIIA	IIIB
T2a	IB	IIB	IIIA	IIIB
T2b	IIA	IIB	IIIA	IIIB
T3	IIB	IIIA	IIIB	IIIC
T4	IIIA	IIIA	IIIB	IIIC
M1a	IVA	IVA	IVA	IVA
M1b	IVA	IVA	IVA	IVA
M1c	IVB	IVB	IVB	IVB

Figure 1-2 TNM Staging for Lung Cancer

Adapted from Detterbeck and Colleagues, Chest (2017)[44]

1.5.2.2 Staging: Role of Transthoracic Needle Biopsy and Endobronchial Ultrasound

Transthoracic needle biopsy and EBUS are important procedures in the diagnosis and staging of lung cancer. A CT-guided transthoracic needle biopsy is an invasive technique used to obtain a tissue sample from a lung nodule, aiding in diagnosis and potentially insight into the nature of the nodule, whether it is inflammation, infection, or cancer.[46] EBUS guided bronchoscopy is a minimally invasive procedure that utilizes a scope equipped with a video camera and an ultrasound probe to visualize and sample nearby lymph nodes, which aids in determining the presence of cancer cells in the nodes (N and M staging).[47]

1.5.2.3 Staging: Role of Imaging Modalities

Imaging modalities, particularly chest radiography, CT, and positron emission tomography (PET), are frequently used to identify patients who may or may not be surgical candidates.

Chest X-ray

Chest radiography, commonly known as a chest X-ray, is a routine medical imaging procedure that uses X-rays to generate two-dimensional projections of the chest and its internal structures. During a standard chest X-ray, the patient is positioned in the posterior-anterior orientation, facing the detector, while X-ray beams are projected from the posterior to the anterior of the chest (~0.01 mSV dose[48]).[49] X-rays traverse through the chest with the extent of radiation absorption by different tissues being dependent on their density. Attenuation, defined as the reduction in radiation intensity as it travels through the body, characterizes how different anatomical structures interact with X-rays. Tissues with high attenuation, such as bones, absorb a significant number of X-rays, causing them to appear white in X-ray images. Conversely, tissues characterised by low attenuation, like lung parenchyma, absorb minimal X-rays, leading to a darker appearance in X-ray images.

Chest radiography is rarely used in the diagnosis and monitoring of lung cancer. It can reveal the presence of lung nodules, masses, or abnormalities in the lung parenchyma. When lung cancer is suspected, additional imaging and diagnostic tests, such as CT scans, are necessary for a higher resolution evaluation and staging of the disease.

Computed Tomography

CT can be used to scan the entire thorax during a single breath-hold. The volumetric imaging allows for the reconstruction of various image types from the acquired data, such as multiplanar and three-dimensional reconstructions. CT attenuation values, quantified in Hounsfield units (HU),[50] are used to define the grayscale appearance of CT images. These values are determined based on the X-ray attenuation characteristics of different tissues. For example, air exhibits low attenuation defined as -1000 HU, while water is 0 HU. In contrast, dense structures with greater attenuation, such as bone, have HU values of around 1000 HU. Although CT imaging offers enhanced spatial resolution in comparison to alternative imaging modalities, and is the primary modality to evaluate lung structure, it presents a drawback, due to the exposure to ionizing radiation and lack of functional information.

In lung cancer, CT is used to evaluate the staging of pulmonary nodules, and their anatomic relationship to structures such as the mediastinum or the pleural space and provides information on the size of mediastinal lymph nodes. Beyond routine visual assessment by radiologists, quantitative imaging for prognostic or prediction of post-operative lung function is rarely performed in clinical practice. Interestingly, studies on CT-derived metrics of emphysema have shown association with poor prognosis in smokers with early-stage lung cancer,[51] and a higher risk of post-operative pulmonary complications with reduced survival than patients without emphysema.[52]

Positron Emission Tomography

PET imaging relies on the use of radiolabeled tracers to visualize metabolic activity in tissues, with the most common tracer in clinical practice being ^{18}F-fluorodeoxyglucose (^{18}F-FDG).[53] This radiotracer is used to identify and visualize regions exhibiting heightened metabolic activity, frequently indicative of tumors within the lungs and mediastinum. The underlying principle is that malignant cells, such as those found in tumors, have an elevated metabolic rate, leading them to consume more of the tracer than surrounding healthy cells. Consequently, these malignant cells exhibit a rapid uptake of the ^{18}F-FDG tracer, enabling the visualization and detection of suspected cancerous lesions. PET is particularly useful in N and M staging of lung cancer. In lung cancer treatment, intrathoracic lymph nodes serve as indicators of disease progression and treatment strategy. Generally, the presence of cancer in lymph nodes indicates an advanced stage of the disease and may necessitate more aggressive treatment strategies, such as radiation therapy, or chemotherapy. Specific lymph node stations, like the hilar lymph nodes, and mediastinal lymph nodes hold particular significance in lung cancer diagnosis and staging. High metabolic activity in these lymph nodes detected by PET may indicate the spread beyond the lung and into the mediastinum. The standard of care for patients with stage I, stage II, and some stage IIIA disease is surgical resection.[44] Patients with stage IIIB and above may require neoadjuvant therapy to reduce the size of the tumor prior to resection.[44]

1.5.3 *Type of Resection Surgery*

The two primary surgical approaches are open thoracotomy and minimally invasive surgery (MIS). Open thoracotomy involves creating a large incision in the chest wall, typically between the ribs, to gain direct access to the lung and the tumor. MIS can be performed in one of two ways: video-assisted thoracoscopic surgery (VATS) or robotic-assisted thoracoscopic surgery

(RATS). This approach involves making small incisions in the chest wall, usually about 1-2 cm in size, and through these small incisions, a thoracoscope (a thin, flexible tube with a camera) and specialized surgical instruments are inserted. Compared with thoracotomy, the VATS approach has shown reduced post-operative complications,[54,55] shorter hospital stays,[56] fewer adverse events,[54,57] and lower morbidity and mortality rates.[58-60]

1.5.4 *The Extent of Resection*

The extent of resection refers to the amount of lung that is removed during the surgical procedure. The extent of resection depends on the type and stage of lung cancer as well as the patient's functional status. For curative intent surgery, the principal aim is to achieve negative margins while preserving as much healthy tissue as possible to maintain optimal post-operative respiratory function. As shown in **Figure 1-3,** standard lung resections include wedge resection (removal of wedge-shaped parenchyma), segmentectomy (removal of a single segment), lobectomy (removal of a single lobe), and pneumonectomy (resection of the entire lung).[61,62]

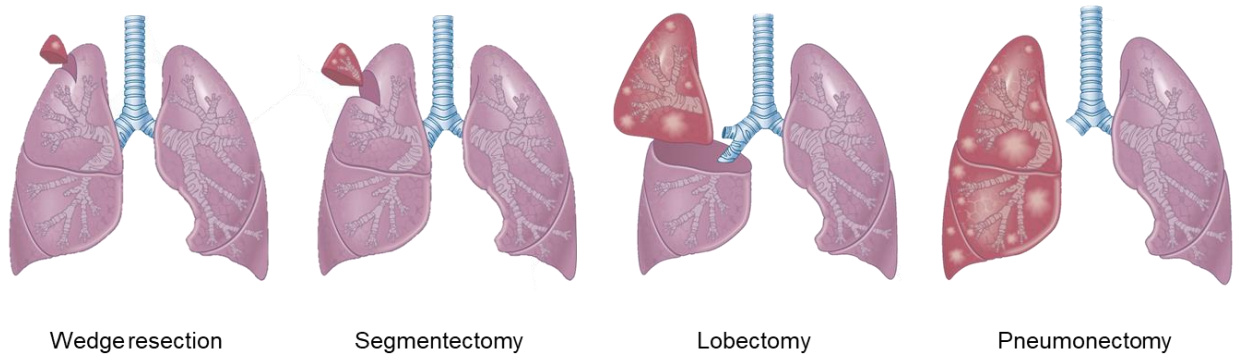

Figure 1-3 Extent of lung cancer resection

Adopted from Murray and Nadel's textbook of Respiratory Medicine

1.6 Post-operative Care and Follow-up

Following surgical resection of lung cancer, patients are closely monitored in-hospital by a multidisciplinary clinical team for surveillance of the patient's health and management of complications. Post-operative pulmonary and plural complications are adverse respiratory events following surgery that increase the length of stay, often require unplanned intensive care unit stays, need for bronchoscopy, and increase risk of mortality. At our institution, post-operative pulmonary and plural complications are classified as per the Ottawa Thoracic Morbidity & Mortality (Ottawa TM&M) classification system.[63,64] Pulmonary complications include atelectasis, pneumonia, initial ventilator support for 48 hours, and acute respiratory distress syndrome. Plural complications include prolonged air leak, pneumothorax, empyema, prolonged pleural drainage, and chylothorax. Following discharge from the hospital, patients are followed up at four weeks to document relevant post-operative complications and clinical outcomes.

1.7 Ventilation Imaging Modalities

Pulmonary ventilation imaging modalities have been developed to provide a regional evaluation of airflow obstruction at high resolution and thus ultimately improve the clinical management of a variety of lung diseases. Nuclear medicine[18,65,66] and magnetic resonance imaging (MRI)[14,67,68] based methods have all demonstrated abnormal and heterogeneous ventilation in patients with obstructive lung diseases, including COPD and asthma. While the potential added value of ventilation imaging modalities over conventional global measures of lung function made by breathing tests is recognized, few are widely available or used in the pre-operative management of lung cancer. A comprehensive summary of the imaging modalities is provided in **Table 1-2**.

Table 1-2 Comparison of lung imaging modalities

	CT	SPECT	PET	HP MRI
Ionizing Radiation	High	Moderate	High	None
Ventilation Contrast Agents	NA	Technegas, DTPA	^{68}Ga	^{3}He, ^{129}Xe
Breath Maneuver	Breath-hold	Tidal breathing	Tidal breathing	Breath-hold
Scan Length	Seconds	Minutes	Minutes	Seconds
Availability in Canada	Widely available in clinical setting	Widely available in clinical setting	Widely available in clinical setting	2-3 national centres*
Assessments	-Lung Density -Lung Volume -Airway -Vasculature	-Ventilation -Perfusion	-Ventilation -Perfusion	-Ventilation -Gas-exchange
Clinical Applications	-Cancer staging -Diagnosis of lung diseases	-Pulmonary embolism diagnosis -Radiation therapy planning -Lung volume reduction surgery planning	Cancer staging	Radiation therapy planning

CT=computed tomography; SPECT= single-photon emission computed tomography; PET = positron emission tomography HP=hyperpolarized; MRI=magnetic resonance imaging; DTPA= Diethylenetriamine pentaacetate. *HP MRI is limited to research applications.

1.7.1 *Nuclear Medicine*

Nuclear imaging methods such as SPECT and PET are clinically well-established methods to visualize regional ventilation and perfusion for the diagnosis of pulmonary embolism (**Table 1-2**). Additionally, these techniques have also been utilized to aid in pre-surgical planning of lung volume reduction surgery and functional lung avoidance in radiation therapy planning. However, nuclear imaging methods such as SPECT and PET are limited by long acquisition times during free-breathing, motion artifacts, and the use of ionizing radiation.

1.7.1.1 Single Photon Emission Computed Tomography (SPECT)

SPECT can be used to evaluate ventilation and perfusion in the lungs using single photon emitting radiotracers. Following inhalation or injection of the radioactive tracer, the radioactive decay process results in the emission of gamma rays. A gamma camera equipped with a collimator and scintillation crystal detects these gamma rays, converting them into electrical signals. Data is collected as the gamma camera rotates around the patient. Advanced computer algorithms then reconstruct three-dimensional images, allowing visualization of the radiopharmaceutical's distribution within the body. While scintigraphy produces planar images, SPECT extends this by providing cross-sectional images of the distribution of radioactive tracers within the lungs.

SPECT is the most clinically established and widely used ventilation imaging modality using a range of inhaled ventilation agents including krypton-81m gas (^{81m}Kr) and ^{99m}Tc-labelled aerosols (e.g. diethylene-triamine-pentaacetate [DTPA] and Technegas).[69,70] In clinical practice, beyond its primary use in conjunction with perfusion SPECT for the diagnosis of pulmonary embolism, ventilation SPECT is rarely utilized for other indications such as pre-operative quantification of lung function[71] and functional lung avoidance in radiation therapy planning[72,73]. In patients with asthma, SPECT has been used to demonstrate ventilation defects compared to healthy controls[74] and demonstrate increased ventilation abnormalities observed following bronchoconstriction induced by a methacholine challenge[75]. In patients with COPD, SPECT has demonstrated ventilation abnormalities compared to healthy participants,[76] determined the severity of airflow limitation,[77] and determined the extent of intrabolus ventilation in patients with pulmonary emphysema[78]. For ventilation imaging, inhaled radiotracers are typically used, and for perfusion imaging, injected radiotracers like Technetium-99m (^{99m}Tc) macroaggregated albumin (MAA) are employed.

1.7.1.2 Positron Emission Tomography

A PET camera captures signals indicating the distribution of radioactivity within the patient's body, which are used to generate tomographic images that represent the three-dimensional distribution of radioactivity. Molecules labeled with a positron-emitting radionuclide can be used to generate PET images. First, the positron-emitting radioactive isotope is inhaled or injected into the patient's body. As the radioactive isotopes decay, positrons are emitted. When a positron encounters an electron within the body, annihilation occurs, releasing energy in the form of two high-energy gamma rays traveling in opposite directions. The PET camera consists of a few rings containing several thousands of scintillation detectors that detect high-energy photons. Following which, a three-dimensional map of the radioactive tracer is produced. Ventilation and perfusion can be evaluated with tracers such as nitrogen-13 (^{13}NN)[79] and gallium-68 (^{68}Ga).[80,81]

1.7.2 *Magnetic Resonance Imaging*

Magnetic resonance imaging (MRI) utilizes radiofrequency (RF) waves, a type of non-ionizing radiation to manipulate nuclear spins, predominantly those of proton (^{1}H) atoms. It generates high-resolution images with soft tissue contrast to help visualize anatomy. Despite the advantages, there are three main reasons why conventional ^{1}H MRI of the lungs is challenging. Firstly, the lungs have a low tissue density of 0.1 g/cm^3 which results in a very low ^{1}H signal intensity.[82] Secondly, the presence of millions of alveoli and air-tissue interfaces in the lungs cause susceptibility artifacts (local magnetic field inhomogeneities) that degrade the ^{1}H MRI signal.[83] Finally, respiratory and cardiac motion during tidal breathing can introduce motion artifacts in the image. The combined effect of these limitations makes ^{1}H MRI of the lung difficult, resulting in images where the lungs appear as black signal voids that provide limited insight on lung structure and function. This is illustrated in **Figure 1-4**, where ^{1}H images are difficult to distinguish between

a healthy volunteer and those from a participant with lung disease (asthma and COPD). Efforts to overcome these technical challenges and enhance lung MRI signals for structural/functional information have led to the development of ^{1}H MRI techniques such as ultra-short echo time (UTE),[84] oxygen-enhanced,[85] and Fourier decomposition methods[86].

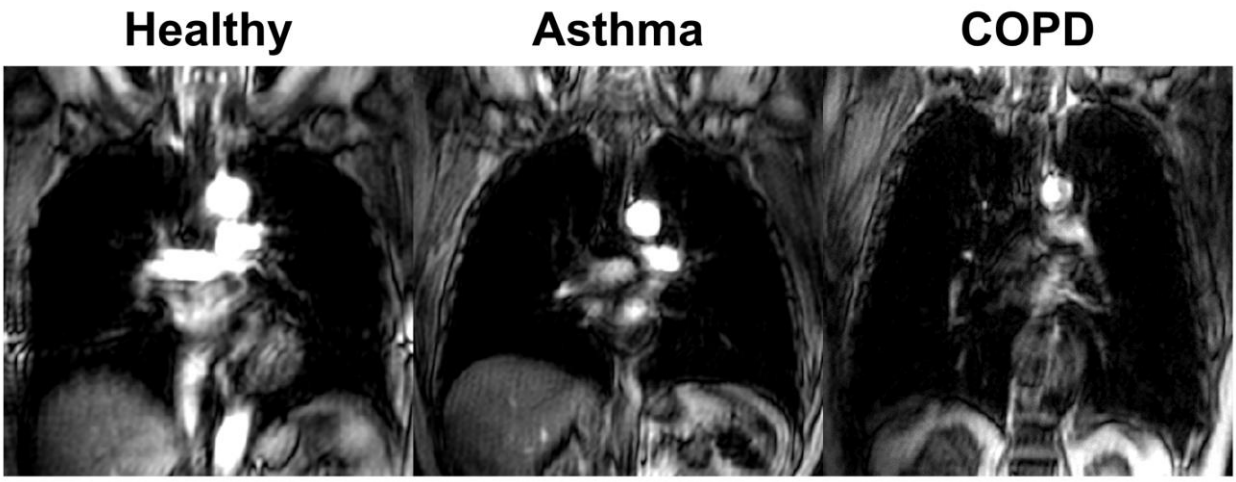

Figure 1-4 Representative conventional ^{1}H MRI coronal center slices for a healthy participant and participants with asthma and COPD.

Ventilation imaging can be performed using exogenous contrast agents such as ^{19}F, O_2,^{3}He, and ^{129}Xe. This section will focus on noble gas MRI using stable isotopes such as hyperpolarized ^{3}He or ^{129}Xe gases for non-invasive measurements of lung ventilation. Albert and colleagues were the first to apply the technique of hyperpolarization of noble gasses to increase the polarization of ^{3}He and ^{129}Xe gas nuclei by approximately 100 000.[87] Hyperpolarization can be achieved using the spin-exchange optical pumping technique.[88] During optical pumping, a circularly polarized laser is used to alter the orientation of angular momentum in the electrons of alkali metal atoms, most commonly rubidium. Following this, spin polarization involves the transfer of angular momentum from the optically polarized alkali metal electrons to the xenon-129 nuclear spins via collisions.

While the first hyperpolarized gas ventilation MRI studies utilized ^{129}Xe, there was a transition to using ^{3}He. This transition occurred because of higher signal-to-noise ratio achievable due to the inherent properties of ^{3}He and available polarization technology at that time. The gyromagnetic ratio of ^{3}He is approximately three times that of ^{129}Xe (^{3}He: 32.3MHz/T; ^{129}Xe: 11.8MHz/T), and ^{3}He has a higher attainable polarization than ^{129}Xe (^{3}He: 30-40%; ^{129}Xe: 8-25%). The higher gyromagnetic ratio and polarization of ^{3}He allowed for a greater MRI signal while using smaller volumes of ^{3}He gas. However, because of ^{3}He's limited supply and increased cost, there has been a shift back to using ^{129}Xe.[89] Fortunately, with recent advances in polarizer technology, higher polarization of ^{129}Xe is now achievable, resulting in similar signal-to-noise ratios to that obtained by ^{3}He MRI.

Imaging of spin densities of hyperpolarized ^{3}He and ^{129}Xe provides visualization of the distribution of noble gases in the lungs following inhalation. As illustrated in **Figure 1-5**, the healthy participant has homogenous distribution of ^{129}Xe gas within the lung. However, as shown in the participants with asthma and COPD, both have heterogeneous ventilation, with regions of the lung not participating in ventilation, termed 'ventilation defects.' These ventilation defects can be quantified using visual scoring and manual segmentation approaches; fortunately, more recently semi-automated segmentation[90,91] and automated segmentation approaches[92] are used. The most commonly reported quantitative metric of ventilation defects observed by ventilation MRI is the ventilation defect percent (VDP), where, as shown in **Equation 3**, ventilation defect volume is normalized to the thoracic lung volume.

$$\text{Ventilation Defect Percent} = \frac{\text{Ventilation Defect Volume}}{\text{Thoracic Cavity Volume}} \text{ x } 100 \qquad \textbf{(3)}$$

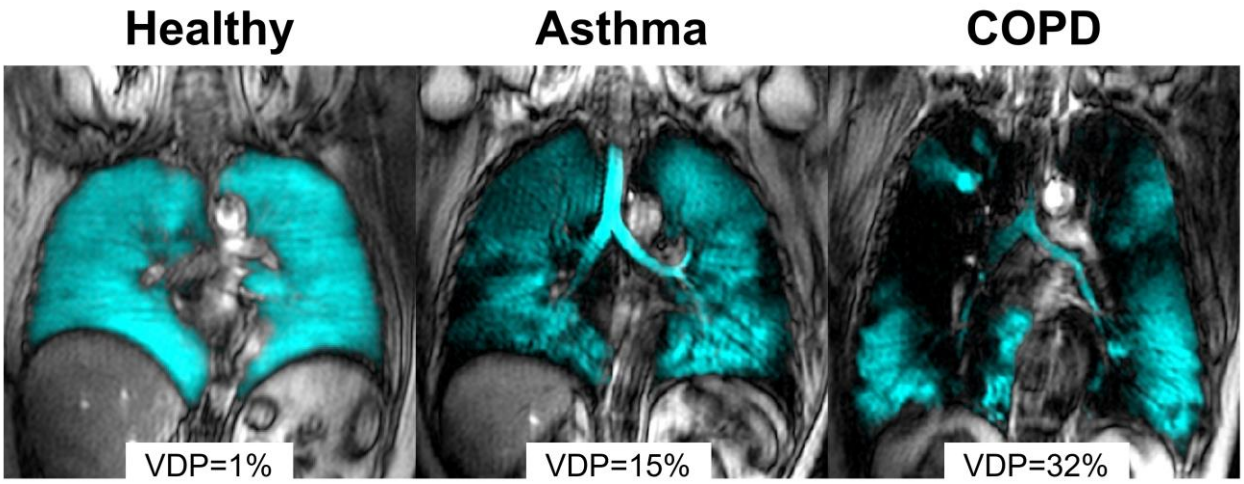

Figure 1-5 Representative hyperpolarized ^{129}Xe MRI coronal images for healthy participant and participants with asthma and COPD.

^{129}Xe MRI static ventilation coronal slices (in cyan) are co-registered to the ^{1}H anatomical MRI (in greyscale) for a representative healthy volunteer, and participant with asthma and COPD.

Previous studies have demonstrated that patients with asthma display heterogeneous ventilation compared to healthy participants.[93-95] Furthermore, it has been observed that ventilation defects persist, both spatially and temporally, when patients were re-imaged the same-day,[95,96] 7 days,[97] 1.5 years[96,98] and 6 years later[99]. Ventilation defects have been observed to significantly correlate with older age,[100] airflow obstruction quantified by spirometry,[101-103] CT measurements of gas trapping,[102] disease severity,[4,101,104] and poor asthma control and lower quality of life measurements in mild[105] and severe asthma.[106] Additionally, higher ventilation defect burden has been associated with exacerbation related hospitalizations[107] and is predictive of two-year asthma exacerbation frequency[105].

Similarly, patients with COPD have heterogeneous ventilation compared to healthy controls.[90,108,109] Ventilation defects have been observed to increase with COPD severity,[109,110] are correlated to measurements of airflow obstruction,[17,111] emphysematous regions on CT,[112] symptoms and exercise capacity,[113] and are predictors of exacerbations requiring hospitalization.[114] More importantly, subclinical abnormal ventilation has been observed in

asymptomatic participants without airflow limitation (assessed by FEV_1), including healthy elderly never-smokers,[16] former smokers,[15,115,116] and current smokers without a clinical diagnosis of lung disease.[117-119]

The application of hyperpolarized gas ventilation MRI in lung cancer has been limited to functional lung avoidance in radiation therapy planning.[20,120-122] Ventilation imaging can assist in optimizing radiation therapy plans by strategically avoiding functioning lung regions, thereby aiming to reduce post-treatment pulmonary toxicity. In one study, Mathew and colleagues reported a prevalence of abnormal ventilation of 67% in a small cohort of patients (n=15) undergoing radical radiotherapy.[20] However, no studies have assessed pre-operative abnormal ventilation in patients scheduled to undergo first-time lung resection.

1.7.3 *Comparison of Ventilation assessed by different Imaging Modalities*

Previous cross-modality investigations have demonstrated the comparability of ^{81m}Kr SPECT with ^{3}He MRI in 23 patients with COPD and 9 healthy volunteers,[123] and ^{99m}Tc-DTPA SPECT with ^{129}Xe MRI in 11 patients with COPD.[124,125] While these preliminary investigations report good comparability, they were limited by the small number of patients and disease populations evaluated. Most importantly, the studies were conducted using SPECT contrast agents that were formerly employed in clinical practice but have since been phased out, highlighting the need for further research with current contrast agents to ensure the relevance and applicability of the findings.

1.8 Risk Factors for Complications following Lung Cancer Resection

Previous clinical studies have identified age, poor lung function, smoking history, and COPD as risk factors for developing pulmonary complications following lung cancer resection.[2-5,9] In a cohort of 234 patients who underwent lung cancer resection, Agostini and colleagues

identified older age (>75 years), BMI (>30 kg/m^2), high American Society of Anesthesia score (>3), smoking history, and COPD as independent risk factors for the development of post-operative complications.[4] Similarly, in a larger prospective cohort of 670 patients, Lugg and colleagues identified COPD and smoking history as independent predictors of post-operative complications.[9] Lickner and colleagues performed a retrospective analysis of 1222 patients with varying lung cancer burdens that underwent lung resection. They reported that pre-operative FEV_1<60%$_{pred}$ was a strong independent risk factor of developing respiratory complications (OR=2.7, CI: 1.3 to 6.6) and 30-day mortality (OR=1.9, CI: 1.2 to 3.9).[2] Furthermore, in patients with non-small cell lung cancer, developing a post-operative complication was an independent risk factor for late death, defined as mortality beyond 30 days following resection.

As previously discussed in **Chapter 1.5.1.2**, pulmonary function testing using spirometry (FEV_1) and diffusion capacity (DL_{CO}) is recommended by BTS and ACCP clinical practice guidelines for risk stratification and as standard first-line screening tools for the selection of patients suitable for lung resection surgery. However, PFT measurements can only capture a global estimation of the pulmonary function and fail to localize the contribution of each lung zone to the overall respiratory impairment. It is therefore difficult to accurately detect and quantify the severity of underlying lung disease using whole-lung function tests. Furthermore, various imaging studies suggest that it is not until lung pathology is well-advanced that symptoms are recognized and conventional clinical measurements such as FEV_1 and DL_{CO} detect abnormalities.[15,63,126] In contrast to global lung function assessments, ventilation imaging offers the advantage of identifying regional ventilation abnormalities within the lungs. In lung cancer, this is an important advantage as clinical and subclinical lung disease may be evaluated in the parts of the lung which

are not involved with the tumor. Thus, ventilation imaging may be more sensitive to early or subclinical lung pathology that is of functional relevance.

In the context of lung cancer, pre-operative ventilation imaging is not incorporated into the standard clinical workup. While previous studies have used ventilation-perfusion scintigraphy and SPECT to predict pulmonary function following lung resection (post-op FEV_1),[127-130] ventilation imaging is not commonly used in clinical practice for risk stratification or predicting post-operative complications.

Using ventilation imaging, abnormal ventilation has been observed in ex-smokers without airflow limitation,[15] healthy elderly,[16] asthmatics, COPD,[17-19], and lung cancer patients.[20-24] A common and modifiable component of airway disease that may contribute to abnormal ventilation is intraluminal inflammation. Eosinophilic and neutrophilic airway inflammation can be evaluated using the cytology of spontaneous or induced sputum.[25] As such, pre-operative identification of abnormal ventilation and airway inflammation can be the first step towards identifying modifiable risk factors for post-operative complications.

1.9 Thesis Hypotheses and Objectives

A significant proportion of patients who undergo lung cancer resection surgery are current or former smokers and often have concurrent respiratory diseases such as COPD, all of which are known contributors to abnormal ventilation and well-known risk factors for developing post-operative complications. Despite this, the prevalence and clinical significance of abnormal ventilation in lung cancer patients prior to resection have not been thoroughly investigated using modern ventilation imaging modalities. This knowledge gap served as the basis for this thesis, which aimed to evaluate ventilation defect burden and its clinical relevance in patients scheduled for lung cancer resection. The central hypotheses that this thesis aimed to address were that

abnormal ventilation is **(1)** present in a subset of patients with lung cancer at the time of lung resection and **(2)** is a predictor of the occurrence and clinical impact of post-operative pulmonary complications.

Intraluminal inflammation may contribute to abnormal ventilation, and eosinophilic and neutrophilic inflammation have been documented in the airways of COPD patients,[131,132] asymptomatic smokers, and former smokers,[133,134] collectively encompassing approximately 70% of patients who undergo lung cancer resection at our institute. Therefore, it is hypothesized that intraluminal cellular inflammation is present in a subset of patients prior to lung cancer resection. Recognizing that intraluminal inflammation is a modifiable factor, identifying the prevalence of intraluminal inflammation can be the first step towards implementing targeted interventions to improve abnormal ventilation prior to resection.

Finally, for ventilation imaging, the current ideal contrast agents for ventilation SPECT and MRI are generally accepted to be Technegas[70] and ^{129}Xe gas,[135] respectively, and they have not been directly compared to each other. With broadening interest in the clinical utility of ventilation imaging and the recent approval of ^{129}Xe MRI and Technegas SPECT by the U.S. Food and Drug Administration, a direct quantitative comparison of the modalities to assess ventilation was performed. The hypothesis was that the abnormal ventilation assessed by Technegas SPECT would be comparable to that assessed by hyperpolarized ^{129}Xe MRI.

Therefore, the objectives of this thesis were to:

1) Determine the prevalence of abnormal ventilation (as measured by Technegas SPECT and hyperpolarized ^{129}Xe MRI) and airway inflammation (as measured by sputum induction) in patients prior to lung cancer resection.

2) Determine if abnormal ventilation (as measured by Technegas SPECT and hyperpolarized ^{129}Xe MRI) prior to lung cancer resection is associated with the incidence and clinical impact of post-operative complications following lung cancer resection.
3) Compare the ventilation defect burden assessed by Technegas SPECT and hyperpolarized ^{129}Xe MRI in patients prior to lung cancer resection.

Chapter 2: Methods

2.1 Participants and Study Design

Patients who were scheduled to undergo first-time lung cancer resection at St. Joseph's Healthcare Hamilton as part of their clinical care were enrolled in a single-center, prospective, six-week proof-of-concept observational study. As this was a proof-of-concept study, broad inclusion criteria were selected. As such, no enrollment restrictions were placed on the disease malignancy type or clinical stage, location of the tumour, surgical approach, or extent of the resection. Eligible patients were greater than 18 years of age, able and willing to provide written informed consent, lung resection candidates in accordance with the British Thoracic Society guidelines and were undergoing first-time lung resection for lung cancer at St. Joseph's Healthcare Hamilton (Hamilton, Canada). Eligible patients could not have had a history of previous lung resection, undergone previous chest radiation, or have an MRI contraindication (such as an implanted mechanically, electrically, or magnetically activated device, or any non-removable metal in their body, such as pacemakers, neurostimulators, biostimulators, or surgical staples, or suffered from any physical, psychological, or other condition(s) that might prevent the performance of the MRI, such as severe claustrophobia). Eligible patients could not be pregnant or breastfeeding. All patients provided written informed consent to an ethics-board-approved (Hamilton Integrated Research Ethics Board #7770) and registered (ClinicalTrials.gov #NCT04191174) protocol. The study design and assessments are summarized in **Figure 2-1**. Briefly, following enrollment, participants completed a pre-operative assessment visit (Visit 1), underwent lung resection in accordance with standard-of-care, and were followed post-operatively for 4-weeks.

A

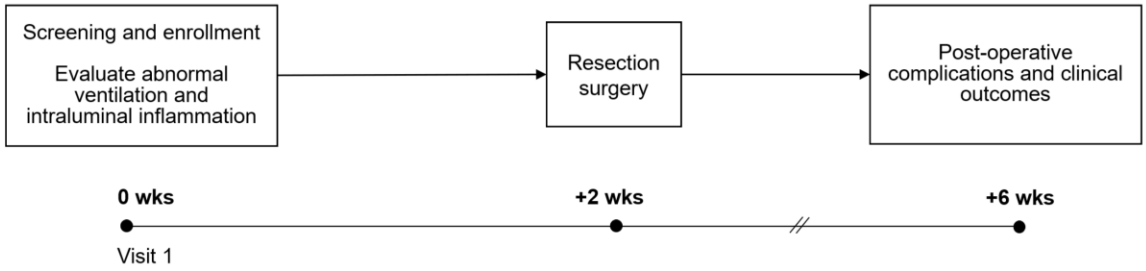

B

Assessment/activity	Visit 1 (V1)	During Surgery	Postop period
Week	0	2	2-6
Inclusion/exclusion criteria	√		
Age, sex, BMI, smoking status	√		
American Society of Anesthesiologists score	√		
Charlson Comorbidity Index	√		
Technegas SPECT/CT	√		
^{129}Xe MRI	√		
Sputum induction	√		
Pulmonary function tests (FEV_1, DLCO)			
Type of surgery and extent of resection		√	
Ottawa TM&M			√*
Length of hospital stay, intensive care unit stay, requirement for mechanical ventilation, intubation, bronchoscopy, hospital readmission, emergency room visit, and post-discharge home oxygen use			√*

*Completed daily until patient discharge.

Figure 2-1 Study design and assessments

2.2 Pre-operative Assessments

During the pre-operative study visit, baseline demographic data and clinical history were collected, and participants performed standard-of-care pulmonary function testing, sputum induction, Technegas SPECT and ^{129}Xe MRI.

2.2.1 Demographic and Clinical Characteristics

Baseline demographic data comprising of age, sex, smoking status, smoking history, body mass index (BMI), American Society of Anesthesiologists (ASA) score,[40] Charlson Comorbidity Index (CCI),[136] and history of respiratory diseases were collected.

2.2.2 Pulmonary Function Tests

In accordance with the American Thoracic Society guidelines, participants performed PFTs using an Elite Series plethysmograph (MGC Diagnostics Corporation, Saint Paul, USA).[137,138] Spirometry was performed to measure FEV_1, FVC, and FEV_1/FVC, while diffusion capacity was performed to measure DL_{CO}.

2.2.3 Airway Inflammation

Luminal cellular inflammation was assessed by quantitative cytometry of spontaneous or induced sputum using well-established methods.[25] Sputum was induced, processed, and quantified according to standardized methods as previously described[25] to report the percentage of eosinophils and the percentage of neutrophils in the airway.[139] The nature of luminal cellular inflammation was classified as: [1] *eosinophilic* (>2.3% eosinophils, and/or presence of eosinophil free granules), [2] *neutrophilic* (≥64% neutrophils with a total cell count of ≥9.7 million cells/g), [3] *mixed-granulocytic* (eosinophilic and neutrophilic), [4] *trivial neutrophilic* (≥64% neutrophils with total cell count of <9.7 million cells/g), and [5] *paucigranulocytic* (total cell count $<9.7 \times 10^6$ cells/g, <2.3% eosinophils, and <64% neutrophils). Participants were considered to have airway inflammation if their sputum was eosinophilic, neutrophilic, trivial-neutrophilic, or mixed-granulocytic.

2.2.4 Technegas SPECT-CT Acquisition

Technegas (Cyclomedica Australia, Sydney) was prepared with a Technegas Generator (Cyclomedica Australia, Sydney) according to the manufacturer recommendations and a 40 MBq dose was administered to the participant in the supine position via inhalation. The participant was coached to inhale Technegas, starting at functional residual capacity, until 40μSv/h was measured by a hand-held Geiger counter positioned over the chest. Technegas SPECT was then acquired

while supine, during 15-minutes of tidal breathing using an Optima™ Nuclear Medicine (NM)/Computed Tomography (CT) 640 hybrid imaging system (GE Healthcare, Milwaukee, USA) and in accordance with The Canadian Association of Nuclear Medicine guidelines using the following acquisition parameters: LEHR collimator, energy window: 140keV±20%, zoom factor of 1.0, 128x128 matrix and 4.42 mm isotropic voxels, step and shoot, 25 seconds/image, 60 images per acquisition (30 images per camera head), 360º rotation, 6º steps, body contour. A low dose non-contrast chest CT was subsequently acquired on the same NM/CT system during free breathing for attenuation correction and to allow for delineation of the thoracic cavity volume using the following acquisition and reconstruction parameters: 120 kVp, 20 mA, 1 s tube rotation time, 1.25 pitch, 512x512 matrix, 2.5 mm slice thickness, 2.5 mm slice spacing, standard reconstruction kernel, and 50 cm display field of view. Technegas SPECT reconstruction was performed using a Hermes Workstation (Hermes Medical Solutions, Stockholm, Sweden) with the following settings: OSEM reconstruction (2 iterations, 10 subsets), 3D Gaussian filter with 1.20 cm FWHM with corrections for attenuation, scatter, and collimator resolution recovery.

2.2.5 MRI Acquisition

^{129}Xe ventilation MRI and ^{1}H MRI were acquired using a Discovery™ MR750 3T system (General Electric Health Care; Milwaukee, USA) as previously described.[140] Participants were instructed to inhale 1 L of gas (N_2 for ^{1}H MRI and a hyperpolarized ^{129}Xe/N_2 mixture for ^{129}Xe MRI) from functional residual capacity, and coronal slices were acquired under breath-hold conditions. Spin-exchange polarizer systems (Polarean 9800 or 9820, Polarean, Durham, USA) were used to polarize isotopically enriched ^{129}Xe gas (86%; ~600 mL) that was dispensed into a pre-filled mixing syringe (~400 mL of N_2) to achieve a fixed dose of 1 L that was transferred to a Tedlar bag (Jensen Inert Products, Coral Springs, USA) for participant delivery. ^{129}Xe polarization

was measured using a polarization measurement station (Polarean Inc., Durham, USA) and the dose-equivalent (DE) volume of 100% enriched, 100% polarized ^{129}Xe was calculated as previously described.[141] Following inhalation of the 1 L dose from functional residual capacity, hyperpolarized ^{129}Xe static ventilation MRI was performed using a custom-built, unshielded quadrature-asymmetric bird-cage coil and a 3D fast gradient recalled echo sequence (acquisition time=10 s, TE=1.5 ms, TR=5.1 ms, variable flip angle, initial flip angle=1.3°, receive bandwidth=16 kHz, field of view = 40x40x24 cm^3, reconstructed matrix size=128x128x16, voxel size=3.125x3.125x15 mm^3). A matching ^{1}H MRI was performed using the whole-body radiofrequency coil and a fast-spoiled gradient echo sequence (acquisition time=9 s, TE=1.2 ms, TR=4.3 ms, flip angle=20°, FOV=40x40 cm, matrix size=128x128, 16 slices, voxel size=3.125x3.125x15 mm^3).

2.2.6 Ventilation Defect Percent (VDP) Quantification

The burden of ventilation defects observed by Technegas SPECT and ^{129}Xe MRI were quantified as the VDP for the whole lung (WL), ipsilateral lung (IL), and contralateral lung (CL) using two different segmentation methods: adaptive thresholding (VDP_T) and k-means clustering (VDP_K), which have been optimized and validated for Technegas SPECT[75] and ^{129}Xe MRI,[17] respectively. For the adaptive thresholding method,[75] voxels within the thoracic cavity were defined as "ventilation defect" if they were below a threshold determined as 0.5 x $Mean_{5\text{-}80}$, where $Mean_{5\text{-}80}$ is the mean intensity of all voxels in the thoracic cavity that fall between the 5th and 80th percentile of voxel intensities. The k-means method[17] used an iterative algorithm to bin the voxel intensities into five clusters, with the lowest signal cluster being considered "ventilation defect." For both segmentation methods, the whole lung VDP was calculated as the volume of ventilation defects normalized to the thoracic cavity volume. Similarly, ipsilateral and contralateral lung VDP

were calculated by normalizing the ventilation defect volume for the specific lung to the corresponding lung volume.

SPECT segmentation: The thoracic cavity was delineated by registering the CT to the Technegas SPECT and then segmenting the CT using semi-automated segmentation and registration software implemented on a HERMES workstation. Technegas SPECT ventilation segmentation using the threshold method was implemented on a HERMES workstation and the k-means method was implemented using the Image Processing Toolbox provided by MATLAB R2022b (The MathWorks Inc., Natick, MA, USA).

MRI segmentation: The thoracic cavity was delineated by registering the ^{1}H MRI to the ^{129}Xe MRI and then segmenting the ^{1}H MRI using a previously described semi-automated pipeline implemented in MATLAB.[17] ^{129}Xe MRI ventilation segmentation using the threshold method was implemented in MATLAB and the k-means method was performed using the previously described MATLAB pipeline.[17]

2.3 Post-operative Follow-up

Following resection surgery, participants were followed in accordance with standard clinical care for 4-weeks post-surgery to document the incidence of post-operative complications and clinical outcomes. Post-operative complications were defined in accordance with the Ottawa Thoracic Mortality and Morbidity (TM&M) classification system.[63,64] A post-operative complication was defined in those participants experiencing one or more pulmonary (atelectasis, acute respiratory distress syndrome (ARDS), initial ventilator support greater than 48 hours, or pneumonia) or pleural complication (bronchopulmonary fistula, chylothorax, effusion, empyema, hemothorax, pneumothorax, prolonged alveolar air leak, prolonged pleural drainage, and subcutaneous emphysema). The clinical impact of post-operative complications was measured as

post-operative length of hospital stay, intensive care unit stay, the requirement for mechanical ventilation, intubation, thoracentesis, bronchoscopy, hospital readmission, emergency room visits, and post-discharge home oxygen use.

2.4 Statistical Analysis

As a proof-of-concept study, no formal sample size calculation was performed. The aim for the sample size was set at 100 participants, and considering a 15% attrition, a plan was made to recruit 115 participants. A sample size of 100 was based on [1] previous findings of Mathews et al. and Sheihk et al. who reported that 67-71% of lung cancer patients prior to radiation therapy had non-tumour specific abnormal ventilation identified by hyperpolarized ^{3}He MRI,[20,120] and [2] that 30% of patients who undergo lung resection surgery at our institute experience post-operative complications (unpublished data).

Differences in demographic and clinical characteristics between enrolled and evaluated participants were determined using an unpaired t-test (parametric data) or Mann-Whiney test (non-parametric data) for continuous variables and a Chi-Square test or Chi-Square test with Yates correction for categorical variables. The difference between Technegas SPECT and ^{129}Xe MRI ipsilateral and contralateral lung VDP was determined using the Wilcoxon test (non-parametric data). Differences in Technegas SPECT and ^{129}Xe MRI VDP between participants with no history of lung disease, asthma, and COPD were determined using a one-way ANOVA with Tukey's multiple comparisons test for parametric data or Kruskal Wallis with Dunn's multiple comparisons test for non-parametric data. The relationship of VDP measured by Technegas SPECT and ^{129}Xe MRI with demographic and clinical characteristics were evaluated by Pearson (r) or Spearman (ρ) correlation coefficients. The correlation and agreement between VDP, measured by Technegas

SPECT and ^{129}Xe MRI, were evaluated by Spearman (ρ) correlation coefficients and Bland-Altman analysis, respectively.

The following analyses [1-4] were performed in (1) the evaluated population, and (2) in the subgroup of participants who underwent lobectomy by minimally invasive surgery. [1] Differences in demographic and clinical characteristics between participants with post-operative complications and without complications were determined using unpaired t-test or Wilcoxon test. [2] Univariate relationships of demographic and clinical characteristics with length of hospital stay were evaluated by Pearson (r) or Spearman (ρ) correlation coefficients. [3] Binary logistic regression models were generated using the forward stepwise method to identify independent predictors of post-operative complications. [4] Multivariate linear regression models were generated using the forward stepwise method to identify independent predictors of post-operative length of hospital stay. For both regression analyses, variables were added to the model when $p<0.2$ and removed when $p>0.21$. Statistical analyses were performed using GraphPad Prism 9.0 (GraphPad Software, San Diego, CA, USA) or using IBM SPSS Statistics 20.0 (SPSS Inc., Chicago, IL, USA) and were considered significant when the probability of making a Type I error was less than 5% ($p < 0.05$).

Chapter 3: Results

3.1 Study Participants

Between January 2020 and December 2023, 217 patients scheduled to undergo first time lung cancer resection were screened for study eligibility and 123 were subsequently enrolled. Of the 123 participants enrolled, 105 completed pre-operative assessments. Eighteen participants did not complete pre-operative assessments and were excluded from the study for the following reasons: seven were withdrawn due to COVID-19 pandemic restrictions, four withdrew consent, two missed their pre-operative study visit, and five could not complete pre-operative assessments due to scheduling conflicts. Of the 105 participants that completed pre-operative assessments, 103 underwent surgical resection 7 [0-44] days later; surgery was cancelled for one participant due to change in clinical course of the disease, and surgery was postponed in one additional participant due to pending cardiac clearance. Therefore, in total, 103 participants completed pre-operative study assessments, surgical resection, and the 4-week post-operative follow-up period and were included in the evaluated population. The study participant flow diagram is provided in **Figure 3-1** and missing data in the evaluated population is summarized in **Table 3-1**.

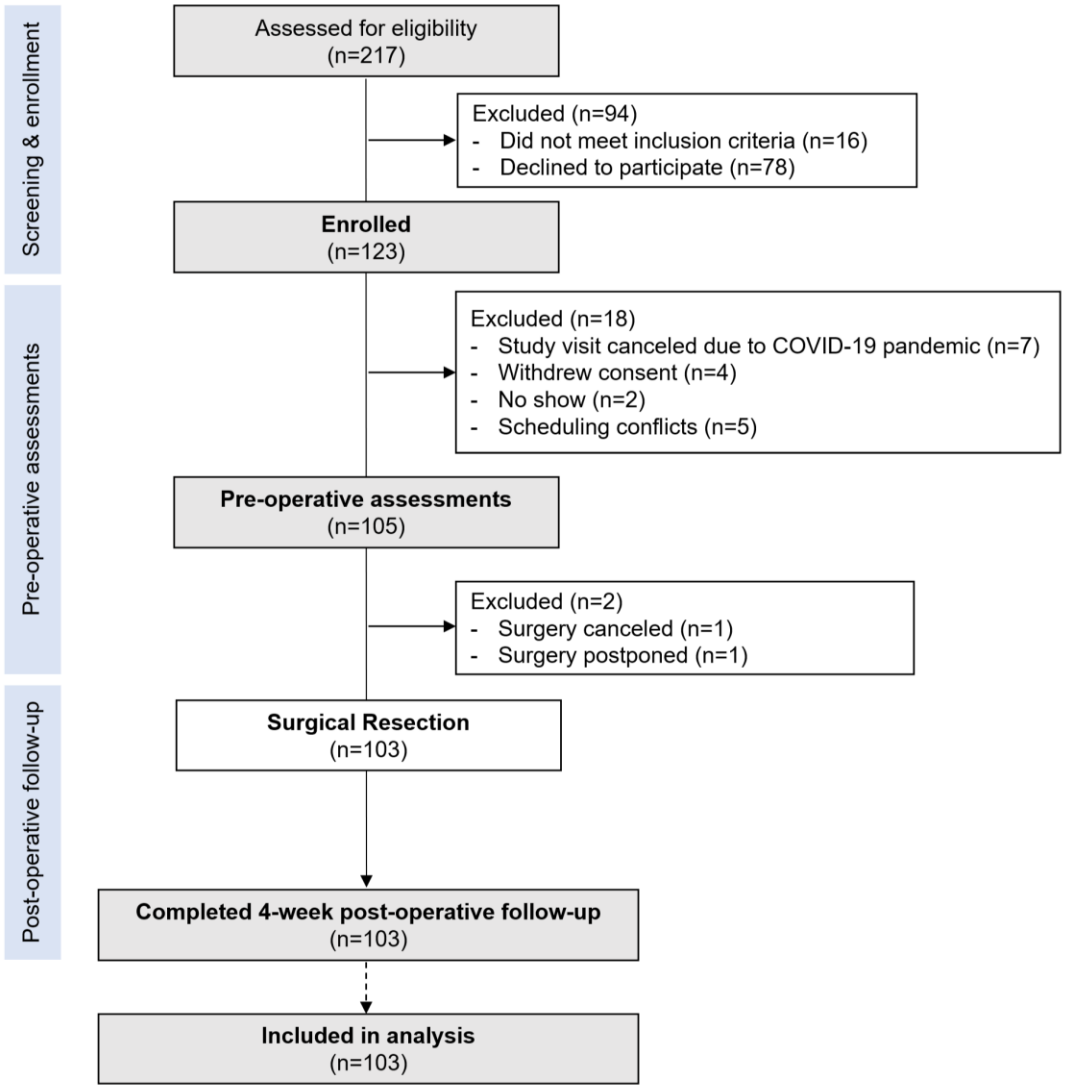

Figure 3-1 Study participant flow diagram.

Table 3-1 Summary of missing data in evaluated population.

	Missing values n (%)
Sputum cell count	34 (33)
Technegas SPECT	4 (4)
^{129}Xe MRI	5 (5)
Spirometry and DL_{CO}	0 (0)

Values are absolute numbers with percentage of total evaluated population (n=103).

3.1.1 Pre-operative Demographics and Clinical Characteristics

Pre-operative participant demographics, clinical characteristics, and comorbidities are summarized in **Table 3-2** for the enrolled (n=123) and evaluated populations (n=103), which were not different (all $p>0.05$). For the evaluated population, the mean age was 69±8 years, 58% were female, and the mean BMI was 28±6 kg/m^2. Regarding smoking status, 17% of participants were never smokers, 57% were past smokers, and 26% were current smokers. The median pack-year smoking history was 26 [0-130]. The Charlson Comorbidity Index revealed that 7% of participants had a history of myocardial infarction, 9% reported with peripheral vascular disease, 17% had a history of transient ischemic attack, 6% were diagnosed with liver disease, and 11% were diabetic. 60% of participants reported no concomitant history of lung disease, while 10% reported a history of asthma, 29% had COPD, and 1% had interstitial lung disease. Participants with no history of lung disease, asthma, and COPD were relatively well-balanced with respect to age, biological sex, and BMI (all $p>0.05$). However, they were different with respect to pack-year smoking history ($p<0.0001$), FEV_1/FVC ($p<0.0001$), $DL_{CO}\%_{pred}$ ($p<0.0001$), and the Charlson Comorbidity Index ($p=0.002$).

Table 3-2 Pre-operative demographics and clinical characteristics for the enrolled and evaluated populations.

	Enrolled (n=123)	**Evaluated** (n=103)	**p-value***
Age, years	69±9	69±8	0.73
Female sex, n (%)	70 (58)	60 (58)	0.99
BMI, kg/m^2	27±6	28±6	0.75
Smoking history			
Never, n (%)	21 (18)	17 (17)	0.84
Past, n (%)	69 (57)	59 (57)	0.97
Current, n (%)	30 (25)	27 (26)	0.84
Pack-years	26 [0-130]	26 [0-130]	0.99
History of lung disease			
No history, n (%)	71 (59)	62 (60)	0.88
Asthma, n (%)	11 (9)	10 (10)	0.89
COPD, n (%)	37 (31)	30 (29)	0.78
ILD, n (%)	1 (1)	1 (1)	0.94
Pulmonary function tests			
$FEV_1\%_{pred}$	--	83±21	--
$FVC\%_{pred}$	--	96±17	--
FEV_1/FVC %	--	67±12	--
$DLco\%_{pred}$	--	87±25	--
Comorbidities			
ASA score	4 [2-4]	4 [2-4]	0.92
CCI	5 [2-12]	5 [2-12]	0.80
Myocardial infarction, n (%)	8 (7)	7 (7)	0.89
Peripheral vascular disease, n (%)	10 (8)	9 (9)	0.91
Transient ischemic attack, n (%)	19 (16)	18 (17)	0.74
Liver disease, n (%)	6 (5)	6 (6)	0.78
Diabetes, n (%)	13 (11)	11 (11)	0.97

Values are mean ± standard deviation or median [minimum-maximum] except when indicated otherwise. BMI=body mass index; COPD=chronic obstructive pulmonary disease; ILD=interstitial lung disease; FEV_1=forced expiratory volume in one second; FVC=forced vital capacity; DLco=diffusion capacity for carbon monoxide; $\%_{pred}$=percent of predicted value; ASA=American Anesthesiologist score. *Significance of the difference between groups was determined using unpaired t-test (parametric data) or Mann-Whiney test (non-parametric data). For categorical data, Chi-Square test or Chi-Square test with Yates correction was used.

3.2 Characterization of Ventilation Defect Burden prior to Lung Cancer Resection

Technegas SPECT and ^{129}Xe MRI were well-tolerated by all participants, with no occurrence of adverse events. The scanning sessions were performed 90±30 minutes apart [minimum of 12 minutes, maximum of 120 minutes], except for one participant who underwent

Technegas SPECT and ^{129}Xe MRI two days apart due to SPECT unavailability. Dosing and measurements of image quality are provided in **Table 3-3** for both ventilation imaging modalities.

Table 3-3 Dosing and measurements of image quality

	Participants
Technegas SPECT (n=99)	
Dose	
Activity of ^{99m}Tc sodium pertechnetate loaded in crucible (MBq)	607 [396-993]
Number of breaths	5 [2-15]
Image quality	
Count rate from lungs on γ-camera, posterior (counts/second)†	2300 [930-4350]
Count rate from lungs on γ-camera, anterior (counts/second)†	2400 [720-4520]
^{129}Xe MRI (n=98)	
Dose	
Volume of ^{129}Xe delivered (mL)	500 [450-730]
Polarization (%)	23 [9-38]
Dose equivalent volume (mL)‡	99 [45-165]
Image quality	
Signal-to-noise ratio*	37 [14-92]

Values are median [minimum-maximum]. †A lower limit of 1500 counts/second is recommended. ‡A lower limit of 50mL is recommended. *Signal-to-noise ratio (SNR) for ^{129}Xe MRI was calculated as the mean voxel value within four representative regions of interest (ROI) within the ventilated lung divided by the standard deviation of the voxel values for noise inside four representative ROIs of the same size outside of the thoracic cavity (i.e., background).

Figure 3-2 shows coronal Technegas SPECT, ^{129}Xe MRI, and corresponding structural ^{1}H MRI slices acquired pre-operatively for four representative participants. For participant A, a never-smoker with no history of lung disease, both modalities revealed relatively normal ventilation. For participant B, an ex-smoker with no history of lung disease, both modalities revealed peripheral ventilation defects despite normal lung function assessed by spirometry. For participants C and D, past smokers with COPD, large and spatially concordant ventilation defects were observed by both modalities.

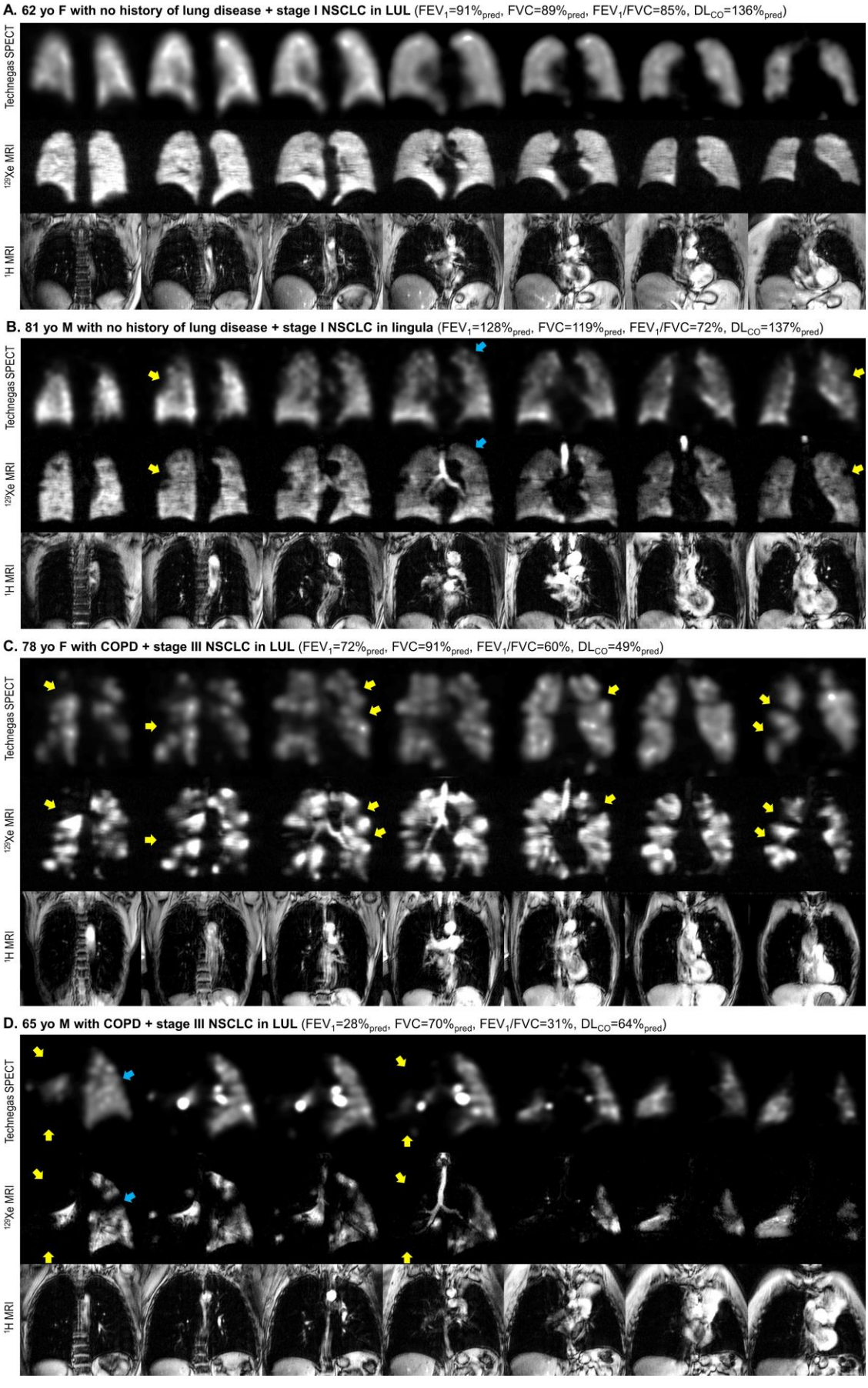
A. 62 yo F with no history of lung disease + stage I NSCLC in LUL (FEV1=91%pred, FVC=89%pred, FEV1/FVC=85%, DLCO=136%pred)
Technegas SPECT
129Xe MRI
1H MRI
B. 81 yo M with no history of lung disease + stage I NSCLC in lingula (FEV1=128%pred, FVC=119%pred, FEV1/FVC=72%, DLCO=137%pred)
Technegas SPECT
129Xe MRI
1H MRI
C. 78 yo F with COPD + stage III NSCLC in LUL (FEV1=72%pred, FVC=91%pred, FEV1/FVC=60%, DLCO=49%pred)
Technegas SPECT
129Xe MRI
1H MRI
D. 65 yo M with COPD + stage III NSCLC in LUL (FEV1=28%pred, FVC=70%pred, FEV1/FVC=31%, DLCO=64%pred)
Technegas SPECT
129Xe MRI
1H MRI

Figure 3-2 Ventilation visualized by Technegas SPECT and ^{129}Xe MRI.

Anatomically matched coronal Technegas SPECT, ^{129}Xe MRI, and ^{1}H MRI slices for four representative participants. Select examples of spatially concordant and discordant ventilation defects are highlighted by yellow and blue arrows, respectively.

(A) 62-year-old female with necrotizing granuloma in left upper lobe and no history of lung disease. Technegas SPECT: VDP_T=12%*, VDP_K=5%; ^{129}Xe MRI: VDP_T=22%, VDP_K=1%*; FEV_1=91%$_{pred}$, FVC=89%$_{pred}$, FEV_1/FVC=85%, DLco=136%$_{pred.}$

(B) 81-year-old male with stage I NSCLC in lingula and no history of lung disease. Technegas SPECT: VDP_T=28%*, VDP_K=14%; ^{129}Xe MRI: VDP_T=18%, VDP_K=4%*; FEV_1=128%$_{pred}$, FVC=119%, FEV_1/FVC=72%, DLco=137%$_{pred}$.

(C) 78-year-old female with stage III NSCLC in left upper lobe and concomitant COPD. Technegas SPECT: VDP_T=47%*, VDP_K=20%; ^{129}Xe MRI: VDP_T=31%, VDP_K=19%*; FEV_1=72%$_{pred}$, FVC=91%$_{pred}$, FEV_1/FVC=60%, DLco=49%$_{pred}$.

(D) 65-year-old male with stage III NSCLC in left upper lobe and concomitant COPD. Technegas SPECT: VDP_T=84%*, VDP_K=52%; ^{129}Xe MRI: VDP_T=37%, VDP_K=48%*; FEV_1=28%$_{pred}$, FVC=70%$_{pred}$, FEV_1/FVC=31%, DLco=64%$_{pred}$.

COPD=chronic obstructive pulmonary disease; FEV_1=forced expiratory volume in one second; FVC=forced vital capacity; DL_{CO}=diffusing capacity for carbon monoxide; LUL=left upper lobe; NSCLC=non-small cell lung cancer; %$_{pred}$=percent of predicted value. *Thresholding (VDP_T) and k-means clustering (VDP_K) methods previously optimized and validated for Technegas SPECT and ^{129}Xe MRI, respectively.

3.2.1 Prevalence of abnormal pre-operative VDP quantified by Technegas SPECT and ^{129}Xe MRI

Figure 3-3 shows the whole lung (WL), ipsilateral lung (IL) and contralateral lung (CL) VDP for Technegas SPECT and ^{129}Xe MRI quantified using adaptive thresholding and k-means clustering methods, respectively. The mean and median whole lung VDP for Technegas SPECT was 21.8±12.3% and 18.5% [10.3-84.0%], respectively. The mean and median whole lung VDP for ^{129}Xe MRI was 9.7±9.5% and 6.4% [1.0-49.5%], respectively. To determine if the tumor burden contributed to VDP, VDP was compared between the ipsilateral and contralateral lungs. For both modalities, VDP of the ipsilateral and contralateral lung was not different (Technegas SPECT: 21.3±10.9% vs. 20.9±12.5%, p=0.60; ^{129}Xe MRI: 9.6±4.4% vs. 9.5±10.5%, p=0.50).

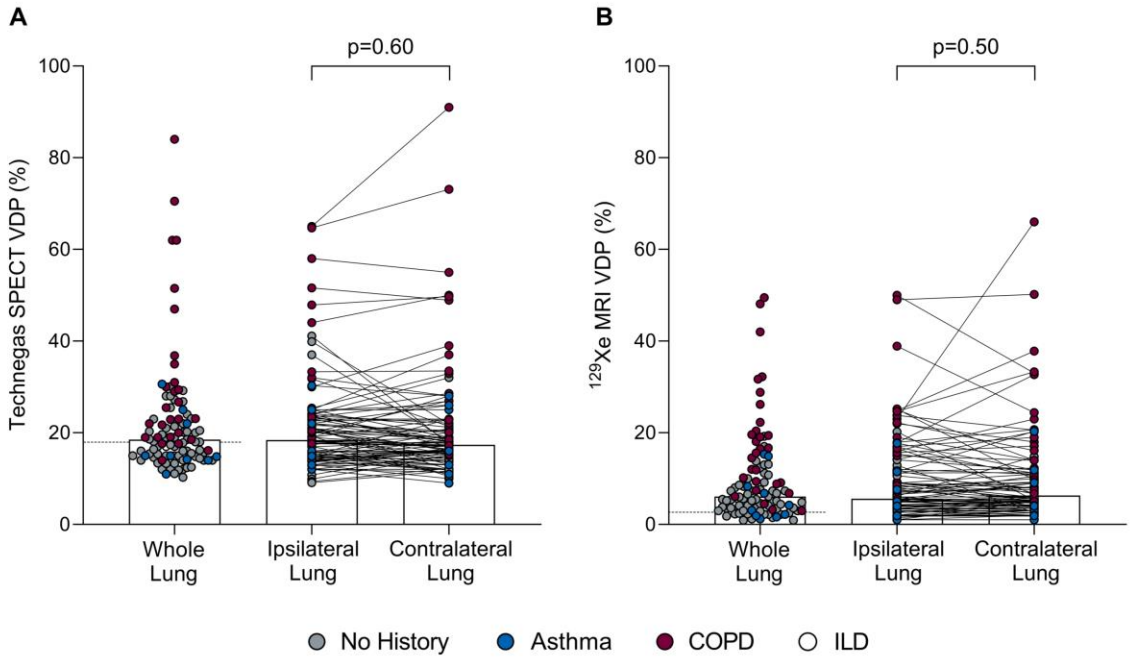

Figure 3-3 Whole lung, ipsilateral lung, and contralateral lung VDP for Technegas SPECT and ^{129}Xe MRI.

(A) Technegas SPECT VDP for the whole lung (21.8±12.3%, 18.5% [10.3-84.0%]), ipsilateral lung (21.3±10.9%, 18.4 [9.1-65.0%]) and contralateral lung (20.9±12.5%, 17.4 [9-91%]).

(B) ^{129}Xe MRI VDP for the whole lung (9.7±9.5%. 6.4% [1.0-49.5%]), ipsilateral lung (9.6±4.4%, 6.1[1.0-50.0%]) and contralateral lung (9.5±10.5%, 5.6 [1.0-66.0%]).

Bars represent median with whole lung, ipsilateral and contralateral lung values for all participants superimposed on the plot. Dashed lines represent the threshold for abnormal ventilation defined as VDP greater than the upper limit of normal of a healthy cohort (Technegas SPECT=18%, ^{129}Xe MRI=2.6%). Difference between ipsilateral and contralateral lung VDP was determined using Wilcoxon test (non-parametric data).

Abnormal ventilation assessed by Technegas SPECT and ^{129}Xe MRI was defined as whole lung VDP greater than the upper limit of normal, determined as the mean + 2 standard deviations of a healthy control group imaged at our institution. The upper limits of normal for Technegas SPECT VDP and ^{129}Xe MRI VDP were 18.0% and 2.6%, respectively. **Figure 3-4Ai** shows that ventilation quantified by Technegas SPECT VDP was abnormal (VDP>ULN) for 58 of 99 (59%) participants. As shown in **Figure 3-4Aii,** of the 58 participants with abnormal ventilation quantified by Technegas SPECT VDP, 47% reported no history of lung disease, 5% had asthma,

and 45% had COPD. Notably, 20 of 58 participants (34%) with abnormal ventilation quantified by Technegas SPECT VDP had normal pre-operative FEV_1 and DL_{CO} (both $\geq 80\%_{pred}$). **Figure 3-4Bi** shows that ventilation quantified by ^{129}Xe MRI VDP was abnormal for 82 of 98 (84%) participants. As shown in **Figure 3-4Bii,** of the 82 participants with abnormal ventilation quantified by ^{129}Xe MRI VDP, 56% reported no history of lung disease, 7% reported asthma, and 35% had COPD. 28 of 82 (34%) participants with abnormal ventilation quantified by ^{129}Xe MRI VDP had normal pre-operative FEV_1 and DLco ($\geq 80\%_{pred}$).

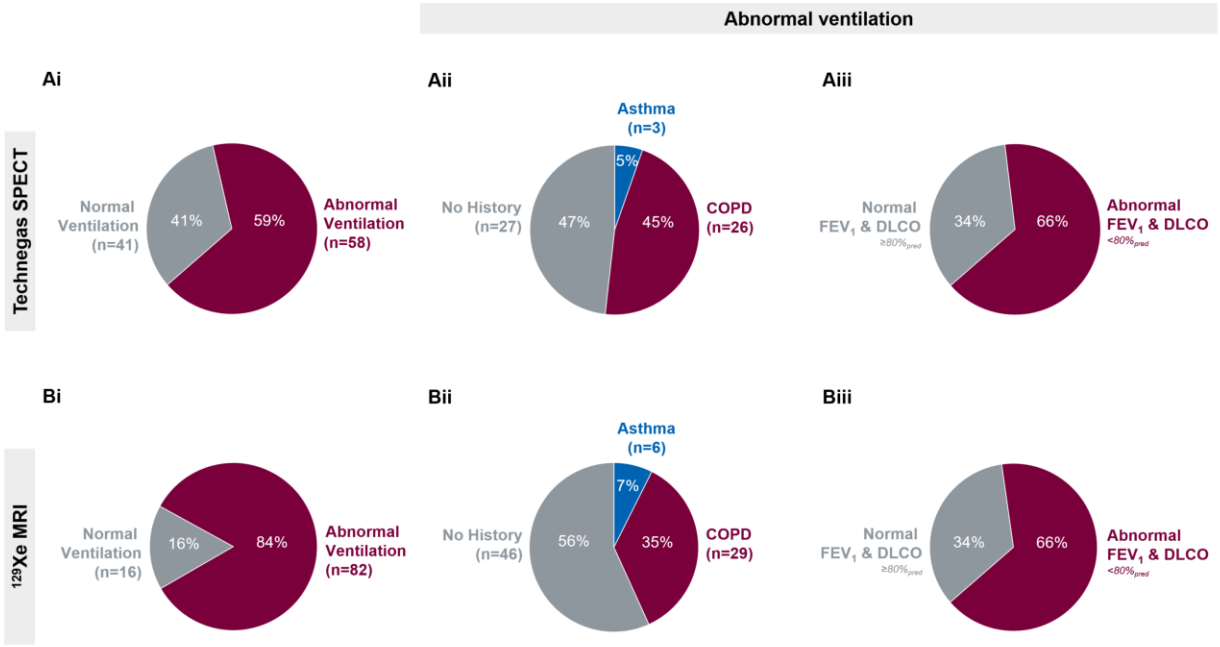

Figure 3-4 Prevalence of abnormal ventilation prior to lung cancer resection.

A. **(i)** Of the 99 participants that completed Technegas SPECT, 58 (59%) had abnormal ventilation. **(ii)** In participants with abnormal ventilation assessed by Technegas SPECT, 47% (27 of 58) reported no history of lung disease, 5% (3 of 58) had asthma, and 45% (26 of 58) had COPD. **(iii)** In participants with abnormal ventilation, 34% (20 of 58) had normal pre-operative FEV_1 and DL_{CO} (both $\geq 80\%_{pred}$).

B. **(i)** Of the 98 participants that completed ^{129}Xe MRI, 82 (84%) had abnormal ventilation as assessed by ^{129}Xe MRI. **(ii)** In participants with abnormal ventilation assessed by ^{129}Xe MRI, 56% (46 of 82) reported no history of lung disease, 7% (6 of 82) had asthma, and 35% (29 of 82) had COPD. **(iii)** In participants with abnormal ventilation, 34% (28 of 82) had normal pre-operative FEV_1 and DL_{CO} (both $\geq 80\%_{pred}$).

3.2.2 Pre-operative VDP and history of obstructive lung disease

Figure 3-5 summarizes whole lung, ipsilateral lung, and contralateral lung VDP for participants with no concomitant obstructive lung disease, those with a history of asthma, and those with COPD. The one (1%) participant with interstitial lung disease was excluded from this cross-sectional comparison. Whole lung Technegas SPECT VDP and ^{129}Xe MRI VDP were significantly higher for participants with COPD than with those with no history of lung disease (both p<0.0001), and asthma (p=0.006 and p=0.0006). Similar results were observed for ipsilateral (**Figure 3-5 C** and **D**) and contralateral lung VDP (**Figure 3-5 E** and **F**). There was no difference in whole lung, ipsilateral lung, and contralateral lung Technegas SPECT VDP or ^{129}Xe MRI VDP between participants with asthma and those with no history of lung disease (all p>0.99).

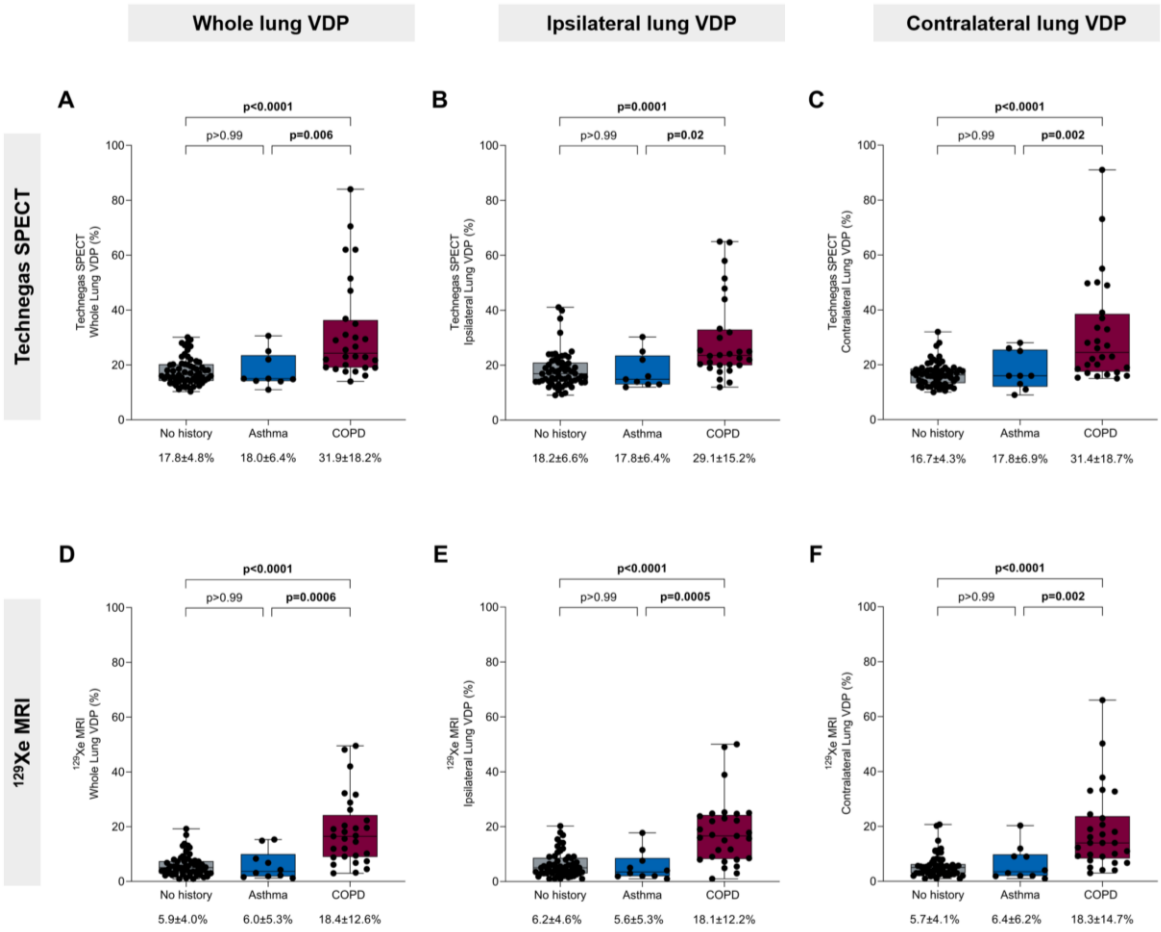

Figure 3-5 Ventilation defect percent and history of obstructive lung disease.

(A) Technegas SPECT VDP_{WL} was higher in participants with COPD than participants with asthma (31.9±18.2% vs. 18.0±6.4, p=0.006) and those with no history of lung disease (31.9±18.2vs. 17.8±4.8, p<0.0001).

(B) Technegas SPECT VDP_{IL} was significantly higher for participants with COPD than those with asthma (29.1±15.2% vs. 17.8±6.4%, p=0.02) and no history of lung disease (29.1±15.2% vs. 18.2±6.6%, p=0.0001).

(C) Technegas SPECT VDP_{CL} was significantly higher for participants with COPD than those with asthma (31.4±18.7% vs. 17.8±6.9%, p=0.02) and no history of lung disease (31.4±18.7% vs. 16.7±4.3%, p<0.0001).

(D) ^{129}Xe MRI VDP_{WL} was higher in participants with COPD than participants with asthma (18.4±12.6% vs. 6.0±5.3, p=0.0006) and those with no history of lung disease (18.4±12.6% vs. 5.9±4.0, p<0.0001).

(E) ^{129}Xe MRI VDP_{IL} was higher in participants with COPD than participants with asthma (18.1±12.2% vs. 5.6±5.3, p=0.0005) and those with no history of lung disease (18.1±12.2% vs. 6.2±4.6, p<0.0001).

(F) ^{129}Xe MRI VDP_{CL} was higher in participants with COPD than participants with asthma (18.3±14.7% vs. 6.46.2, p=0.002) and those with no history of lung disease (18.3±14.7% vs. 5.7±4.1%, p<0.0001).

Box plots show minimum, first quartile, median, third quartile, and maximum VDP with individual values for all participants superimposed on the plot. Difference between groups was determined using one-way ANOVA with Tukey's multiple comparisons test or Kruskal Wallis with Dunn's multiple comparisons test.

3.2.3 Relationships of pre-operative VDP with demographic and clinical characteristics

Univariate relationships of pre-operative Technegas SPECT VDP and ^{129}Xe MRI VDP with age, BMI, pack-year smoking history, spirometry, DL_{CO}, American Society of Anesthesia score, and the Charlson Comorbidity Index are summarized in **Table 3-4**. Whole lung Technegas SPECT VDP was correlated with BMI (r=-0.43, p<0.0001), pack-year smoking history (r=0.30, p<0.0001), $FEV_1\%_{pred}$ (r=-0.23, p=0.03), FEV_1/FVC (r=-0.47, p<0.0001), $DL_{CO}\%_{pred}$ (r=-0.44, p<0.0001), the American Society of Anesthesia score (r=0.21, p=0.03), and the Charlson Comorbidity Index (r=0.29, p=0.002). Similarly, whole lung ^{129}Xe MRI VDP was correlated with BMI (r=-0.29, p=0.004), pack-year smoking history (r=0.45, p<0.0001), $FEV_1\%_{pred}$ (r=-0.45, p<0.0001), FEV_1/FVC (r=-0.56, p<0.0001), $DL_{CO}\%_{pred}$ (r=-0.62, p<0.0001), the American Society

of Anesthesia score (r=0.44, p<0.0001), and the Charlson Comorbidity Index (r=0.40, p<0.0001). For both modalities, similar relationships were observed for the ipsilateral and contralateral lung VDP.

Table 3-4 Univariate relationships of pre-operative Technegas SPECT VDP and ^{129}Xe MRI VDP with participant demographics and clinical characteristics.

	Technegas SPECT VDP						**^{129}Xe MRI VDP**					
	Whole Lung		**Ipsilateral Lung**		**Contralateral Lung**		**Whole Lung**		**Ipsilateral Lung**		**Contralateral Lung**	
	r	**p**	**r**	**p**	**r**	**p**	**r**	**p**	**r**	**p**	**r**	**p**
Age, years	0.12	0.22	0.12	0.23	0.13	0.22	0.14	0.16	0.12	0.23	0.16	0.10
BMI, kg/m^2	-0.43	**<0.0001**	-0.43	**<0.0001**	-0.37	**0.0001**	-0.29	**0.004**	-0.31	**0.001**	-0.23	**0.02**
Pack-year smoking history	0.30	**<0.0001**	0.27	**0.006**	0.30	**0.002**	0.45	**<0.0001**	0.41	**<0.0001**	0.46	**<0.0001**
$FEV_1\%_{pred}$	-0.23	**0.03**	-0.21	**0.04**	-0.26	**0.008**	-0.45	**<0.0001**	-0.42	**<0.0001**	-0.47	**<0.0001**
$FVC\%_{pred}$	0.09	0.40	0.10	0.33	0.03	0.75	-0.17	0.10	-0.12	0.23	-0.21	**0.04**
FEV_1/FVC, %	-0.47	**<0.0001**	-0.44	**<0.0001**	-0.46	**<0.0001**	-0.56	**<0.0001**	-0.54	**<0.0001**	-0.54	**<0.0001**
DLco $\%_{pred}$	-0.44	**<0.0001**	-0.36	**0.0003**	-0.46	**<0.0001**	-0.62	**<0.0001**	-0.60	**<0.0001**	-0.62	**<0.0001**
ASA score	0.21	**0.03**	0.24	**0.02**	0.17	0.09	0.44	**<0.0001**	0.35	**0.0002**	0.49	**<0.0001**
CCI	0.29	**0.002**	0.29	**0.004**	0.29	**0.003**	0.40	**<0.0001**	0.37	**0.0003**	0.44	**<0.0001**

Relationships were evaluated with Pearson correlation coefficients for parametric data and Spearman's correlation coefficients for non-parametric data. VDP=ventilation defect percent; FEV_1=forced expiratory volume in one second; FVC=forced vital capacity; DL_{CO}=diffusion capacity for carbon monoxide. ASA=American Society of Anaesthesiologist score; CCI=Charlson Comorbidity Index.

3.2.4 Comparison of ventilation defects quantified by Technegas SPECT and ^{129}Xe MRI

The ventilation defect burden quantified by Technegas SPECT and ^{129}Xe MRI was compared in 95 participants who completed both imaging sessions. As shown in **Figure 3-3**, most ventilation defects, such as those highlighted by yellow arrows for participants C and D, were spatially concordant across modalities. However, focal discordances were also observed, such as those highlighted by blue arrows for participants B and D. Participant B had ventilation defects in the left upper lobe observed on Technegas SPECT that were not evident on ^{129}Xe MRI. Conversely, for Participant D, a large ventilation defect in the left upper lobe was observed on ^{129}Xe MRI but not Technegas SPECT.

The VDP for Technegas SPECT and ^{129}Xe MRI were quantified using adaptive thresholding (VDP_T) and k-means clustering (VDP_K) methods. The VDP was higher when determined using the threshold method compared to the k-means method for both Technegas

SPECT (VDP_T=22.2±12.5% vs. VDP_K=10.2±8.6%, p<0.0001) and ^{129}Xe MRI (VDP_T=19.7±5.3% vs. VDP_K=9.2±9.5%, p<0.0001). **Figure 3-6** summarizes the correlation and agreement of VDP_T and VDP_K measured by Technegas SPECT and ^{129}Xe MRI. For both quantification methods, VDP measured by Technegas SPECT and ^{129}Xe MRI were correlated (**Figure 3-6A**: VDP_T, r=0.52, p<0.0001; Figure 2C: VDP_K, r=0.57, p<0.0001). Using the threshold method, Bland-Altman analysis (**Figure 3-6B**) indicated a 2.5% bias (95% limit of agreement: -22.0% to 17.2%) for higher VDP_T measured by Technegas SPECT (Technegas SPECT VDP_T=22.2±12.5% vs. ^{129}Xe MRI VDP_T=19.7±5.3%, p=0.20). Using the k-means method, Bland-Altman analysis (**Figure 3-6D**) indicated a similar -0.9% bias (95% limit of agreement: -11.5% to 9.6%) for higher VDP_K measured by Technegas SPECT (Technegas SPECT VDP_K=10.2±8.6% vs. ^{129}Xe MRI VDP_K=9.2±9.5%, p=0.009).

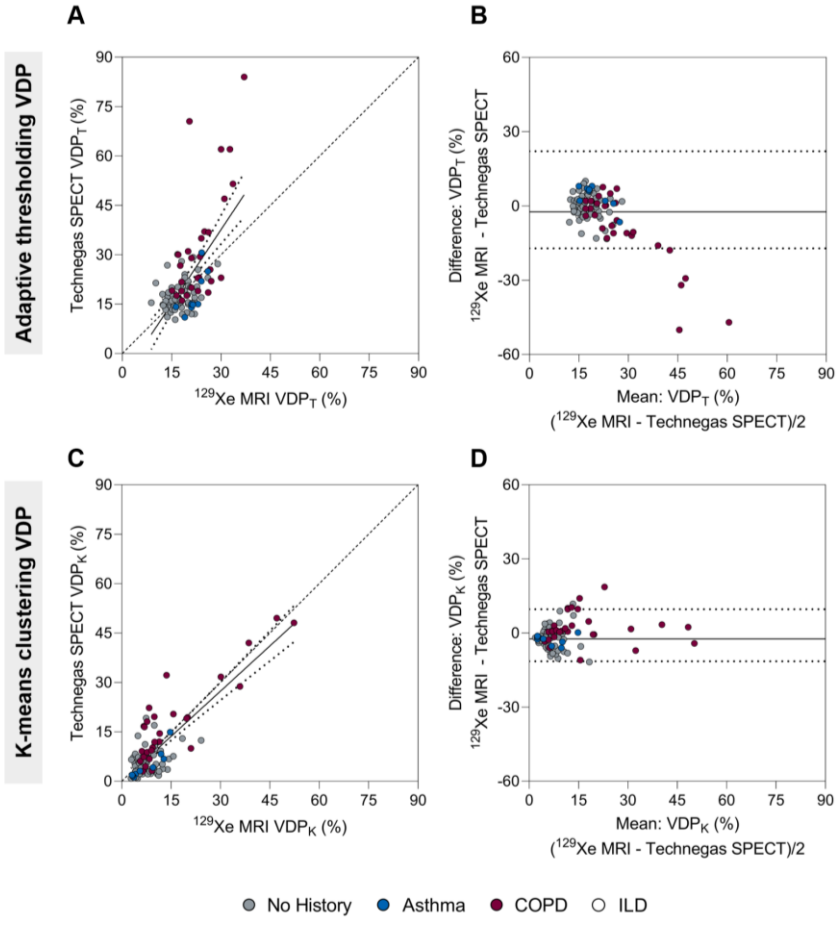

Figure 3-6 Comparison of the ventilation defect percent (adaptive thresholding (VDP_T) and k-means clustering (VDP_K)) quantified by Technegas SPECT and ^{129}Xe MRI.

(A) Positive relationship between Technegas SPECT and ^{129}Xe MRI VDP_T quantified using the adaptive threshold method ($r=0.52$, $r^2=0.40$, $p<0.0001$, $y=1.5x-7.45$).

(B) Bland-Altman plot of the difference between Technegas SPECT and ^{129}Xe MRI VDP_T quantified using the adaptive threshold method. Bias=-2.5% (95% limits of agreement, -22.0% to 17.2%).

(C) Positive relationship between Technegas SPECT and ^{129}Xe MRI VDP_K quantified using the k-means clustering method ($r=0.57$, $r^2=0.69$, $p<0.0001$, $y=0.91x-0.06$).

(D) Bland-Altman plot of the difference between Technegas SPECT and ^{129}Xe MRI VDP_K quantified using the k-means clustering method. Bias=-0.9% (95% limits of agreement, -11.5% to 9.6%).

For correlation plots, the dashed line represents the line of identity (y=x) and the dotted lines represent the 95% confidence intervals of the linear regression line. For Bland-Altman plots, the solid line represents the mean of the paired differences, and the dotted lines represent the 95% limits of agreement. Colored data points represent history of lung disease (no history, n=57; asthma, n=9; COPD, n=28; ILD: n=1). *Thresholding (VDP_T) and k-means clustering (VDP_K) methods previously optimized and validated for Technegas SPECT and ^{129}Xe MRI, respectively.

3.3 Characterization of Airway Inflammation prior to Lung Cancer Resection

Sputum samples were collected from 69 of 103 participants in the evaluated population, of which 34 (49%) were spontaneous and 35 (51%) were induced. Sputum cell counts and airway inflammatory endotypes are summarized in **Table 3-5**. Cellular inflammatory endotype classification based on sputum cytology revealed 35 (51%) participants had luminal cellular inflammation; 10% of whom had eosinophilic inflammation, 12% had neutrophilic inflammation, 14% had trivial neutrophilic inflammation, and 14% had mixed granulocytic inflammation. As shown in **Figure 3-7**, of the participants that had pre-operative airway inflammation, 40% had a reported history of COPD, 20% had asthma, and 40% reported no history of lung disease.

Table 3-5 Pre-operative sputum cell counts and endotype.

	Pre-operative (n=69)
Sputum Cell Counts	
Total cell count, $x10^6$ cells/g	5.4 [0.05-76.4]
$\geq 9.7x10^6$ cells/g, n (%)	20 (29)[†]
Eosinophils, %	0.5 [0-24.8]
≥2.3%, n (%)	16 (23)[‡]
Neutrophils, %	68.2 [12.3-94.3]
≥64%, n (%)	30 (43)[§]
Sputum Cellular Endotype*	
Paucigranulocytic, n (%)	34 (49)
Eosinophilic, n (%)	7 (10)
Neutrophilic, n (%)	8 (12)
Mixed-granulocytic, n (%)	10 (14)
Trivial Neutrophilic, n (%)	10 (14)

[†]n=61, n=58[‡], n=58[§], *Paucigranulocytic: Total cell count (TCC)<$9.7x10^6$ cells/g, <2.3% eosinophils, and <64% neutrophils or produced insufficient sample after 3 rounds of sputum induction; Eosinophilic: ≥2.3% eosinophils and/or moderate or many eosinophil-free-granules; Neutrophilic: ≥64% neutrophils and TCC ≥$9.7x10^6$ cells/g without eosinophilia; Trivial neutrophilic: ≥64% neutrophils or TCC ≥$9.7x10^6$ cells/g without eosinophilia; Mixed-granulocytic: eosinophilic and neutrophilic.

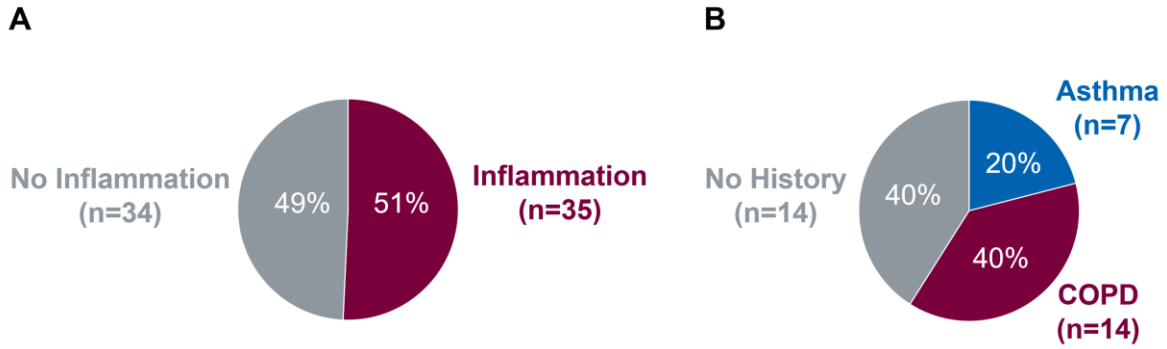

Figure 3-7 Prevalence of intraluminal cellular inflammation prior to lung cancer resection.

(A) Of the 69 participants for whom sputum was collected, 35 (51%) had pre-operative intraluminal inflammation.

(B) Of the 35 participants with pre-operative intraluminal inflammation, 14 (40%) had no reported history of lung disease, 7 (20%) reported asthma, and 14 (40%) reported COPD.

3.4 Surgical Details and Tumor Characteristics

Tumor location, surgical approach, extent of resection, and post-operative histopathological tumor diagnosis are detailed in **Table 3-6**. Minimally invasive surgery (MIS) was the most common surgical approach and was performed for 92 of 103 (89%) participants; 72 (70%) were video-assisted and 20 (19%) were robot-assisted. Only 7% of surgeries were open thoracotomy. Finally, 4% of surgeries were conducted using a combined approach (converted from minimally invasive to open thoracotomy due to complexity of resection). Regarding the extent of resection, 76 (74%) participants underwent lobectomy, 15 (15%) underwent wedge resection, 10 (10%) underwent segmentectomy, and 2 (2%) underwent pneumonectomy.

Histopathological analysis of surgical resections revealed a prevalence of non-small cell lung cancer in 76% (78 of 103) of participants. Among these cases, adenocarcinoma was the predominant subtype, accounting for 51%, while squamous cell carcinoma was identified in 19% of participants. 3% of participants had combined malignancy (2% had both squamous cell carcinoma and adenocarcinoma, and 1% had large cell carcinoma and adenocarcinoma). Other malignancy types included small cell lung cancer (n=1, 1%), carcinoid (n=5, 5%), and secondary metastatic cancer (n=3, 3%) (melanoma, colorectal and endometrial primary cancers). Histopathology revealed that 15% (15 of 103) of resected tumours were not cancerous. Among these cases, necrotizing granuloma was most common (n=10, 10%). Tumor stage information was available for 86 of 103 participants; 65 (76%) had Stage I cancer, 9 (10%) had Stage II cancer, 10 (12%) had Stage III cancer, and 2 (2%) had Stage IV cancer.

Table 3-6 Surgical details and tumor characteristics

	Evaluated Population (n=103)
Tumor Location	
Right upper lobe, n (%)	33 (32)
Right middle lobe, n (%)	4 (4)
Right lower lobe, n (%)	15 (15)
Left upper lobe, n (%)	28 (27)
Left lower lobe, n (%)	21 (20)
Surgical Approach	
Open, n (%)	7 (7)
Minimally invasive, n (%)	92 (89)
Video-assisted, n (%)	72 (70)
Robot-assisted, n (%)	20 (19)
Combined, n (%)*	4 (4)
Extent of resection	
Wedge, n (%)	15 (15)
Segmentectomy, n (%)	10 (10)
Lobectomy, n (%)	76 (74)
Pneumonectomy, n (%)	2 (2)
Post-operative Histopathological Diagnosis	
Malignancy Type	
Non-small cell cancer, n (%)	78 (76)
Adenocarcinoma, n (%)	53 (51)
Squamous cell carcinoma, n (%)	20 (19)
Combined, n (%)	3 (3)
Small cell cancer, n (%)	1 (1)
Carcinoid, n (%)	5 (5)
Secondary cancer, n (%)	3 (3)
No cancer, n (%)	15 (15)
Necrotizing granuloma, n (%)	10 (10)
Primary Tumor Stage, n (%)[†]	
Stage I, n (%)	65 (76)
Stage II, n (%)	9 (10)
Stage III, n (%)	10 (12)
Stage IV, n (%)	2 (2)

*Resection initially started as minimally invasive surgery that later converted to open thoracotomy.
[†]n=86

3.5 Post-operative Complications and Clinical Outcomes

Post-operative pulmonary and pleural complications and relevant clinical outcomes are summarized in **Table 3-7.** Within the 4-week post-operative period, 42 (41%) participants experienced one or more pulmonary or pleural complications and 61 (59%) experienced no complications. 24 (23%) participants experienced a single complication, 15 (15%) experienced

two complications, while 2 (2%) and 1 (1%) experienced three and four complications, respectively. A total of 64 pulmonary and pleural complications occurred within the 4-weeks post-operative period, of which 16 (25%) were pulmonary and 48 (75%) were pleural complication. Regarding the 16 pulmonary complications, the most prevalent was atelectasis (6 of 64, 9%). Among the 48 pleural complications, the most prevalent was prolonged air leak (19 of 64, 30%), followed by subcutaneous emphysema (14 of 64, 22%) and pneumothorax (10 of 64, 16%).

The median post-operative length of hospital stay was 3 days [1-26]. Following resection, six (6%) participants required bronchoscopy, four (4%) were admitted to the intensive care unit, two (2%) required intubation, and one (1%) died. At the time of discharge, three (3%) participants required post-discharge home oxygen use. Following discharge, 12 (12%) participants presented at the emergency room, and five (5%) were readmitted to hospital within the 4-week post-operative period.

Table 3-7 Post-operative complications and clinical outcomes during the 4-week post-operative period.

	Evaluated Population (n=103)
Participants with no respiratory complications, n (%)	61 (59)
Participants with ≥1 respiratory complication, n (%)	42 (41)
1 complication, n (%)	24 (23)
2 complications, n (%)	15 (15)
3 complications, n (%)	2 (2)
4 complications, n (%)	1 (1)
Total Pulmonary and Pleural complications	64
Pulmonary complications, *n (%)**	16 (25)
Atelectasis, n (%)	6 (9)
Acute respiratory distress syndrome, n (%)	4 (6)
Initial ventilator support >48 hours, n (%)	2 (3)
Pneumonia, n (%)	4 (6)
Pleural complications, *n (%)**	48 (75)
Prolonged air leak, n (%)	19 (30)
Subcutaneous emphysema, n (%)	14 (22)
Pleural effusion, n (%)	3 (5)
Pneumothorax, n (%)	10 (16)
Hemothorax, n (%)	1 (2)
Empyema, n (%)	1 (2)
Cardiac complications, n (%)*	
Atrial Arrhythmias, n (%)	2 (2)
Clinical outcomes	
Post-operative length of hospital stay, days, n (%)	3 [1-26]
Intensive care unit admissions, n (%)	4 (4)
Intubation, n (%)	2 (2)
Requirement for bronchoscopy, n (%)	6 (6)
Emergency room visit, n (%)	12 (12)
Hospital re-admission, n (%)	5 (5)
Post-discharge home oxygen use, n (%)	3 (3)
Death, n (%)	1 (1)

*Post-operative pulmonary, pleural, and cardiac complications were defined as per the Ottawa thoracic mortality and morbidity classification system.

3.6 Clinical Relevance of Pre-operative Ventilation Defect Burden

Figure 3-8 shows coronal Technegas SPECT and ^{129}Xe MRI slices acquired pre-operatively for participants with and without post-operative complications. In the subset of participants without post-operative complications, a majority exhibited normal ventilation, as illustrated by cases P33 and P37. These individuals, with no history of lung disease, had a homogenous ventilation pattern, developed no complications, and were discharged within two

days after the procedure. However, within this group, there are discordant cases. For instance, P106 displays bilateral large ventilation defects and abnormal spirometry but did not develop any post-operative complications. P128, a COPD participant with abnormal FEV_1 and DL_{CO}, exhibited relatively well-ventilated lungs, and experienced no complications. Participants with post-operative complications, such as P47, P59, and P88, had abnormal PFTs and exhibited heterogeneous ventilation pattern with significant defects in both ipsilateral and contralateral lungs. For P101, although PFTs were normal, imaging revealed focal ventilation defects and the participant experienced post-operative prolonged air leak and spent five post-operative days in hospital.

No Post-operative Complications

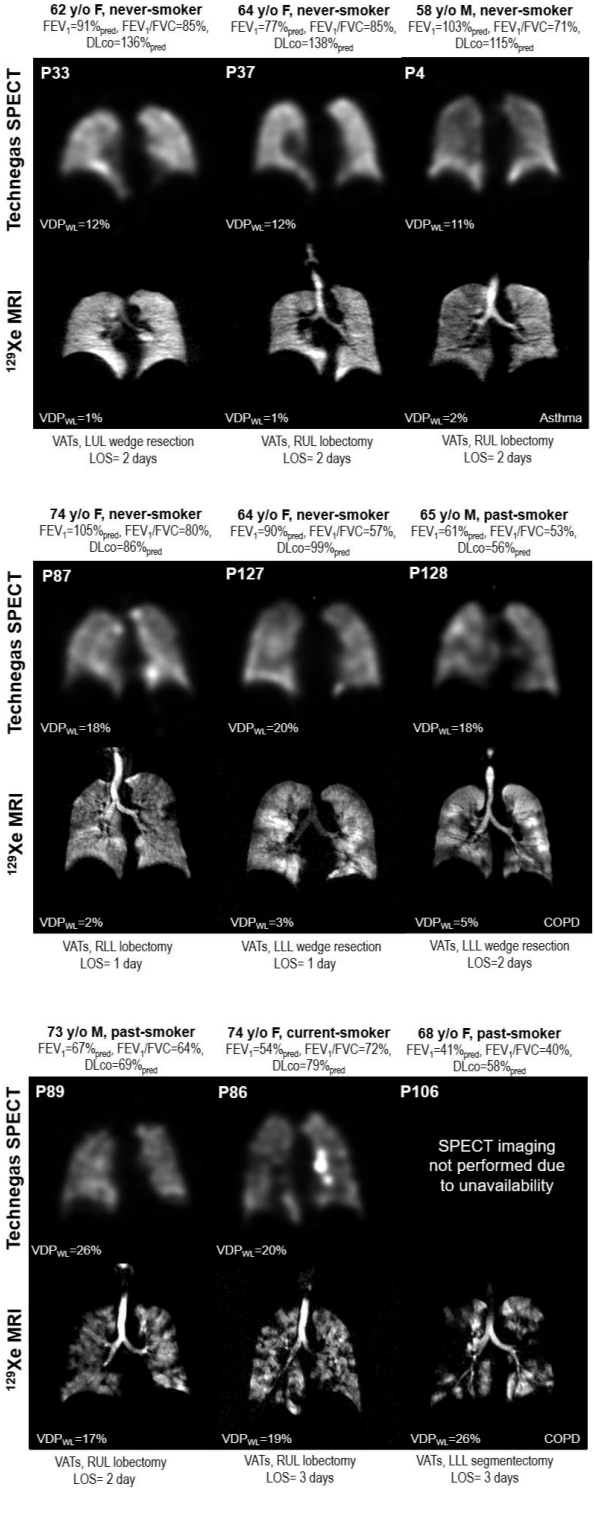

Post-operative Complications

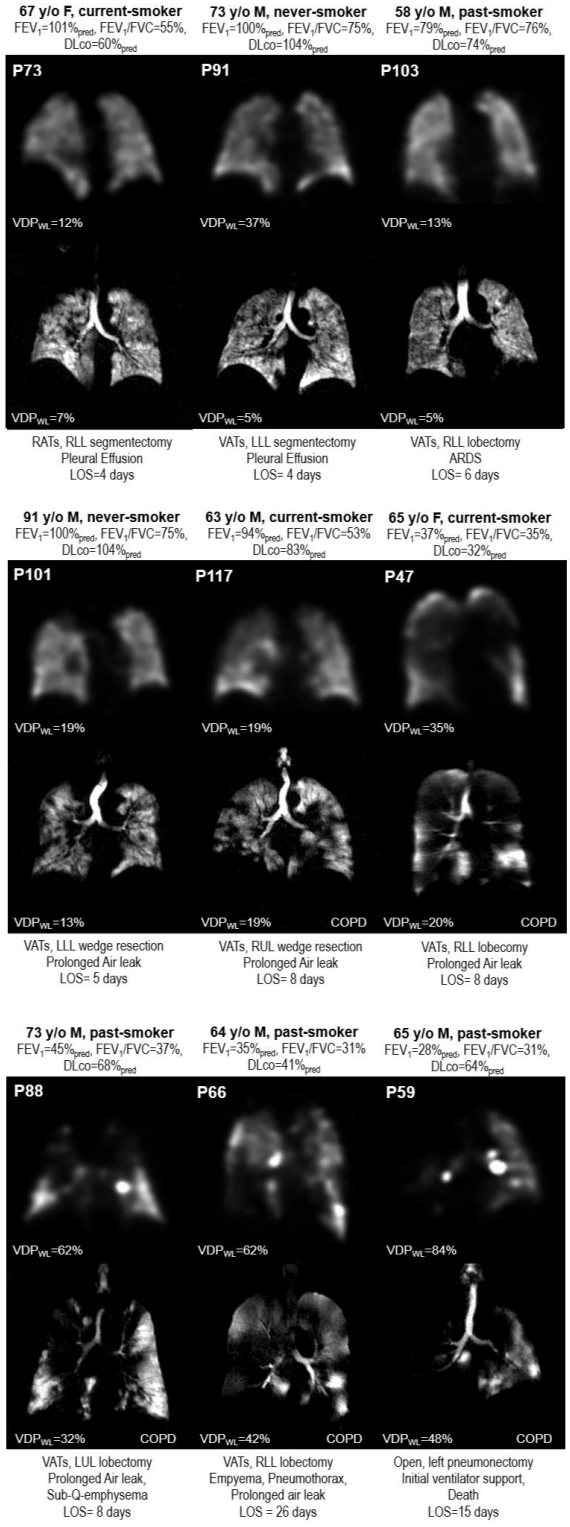

Figure 3-8 Representative Technegas SPECT and ^{129}Xe MRI for participants with and without post-operative complications.

Displayed above are coronal ^{129}Xe MRI slices for nine representative participants without post-operative complications and nine participants with post-operative complications. Pre-operative characteristics are detailed above, and post-operative clinical outcomes are detailed below.

ARDS=acute respiratory distress syndrome; COPD=chronic obstructive pulmonary disease; FEV_1=forced expiratory volume in one second; DL_{CO}=diffusing capacity for carbon monoxide; LUL=left upper lobe; LLL=left lower lobe; RUL=right upper lobe; RLL=right lower lobe; NSCLC=non-small cell lung cancer; POD=post-operative day; $\%_{pred}$=percent of predicted value; VATs=video-assisted thoracoscopic surgery; RATs=robot-assisted thoracoscopic surgery; VDP_{WL}=whole lung ventilation defect percent.

3.6.1 Evaluated Population

3.6.1.1 Comparison of participants with and without post-operative complications

Figure 3-9 shows the pre-operative Technegas SPECT VDP and ^{129}Xe MRI VDP for participants with (n=42, 41%) and without (n=61, 59%) post-operative complications during the 4-week post-operative period. Technegas SPECT VDP and ^{129}Xe MRI VDP measured pre-operatively were higher for participants with post-operative complications compared to those without post-operative complications (all $p<0.05$).

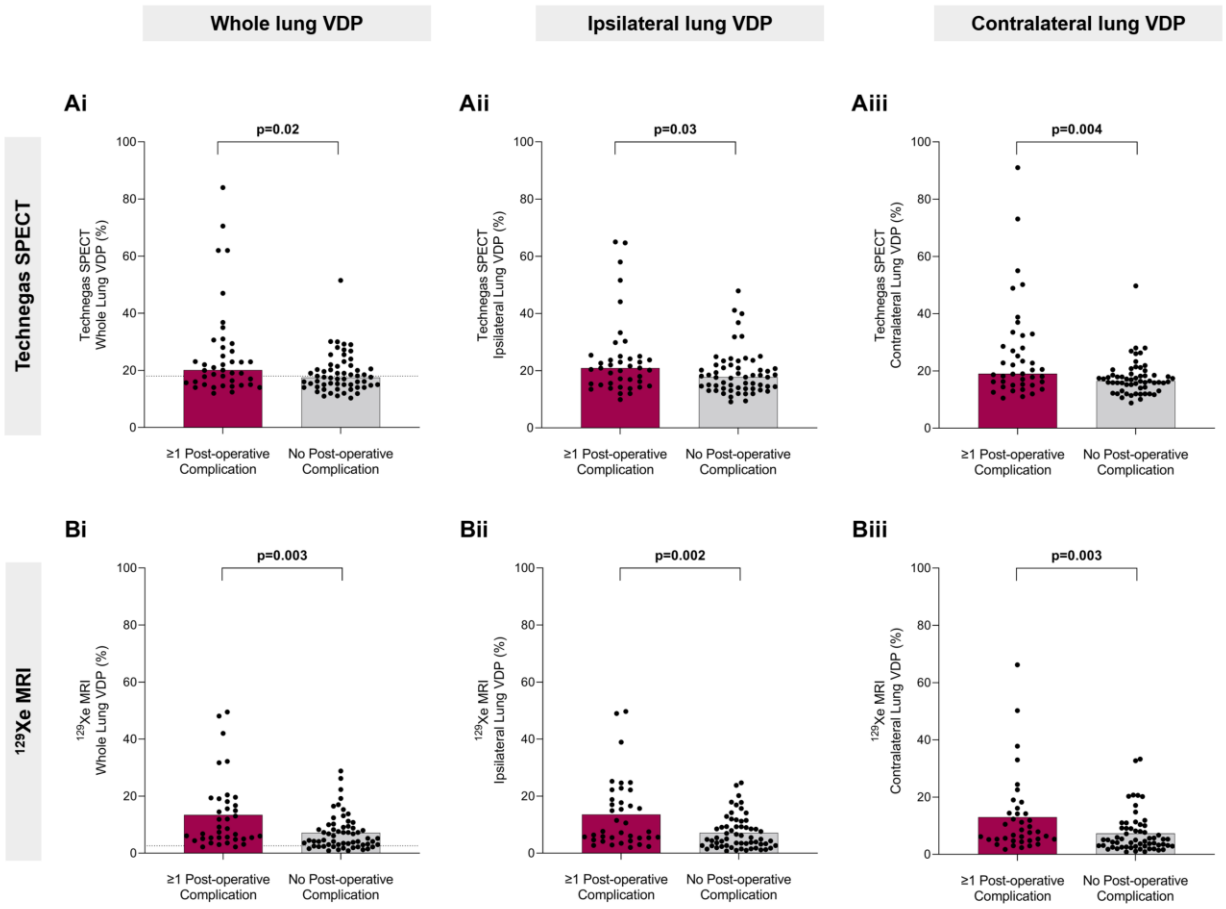

Figure 3-9 Comparison of pre-operative VDP in participants with and without post-operative complications.

(A) Compared to participants without a post-operative complication, those with a post-operative complication had higher Technegas SPECT VDP_{WL} **(i)** (26±17, 20[12-84] vs 19±7, 18[10-52], p=0.02), VDP_{IL} **(ii)** (24±14, 21[10-65] vs 19±8, 18[9-48], p=0.03), and VDP_{CL} **(iii)** (26±17, 19[11-91] vs 18±6, 16[9-50], p=0.004).

(B) Compared to participants without a post-operative complication, those with a post-operative complication had higher ^{129}Xe MRI VDP_{WL} **(i)** (13±12, 8[2-50] vs 7±6, 5[1-29], p=0.003), VDP_{IL} **(ii)** (14±12, 8[2-50] vs 7±6, 5[1-25], p=0.002), and VDP_{CL} **(iii)** (13±14, 8[2-66] vs 7±7, 5[1-33], p=0.003).

Bars represent median with VDP values for all participants superimposed on the plot. Dashed lines represent the threshold for abnormal ventilation defined as VDP greater than the upper limit of normal of a healthy cohort (Technegas SPECT=18%, ^{129}Xe MRI=2.6%). Difference between participants with post-operative complications and without post-operative complications was determined using Wilcoxon test (non-parametric data).

Table 3-8 summarizes participant demographics, clinical characteristics, comorbidities, and surgical characteristics for participants with and without post-operative complications. The groups were comparable with respect to their age, sex, BMI, pack-year smoking history, and comorbidities evaluated by the ASA score and CCI (all $p>0.05$). However, the proportion of current smokers (36% vs. 18%, $p=0.04$) and participants with COPD (40% vs. 21%, $p=0.04$) was higher in the post-operative complication group compared to no post-operative complication group. FEV_1/FVC was significantly lower in the post-operative complication group compared to the no post-operative complication group (64±14% vs. 70±10%, $p=0.01$), but $FEV_1\%_{pred}$, $FVC\%_{pred}$, and $DL_{CO}\%_{pred}$ were not different (all $p>0.05$). The type of surgery and extent of resection were not different between the groups ($p>0.05$). Participants with one or more post-operative complications had a longer hospital stay of 5 days [2-26] compared to 2 days [1-9] for those without complications ($p<0.0001$).

Table 3-8 Comparison of participants with and without post-operative complications.

	≥1 post-operative complication (n=42)	**No post-operative complication (n=61)**	**p-value***
Age, years	69±9	68±8	0.79
Female sex, n (%)	20 (48)	40 (66)	0.07
BMI, kg/m^2	27±6	28±6	0.25
Smoking history			
Never, n (%)	4 (10)	13 (21)	**0.03**
Past, n (%)	23 (55)	36 (59)	0.82
Current, n (%)	15 (36)	11 (18)	**0.04**
Pack-year smoking history	30 [0-130]	25 [0-66]	0.09
History of respiratory disease			
No History, n (%)	22 (52)	40 (66)	0.25
Asthma, n (%)	3 (7)	7 (11)	0.70
COPD, n (%)	17 (40)	13 (21)	**0.04**
Pulmonary function tests			
FEV_1 $\%_{pred}$	81±24	84±17	0.21
FVC $\%_{pred}$	99±18	94±16	0.52
FEV_1/FVC, %	64±14	70±10	**0.01**
DL_{CO} $\%_{pred}$	84±27	89±23	0.34
Co-morbidities			
ASA score	4[2-4]	3[2-4]	0.64
CCI	6[3-9]	5[2-12]	0.07
Surgical Approach			
Open, n (%)	7 (17)	4 (7)	0.19
Minimally invasive, n (%)	35 (83)	57 (93)	0.19
Extent of Resection			
Wedge, n (%)	4 (10)	11 (18)	0.36
Segmentectomy, n (%)	6 (14)	4 (7)	0.34
Lobectomy, n (%)	31 (74)	45 (74)	0.99
Pneumonectomy, n (%)	1 (2)	1 (2)	0.65
Clinical outcome			
Post-operative length of hospital stay, days	5 [2-26]	2 [1-9]	**<0.0001**

Values are mean ± standard deviation or median [minimum-maximum] except when indicated otherwise. BMI=body mass index; COPD=chronic obstructive pulmonary disease; FEV_1=forced expiratory volume in one second; FVC=forced vital capacity; DL_{CO}=diffusion capacity for carbon monoxide; $\%_{pred}$=percent of predicted value; ASA=American Society of Anesthesiologist score; CCI=Charlson Comorbidity Index *Significance of the difference between groups was determined using unpaired paired t-test (parametric data) or Mann-Whitney test (non-parametric data) for continuous variables, and Chi-Square test or Chi-Square test with Yates correction for categorical variables.

3.6.1.2 Univariate relationships with post-operative length of hospital stay

Figure 3-10 shows that pre-operative Technegas SPECT VDP (WL: r=0.43, p<0.0001; IL: r=0.45, p<0.0001; CL: r=0.36, p=0.0002) and ^{129}Xe MRI VDP (WL: r=0.49, p<0.0001; IL: r=0.50,

p<0.0001; CL: r=0.44, p<0.0001) were positively correlated with post-operative length of hospital stay.

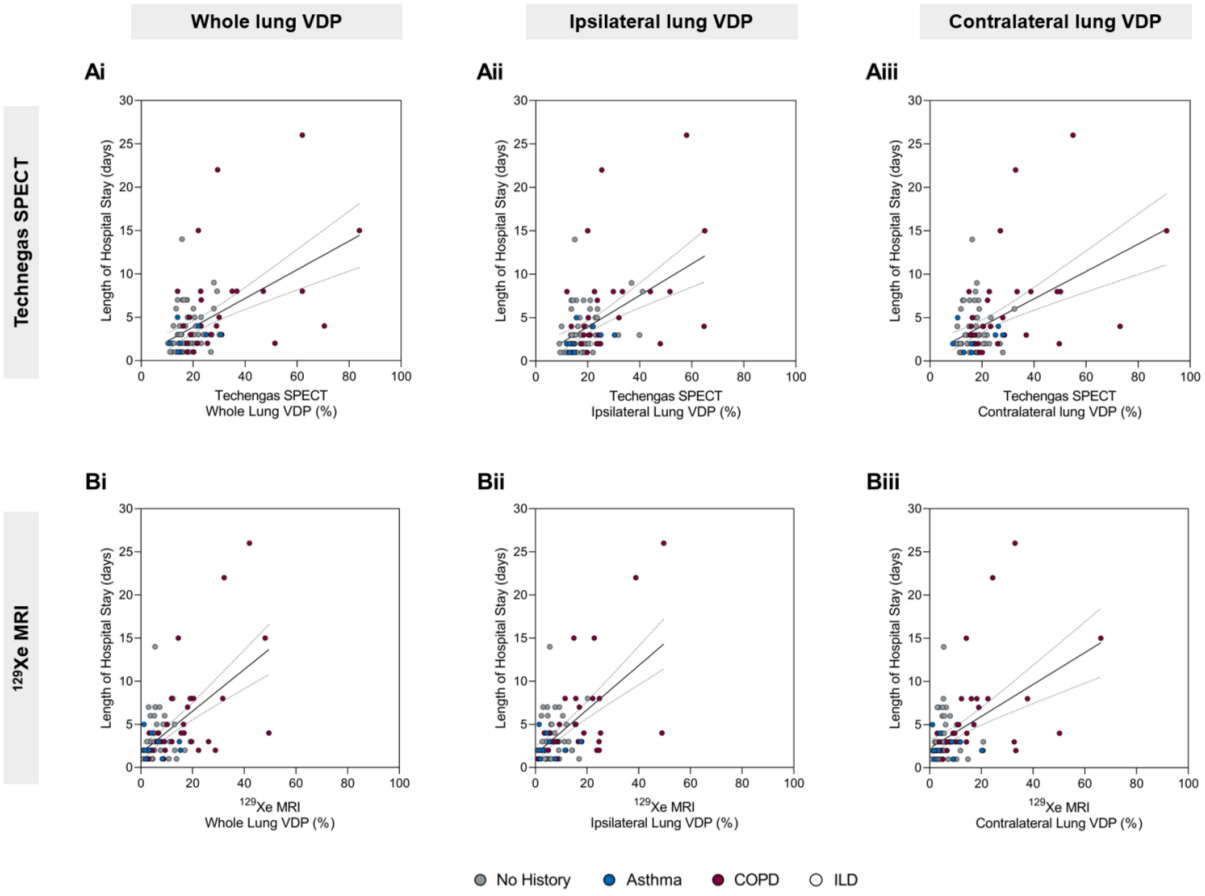

Figure 3-10 Univariate relationships of pre-operative Technegas SPECT VDP and ^{129}Xe MRI VDP with post-operative length of hospital stay.

(A) Pre-operative Technegas SPECT VDP_{WL} (**i**) (r=0.43, p<0.0001), VDP_{IL} (**ii**) (r=0.45, p<0.0001), and VDP_{CL} (**iii**) (r=0.36, p=0.002) were positively correlated with post-operative length of hospital stay.

(B) Pre-operative ^{129}Xe MRI VDP_{WL} (**i**) (r=0.49, p<0.0001), VDP_{IL} (**ii**) (r=0.50, p<0.0001), and VDP_{CL} (**iii**) (r=0.44, p<0.0001) were positively correlated with post-operative length of hospital stay.

Correlations show the best-fit line with 95% confidence bands.

Additional univariate relationships of demographics and clinical characteristics with post-operative length of hospital stay are summarized in **Table 3-9**. Age (r=0.30, p=0.04), pack-year

smoking history (r=0.23, p=0.02), CCI (r=0.28, p=0.004), FEV_1/FVC (r=-0.42, p<0.0001), and $DLco\%_{pred}$ (r=-0.36, p=0.0002) were all correlated with post-operative length of hospital stay.

Table 3-9 Univariate relationships of demographic and clinical characteristics with post-operative length of hospital stay.

	Post-operative length of hospital stay (n=103)	
	r	**p**
Age, years	0.30	**0.04**
BMI, kg/m^2	-0.19	0.05
Pack-year smoking history	0.23	**0.02**
ASA score	0.13	0.16
CCI	0.28	**0.004**
Pulmonary Function Tests		
FEV_1 $\%_{pred}$	-0.13	0.19
FVC $\%_{pred}$	0.13	0.20
FEV_1/FVC, %	-0.42	**<0.0001**
DL_{CO} $\%_{pred}$	-0.36	**0.0002**

Relationships were evaluated with Pearson correlation coefficients for parametric data and Spearman's correlation coefficients for non-parametric data. VDP=ventilation defect percent; FEV_1=forced expiratory volume in one second; FVC=forced vital capacity; DL_{CO}=diffusion capacity for carbon monoxide. ASA=American Society of Anaesthesiologist score; CCI=Charlson Comorbidity Index.

3.6.1.3 Regression models to predict post-operative complications and length of hospital stay

Binary logistic regression models were generated to identify predictors of post-operative complications and multivariate linear regression models were generated to identify predictors of post-operative length of hospital stay following lung resection. Covariates that remained constant in each model included age, pack-year smoking history, Charlson Comorbidities Index, $FEV_1\%_{pred}$, $DL_{CO}\%_{pred}$, history of obstructive lung disease, type of surgery (minimally invasive surgery, open thoracotomy), and extent of resection (wedge, segmentectomy, lobectomy, pneumonectomy). The only varying covariate in each model was VDP – for which Technegas SPECT VDP and ^{129}Xe MRI VDP were evaluated.

Table 3-10 summarizes the logistic regression models using a forward method to identify predictors of ≥1 post-operative complication. In model one, after adjusting for co-variates,

Technegas SPECT VDP_{WL} and the extent of resection (segmentectomy compared to wedge resection) were found to be significantly associated with the incidence of post-operative complications. The odds ratio for Technegas SPECT VDP_{WL} was 1.08 (95% CI: 1.02, 1.14, p=0.005), indicating that for each one-unit increase in pre-operative Technegas SPECT VDP, the odds of post-operative complications increased by 8%. The odds of developing post-operative complications in participants that underwent segmentectomy compared to wedge resection was 9.47 (95% CI: 1.28, 69.59, p=0.03). Model two showed that while adjusting for covariates, ^{129}Xe MRI VDP_{WL} (odds ratio=1.16, 95% CI: 1.06-1.28, p=0.002), minimally invasive surgery compared to open thoracotomy (odds ratio=0.093, 95% CI: 0.012-0.73, p=0.002), segmentectomy compared to wedge resection (odds ratio=13.55, 95% CI: 1.38-133.58, p=0.03) and lobectomy compared to wedge resection (odds ratio= 6.93, 95% CI: 1.07-45.04, p=0.04) were significantly associated with incident of post-operative complications.

Table 3-10 Binary logistic regression analysis for predictors of post-operative complications

Predictor Variables	Odds Ratio	95% CI	p-value
Model 1: Abnormal ventilation assessed by Technegas SPECT VDP			
Technegas SPECT VDP_{WL}, %	1.08	1.02-1.14	**0.005**
Segmentectomy†	9.47	1.28-69.95	**0.03**
Model 2: Abnormal ventilation assessed by ^{129}Xe MRI VDP			
^{129}Xe MRI VDP_{WL}, %	1.16	1.06-1.28	**0.002**
Type of surgery‡	0.093	0.012-0.73	**0.02**
Segmentectomy†	13.55	1.38-133.58	**0.03**
Lobectomy†	6.93	1.07-45.04	**0.04**
$FEV_1\%_{pred}$	1.03	1.00-1.06	0.10
Pack-year smoking history	1.02	1.00-1.05	0.08
$DL_{CO}\%_{pred}$	1.02	0.99-1.05	0.13

Predictor variables in the models included age, pack-year smoking history, Charlson Comorbidities Index, $FEV_1\%_{pred}$, $DL_{CO}\%_{pred}$, history of obstructive lung disease, type of surgery, extent of resection, Technegas SPECT VDP_{WL} and ^{129}Xe MRI VDP_{WL}.
†Compared to wedge resection. ‡Minimally invasive surgery compared to open thoracotomy. VDP_{WL}=whole lung ventilation defect percent; FEV_1=forced expiratory volume in one second; DL_{CO}=diffusion capacity for carbon monoxide.

Table 3-11 summarizes the multivariate regression models generated using a stepwise approach to identify predictors of post-operative length of hospital stay. In the first model, pre-operative Technegas SPECT VDP_{WL} (unstandardized β=0.12, p<0.001), $DL_{CO}\%_{pred}$ (unstandardized β=-0.033, p=0.045), and extent of resection, lobectomy compared to wedge resection (unstandardized β=2.37, p=0.02) added to the prediction of post-operative length of hospital stay (adjusted R^2=0.29; p<0.0001). In the second model, pre-operative ^{129}Xe MRI VDP_{WL} (unstandardized β=0.24, p<0.001), extent of resection, lobectomy compared to wedge resection (unstandardized β=2.58, p=0.008) added to the prediction of post-operative length of hospital stay (adjusted R^2=0.36; p<0.0001). Similar findings were noted for ipsilateral and contralateral lung models for prediction of post-operative length of hospital stay (Appendix 7.3 and 7.4).

Table 3-11 Multivariate regression analysis for predictors of post-operative length of hospital stay

Predictor Variables	Unstandardized β	Standardized β	95% CI	p-value
MODEL 1: Anormal ventilation assessed by Technegas SPECT VDP (R^2=0.33, adjusted R^2=0.29, p<0.001)				
Technegas SPECT VDP_{WL}, %	0.13	0.40	0.063-0.20	**<0.001**
$DL_{CO}\%_{pred}$	-0.031	-0.20	-0.062-(-0.001)	**0.045**
Lobectomy†	2.34	0.25	0.39-4.29	**0.02**
Pneumonectomy‡	4.31	0.15	-1.25-9.87	0.13
Segmentectomy§	2.14	0.15	-0.76-5.05	0.15
MODEL 2: Abnormal ventilation assessed by ^{129}Xe MRI VDP (R^2=0.38, adjusted R^2=0.36, p<0.001)				
^{129}Xe MRI VDP_{WL}, %	0.24	0.58	0.17-0.32	**<0.001**
Lobectomy†	2.58	0.28	0.68-4.49	**0.008**
Pneumonectomy‡	4.67	0.16	-0.38-9.71	0.07
Segmentectomy§	2.24	0.16	-0.52-5.01	0.11

Predictor variables in the model included age, pack-year smoking history, Charlson Comorbidities Index, $FEV_1\%_{pred}$, $DL_{CO}\%_{pred}$, history of obstructive lung disease, type of surgery, extent of resection, Technegas SPECT VDP_{WL} and ^{129}Xe MRI VDP_{WL}.

†‡§Compared to wedge resection. VDP_{WL}=whole lung ventilation defect percent; DL_{CO}=diffusion capacity for carbon monoxide.

3.6.2 *Minimally Invasive Lobectomy*

To account for variations in surgical approach and extent of resection, a subgroup analysis was conducted on the cohort of participants (69 of 103) who underwent minimally invasive lobectomy. **Figure 3-11** shows that pre-operative Technegas SPECT VDP and ^{129}Xe MRI VDP for participants with (n=26, 38%) and without (n=43, 62%) post-operative complications during the 4-week post-operative period. Technegas SPECT VDP and ^{129}Xe MRI VDP measured pre-operatively were higher for participants with post-complications compared to those without post-operative complications (all $p<0.05$).

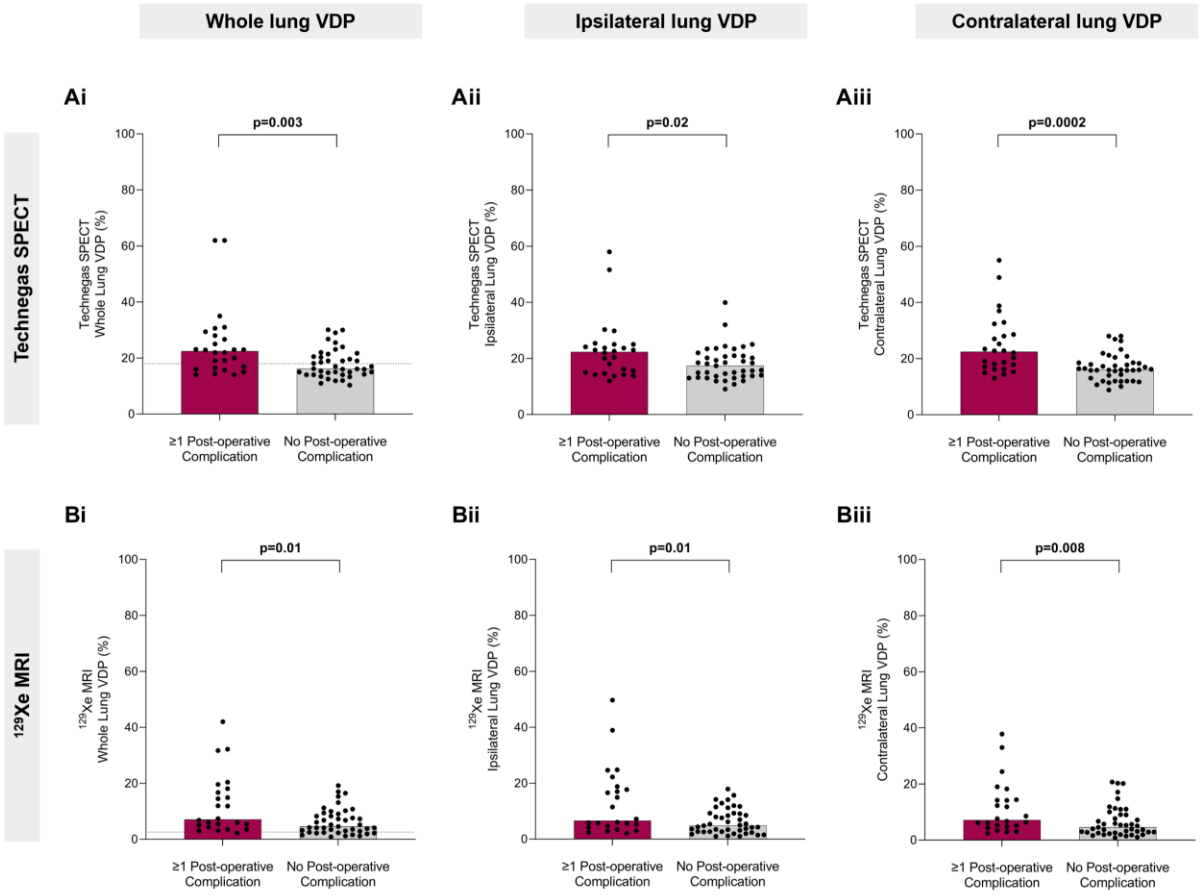

Figure 3-11 Comparison of VDP in participants with and without post-operative complications who underwent minimally invasive lobectomy

(A) Compared to participants without a post-operative complication, those with a post-operative complication had higher Technegas SPECT VDP_{WL} **(i)** (25±12, 22[14-62] vs 18±5, 16[10-30],

p=0.003), VDP_{IL} **(ii)** (23±11, 22[12-58] vs 18±6, 17[9-40], p=0.02), and VDP_{CL} **(iii)** (25±11, 22[13-55] vs 17±5, 16[9-28], p=0.0002).

(B) Compared to participants without a post-operative complication, those with a post-operative complication had higher ^{129}Xe MRI VDP_{WL} **(i)** (12±11, 7[2-42] vs 6±5, 5[1-19], p=0.01), VDP_{IL} **(ii)** (13±12, 7[2-50] vs 6±5, 5[1-18], p=0.01), and VDP_{CL} **(iii)** (11±9, 7[2-38] vs 6±5, 5[1-21], p=0.008).

Bars represent median with VDP values for all participants superimposed on the plot. Dashed lines represent the threshold for abnormal ventilation defined as VDP greater than the upper limit of normal of a healthy cohort (Technegas SPECT=18%, ^{129}Xe MRI=2.6%). Difference between participants with post-operative complications and without post-operative complications was determined using Wilcoxon test (non-parametric data).

Table 3-12 summarizes participant demographics, clinical characteristics, and co-morbidity scores for participants with and without post-operative complications. The groups were comparable with respect to their age, sex, BMI, smoking status, pack-year smoking history, and comorbidities evaluated by the ASA score and CCI (all $p>0.05$). The proportion of participants with COPD was higher in the post-operative complication group compared to no post-operative complication group (COPD: 46% vs 16%, p=0.007). FEV_1/FVC, was significantly lower in the post-operative complication group compared to the no post-operative complication group (63±13% vs 72±8%, p=0.002). Participants with one or more post-operative complications had a longer hospital stay of 6 days [2-26] compared to 2 days [1-6] for those without complications ($p<0.0001$).

Table 3-12 Comparison of participants with and without post-operative complications in subset of participants that underwent lobectomy by minimally invasive surgery.

	≥1 post-operative complication (n=26)	**No post-operative complication (n=43)**	**p-value***
Age, years	68±8	69±8	0.60
Female sex, n (%)	12 (46)	28 (65)	0.20
BMI, kg/m^2	26±6	28±6	0.20
Smoking history			
Never, n (%)	2 (8)	9 (21)	0.26
Past, n (%)	15 (58)	26 (60)	0.82
Current, n (%)	9 (35)	8 (19)	0.13
Pack-years	36[0-130]	22[0-66]	0.09
History of respiratory disease			
No History, n (%)	11 (42)	28 (65)	0.06
Asthma, n (%)	3 (12)	7 (16)	0.59
COPD, n (%)	12 (46)	7 (16)	**0.007**
Pulmonary function tests			
$FEV_1\%_{pred}$	80±25	86±16	0.20
$FVC\%_{pred}$	99±17	94±17	0.26
FEV_1/FVC, %	63±13	72±8	**0.002**
$DLco\%_{pred}$	83±26	92±23	0.15
Co-morbidities			
ASA score	4[2-4]	3[2-4]	0.72
CCI	5[3-8]	5[2-12]	0.37
Clinical outcomes			
Post-operative length of hospital stay, days	6[2-26]	2[1-6]	**<0.0001**

Values are mean ± standard deviation or median [minimum-maximum] except when indicated otherwise. BMI=body mass index; COPD=chronic obstructive pulmonary disease; FEV_1=forced expiratory volume in one second; FVC=forced vital capacity; DL_{CO}=diffusion capacity for carbon monoxide; $\%_{pred}$=percent of predicted value; ASA=American Society of Anesthesiologist score; CCI=Charlson Comorbidity Index. *Significance of the difference between groups was determined using unpaired paired t-test (parametric data) or Mann-Whitney test (non-parametric data) for continuous variables, and Chi-Square test or Chi-Square test with Yates correction for categorical variables.

3.6.2.1 Univariate relationships with post-operative length of hospital stay

Figure 3-12 shows that in the subgroup of evaluated participants that underwent minimally invasive lobectomy (n=69), both Technegas SPECT VDP (WL: r=0.42, p=0.0005; IL: r=0.40, p=0.0007; CL: r=0.43, p=0.0003) and ^{129}Xe MRI VDP (WL: r=0.45, p=0.0001; IL: r=0.47, p<0.0001; CL: r=0.44, p=0.0002) were positively correlated with post-operative length of hospital stay.

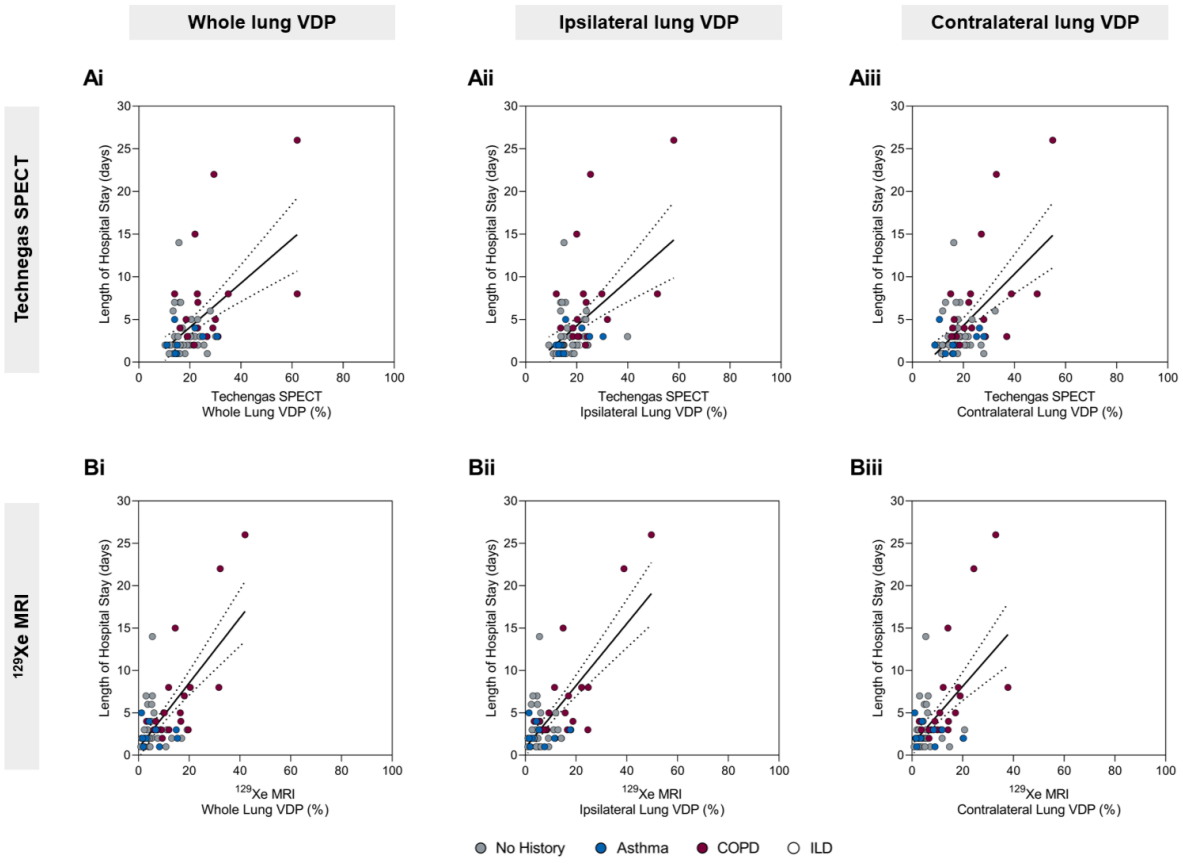

Figure 3-12 Univariate relationships between pre-operative Technegas SPECT and 129Xe MRI VDP and post-operative length of hospital stay. *Correlations show the best-fit line with 95% confidence bands.*

(A) Pre-operative Technegas SPECT VDP_{WL} (**i**) (r=0.42, p=0.005), VDP_{IL} (**ii**) (r=0.40, p=0.0007), and VDP_{CL} (**iii**) (r=0.43, p=0.0003) were positively correlated with post-operative length of hospital stay.

(B) Pre-operative ^{129}Xe MRI VDP_{WL} (**i**) (r=0.45, p=0.0001), VDP_{IL} (**ii**) (r=0.47, p<0.0001), and VDP_{CL} (**iii**) (r=0.44, p=0.0001) were positively correlated with post-operative length of hospital stay.

The univariate relationships of demographics and clinical characteristics with post-operative length of hospital stay in participants who underwent minimally invasive lobectomy are presented in **Table 3-13**. Pack-year smoking history (r=0.35, p=0.003) and CCI score (r=0.30, p=0.01) were positively correlated with post-operative length of hospital stay. $FEV_1\%_{pred}$ (r=-0.28, p=0.02), FEV_1/FVC (r=-0.56, p<0.0001), and DL_{CO} $\%_{pred}$ (r=-0.44, p<0.0001) were negatively correlated with length of hospital stay.

Table 3-13 Univariate relationships of demographic and clinical characteristics with post-operative length of hospital stay in participants who underwent minimally invasive lobectomy

	Length of hospital stay (n=69)	
	r	**p**
Age years	0.16	0.17
BMI, kg/m^2	-0.19	0.12
Pack-year smoking history	0.35	**0.003**
ASA score	0.08	0.50
CCI	0.30	**0.01**
Pulmonary Function Tests		
FEV_1 $\%_{pred}$	-0.28	**0.02**
FVC $\%_{pred}$	0.10	0.41
FEV_1/FVC, %	-0.56	**<0.0001**
DL_{CO} $\%_{pred}$	-0.44	**<0.0001**

Relationships were evaluated with Pearson correlation coefficients for parametric data and Spearman's correlation coefficients for non-parametric data. VDP=ventilation defect percent; VDP_T=VDP determined by thresholding method; VDP_K=VDP determined by k-means method; FEV_1=forced expiratory volume in one second; FVC=forced vital capacity; DL_{CO}=diffusion capacity for carbon monoxide. ASA=American Society of Anaesthesiologist score; CCI=Charlson Comorbidity Index.

3.6.2.2 Regression models to predict post-operative complications and length of hospital stay

The same covariates as described above were used in the subgroup analysis. As shown in **Table 3-14**, Technegas SPECT and ^{129}Xe MRI VDP_{WL} were independent predictors for the occurrence of post-operative complications. The odds ratio for Technegas SPECT VDP_{WL} was 1.13 (95% CI: 1.03, 1.24, p=0.01), indicating that for each one-unit increase in pre-operative VDP_{WL}, the odds of post-operative complications increased by 13%. Similarly, the odds ratio for ^{129}Xe MRI VDP_{WL} was 1.12 (95% CI: 1.03, 1.22, p=0.009), indicating that for each one-unit increase in VDP_{WL}, the odds of any post-operative complications increased by 12%. Comparable results were observed for Technegas SPECT and ^{129}Xe MRI VDP_{CL} but not Technegas SPECT VDP_{IL} (Appendix 7.4 and 7.5).

Table 3-14 Binary logistic regression analysis for predictors of post-operative complications in participants who underwent minimally invasive lobectomy

Predictor Variables	Odds Ratio	95% CI	p-value
Model 1: Abnormal ventilation assessed by Technegas SPECT VDP			
Technegas SPECT VDP_{WL}, (%)	1.13	1.03-1.24	**0.01**
Model 2: Abnormal ventilation assessed by ^{129}Xe MRI VDP			
^{129}Xe MRI VDP_{WL}, (%)	1.12	1.03-1.22	**0.009**

Predictor variables in the model included age, pack-year smoking history, Charlson Comorbidities Index, $FEV_1\%_{pred}$, $DL_{CO}\%_{pred}$, history of obstructive lung disease, Technegas SPECT VDP_{WL} and ^{129}Xe MRI VDP_{WL}. VDP_{WL}=whole lung ventilation defect percent.

Table 3-15 presents the results of multivariate regression models using a stepwise approach to identify predictors of post-operative length of hospital stay in participants that underwent minimally invasive lobectomy. Technegas SPECT VDP_{WL} (unstandardized β=0.21, p<0.001) and $DL_{CO}\%_{pred}$ (unstandardized β=-0.051, p=0.02) added to the prediction of post-operative length of hospital stay (adjusted R^2=0.35; p<0.0001). In the second model, ^{129}Xe MRI VDP_{WL} (unstandardized β=0.41, p<0.001) was the only variable that added to the prediction of post-operative length of hospital stay (adjusted R^2=0.46; p<0.0001). Comparable results were observed for ipsilateral and contralateral lung Technegas SPECT and ^{129}Xe MRI VDP, where in their respective models, both Technegas SPECT and ^{129}Xe MRI VDP were the strongest predictors of post-operative length of hospital stay (Appendix 7.7 and 7.8).

Table 3-15 Multivariate regression analysis for predictors of post-operative length of hospital stay in in participants who underwent minimally invasive lobectomy

Predictor Variables	Unstandardized β	Standardized β	95% CI	p-value
MODEL 1: Anormal ventilation assessed by Technegas SPECT VDP (R^2=0.39, adjusted R^2=0.35, p<0.001)				
Technegas SPECT VDP_{WL}, (%)	0.21	0.42	0.92-0.32	**<0.001**
$DL_{CO}\%_{pred}$	-0.051	-0.28	-0.92-(-0.010)	**0.02**
$FEV_1\%_{pred}$	-0.039	-0.18	-0.088-0.009	0.11
Pack-year smoking history	-0.028	-0.16	-0.028	0.16
MODEL 2: Abnormal ventilation assessed by ^{129}Xe MRI VDP (R^2=0.48, adjusted R^2=0.46, p<0.001)				
^{129}Xe MRI VDP_{WL}, (%)	0.41	0.73	0.30-0.52	**<0.001**
Pack-year smoking history	-0.02	-0.13	-0.06-0.01	0.20

Predictor variables in the model included age, pack-year smoking history, Charlson Comorbidities Index, $FEV_1\%_{pred}$, $DL_{CO}\%_{pred}$, history of obstructive lung disease, Technegas SPECT VDP_{WL} and ^{129}Xe MRI VDP_{WL}. VDP_{WL}=whole lung ventilation defect percent; DL_{CO}=diffusion capacity for carbon monoxide. FEV_1=forced expiratory volume in one second.

Chapter 4: Discussion

The prevalence and clinical relevance of abnormal ventilation prior to lung cancer resection is not well understood. This thesis reports the results of a six-week, prospective, proof-of-concept observational study, which was designed as a first step towards addressing this knowledge gap. One-hundred-three patients scheduled for lung cancer resection surgery underwent ventilation lung imaging using Technegas SPECT and ^{129}Xe MRI, and abnormal ventilation was quantified as the VDP for both modalities. Pre-operative Technegas SPECT VDP and ^{129}Xe MRI VDP were observed to be abnormal for 58% and 84% of participants, respectively, indicating that abnormal ventilation is prevalent prior to lung cancer resection. Pre-operative Technegas SPECT VDP and ^{129}Xe MRI VDP were 1) correlated with one another, 2) correlated with standard measures of airflow limitation and diffusing capacity, and 3) higher in participants with COPD compared to those with asthma and no history of obstructive lung disease. Post-operative follow-up revealed that Technegas SPECT VDP and ^{129}Xe MRI VDP measured pre-operatively were 1) higher in participants that developed one or more complications during the four-week post-operative period compared to those that did not, 2) correlated with post-operative length of hospital stay, and 3) independent predictors of the incidence of post-operative complications and length of hospital stay. These observations provide proof-of-concept evidence that abnormal ventilation, assessed by two ventilation imaging modalities is prevalent and clinically relevant prior to lung cancer resection.

4.1.1 Ventilation Defect Burden prior to Lung Cancer Resection

Quantification of ventilation defect burden revealed a high prevalence, with 58% and 84% of participants observed to have abnormal ventilation prior to lung resection, as assessed by Technegas SPECT and ^{129}Xe MRI, respectively. While this is the first study that evaluated the prevalence of abnormal ventilation in participants scheduled to undergo lung resection, the

observations are comparable to previous investigations that focused on assessing ventilation defects in radiation planning studies for functional lung avoidance.[20,120] Mathew and colleagues, in an exploratory study of 15 non-small cell and small cell lung cancer patients, observed MRI ventilation abnormalities in the contralateral lung in 67% of cases.[20] Similarly, in a prospective study of 17 patients with non-resectable Stage III non-small cell lung cancer, Sheikh and colleagues reported non-tumor-specific MRI ventilation abnormalities in 71% of patients.[120]

It should be noted that the reported prevalence of abnormal ventilation is dependent on the upper limit of normal for VDP, which has not been well established by the ventilation imaging community. For this thesis, the upper limits of normal were determined from a small cohort of healthy individuals imaged at our centre. The threshold of 2.6% used in this thesis for ^{129}Xe MRI VDP may explain the high prevalence of abnormal ventilation, but the threshold is comparable to what has been reported in previous work.[142] Recently, McIntosh et al. established the upper limit of normal for ^{129}Xe MRI VDP as 2.5% for individuals aged 40-59 years and 3.8% for those aged 60-79 years.[142]

The high prevalence of abnormal ventilation is not surprising given that 83% of the study cohort were current or former smokers. The correlation between VDP and pack-year smoking history aligns with previous literature highlighting abnormal ventilation in individuals who are former smokers, [15,115,116] and current smokers without lung disease.[117-119] The association between VDP and smoking may be attributed to smoking-induced effects, such as airway inflammation, increased airway resistance, airway remodeling, and emphysema - all contributing to the observed ventilation defects. Additionally, as 29% of participants reported a diagnosis of COPD, we expected to find a high prevalence of abnormal ventilation, given that previous research has demonstrated that participants with COPD display heterogeneous ventilation compared to healthy

individuals.[90,108,109] Kirby et al. demonstrated that participants with COPD (n=10) exhibited greater VDP and heterogeneous ventilation compared to healthy volunteers (n=8).[143] Indeed, a greater ventilation defect burden quantified by both modalities was observed for participants with COPD compared to those with asthma and no history of obstructive disease. However, VDP assessed by both modalities was not higher in participants who reported a history of asthma compared to those without any known history of obstructive disease. This result may be considered unexpected as abnormal ventilation is a characteristic feature of asthma. It should be noted that the VDPs of asthmatics in the evaluated cohort are similar to what has been previously reported by others, using ^{129}Xe MRI VDP[144] and Technegas SPECT VDP,[66,75] respectively. In this thesis, older age was not a contributor to the ventilation defect burden, contrary to previous findings associating age-related changes in lung structure and function with ventilation defects.[16] Sheikh et al. in a prospective study of 52 older non-smokers with no history of COPD, observed ventilation defects in 75% of the cohort.[16] It is suggested that small ventilation defects found in the periphery of the lungs are indicative of age-related pulmonary changes that involve loss of elastic recoil or irreversible airway narrowing and collapse. We did observe similar ventilation patterns in some participants such as P89 and P101. Given that the participants had lung cancer, to ensure tumor size did not significantly contribute to the burden of ventilation defects quantified by VDP and thus the high prevalence of abnormal ventilation observed, VDP in both the ipsilateral and contralateral lungs was quantified. The VDP of the ipsilateral and contralateral lung were comparable, suggesting that the tumor burden did not significantly contribute to, or had minimal contribution to the observed ventilation defect burden in this cohort.

A notable finding of this thesis is that among participants observed to have abnormal ventilation, 47-51% reported no history of lung disease. As abnormal ventilation is the functional

consequence of airway or parenchymal pathology, this observation suggests that there is a high prevalence of subclinical or undiagnosed lung pathology in the cohort. This may include mild asthma or early-stage COPD that have not been diagnosed, but as previously shown in the literature, may contribute to the ventilation defect burden.[66,75] More importantly, while ventilation burden was associated with established markers of lung function, mainly FEV_1 and DL_{CO}, we observed that 34% of participants with normal lung function assessed by standard lung function tests had abnormal ventilation. Ventilation abnormalities quantified by VDP may represent subclinical or localized lung pathology, that clinical measures of lung function are unable to detect. Participant B shown in **Figure 3-2** is an example of this, where, despite having normal FEV_1 and DL_{CO}, such participants may have subclinical or undiagnosed airway disease contributing to ventilation defects.

To summarize, our observations provide the first evidence that ventilation defects are prevalent prior to lung cancer resection and can be observed by imaging despite normal FEV_1 and DL_{CO}.

4.1.2 Comparison of ventilation defects quantified by Technegas SPECT and ^{129}Xe MRI

This thesis directly compared ventilation defect burden using Technegas SPECT and ^{129}Xe MRI, the two widely accepted contrast agents for ventilation imaging in SPECT and MRI, respectively. With both modalities recently approved by the FDA and increasing interest in their clinical use, this quantitative comparison aimed to enhance the understanding of their correlation and potential equivalency in assessing ventilation defect burden.

Many segmentation methods have been developed and optimized to quantify ventilation defects as the VDP, including linear binning, thresholding, and k-means clustering. In this thesis, VDP was determined for both Technegas SPECT and ^{129}Xe MRI using adaptive thresholding and k-means segmentation methods. The basis for this decision was that the adaptive thresholding

quantification method has been previously optimized and validated for Technegas SPECT by Farrow et al, [75] and the k-means method for ^{129}Xe MRI by Kirby et al.[17] Using both segmentation approaches, we observed that the burden of ventilation defects quantified by Technegas SPECT and ^{129}Xe MRI VDP were correlated. While this is the first comparison of ventilation defects assessed by Technegas SPECT and ^{129}Xe MRI, the observations are consistent with previous investigations demonstrating the comparability of ventilation assessed by SPECT and MRI when utilizing alternative ventilation agents. Stavngaard and colleagues previously reported a good correlation between ^{81m}Kr SPECT and ^{3}He MRI for both visual and quantitative assessments of ventilation defect scores in a cohort of 23 COPD and 9 healthy participants.[123] In a smaller study of 11 COPD patients, Doganay et al demonstrated a good correlation between ^{99m}Tc-DTPA SPECT and ^{129}Xe MRI relative lobar percentage ventilation.[124] For ventilation SPECT, international guidelines now recommend Technegas as the preferred ventilation agent in patients with obstructive lung disease[69,70] limiting the clinical relevance of previous comparisons that used ^{81m}Kr and ^{99m}Tc-DTPA. Additionally, for hyperpolarized gas ventilation MRI, ^{129}Xe gas is now preferred over ^{3}He gas due to its greater availability, lower cost, and higher solubility that permits dissolved-phase imaging.[135]

In most participants, visual assessment showed spatial agreement between focal ventilation defects observed by both modalities. However, as highlighted in **Figure 3-2** by the blue arrows, some discordance was also observed. We also report a mean bias, 2.5% and 0.9%, towards higher VDP measured by Technegas SPECT than ^{129}Xe MRI, which was observed using the adaptive threshold and k-means method, respectively. This inter-modality bias and lack of absolute agreement in ventilation defects were not unexpected and may be explained by several factors. First, fundamental differences in the physical properties of the ventilation agents may contribute

to differences in lung distribution. Technegas is an ultrafine aerosolized particle (0.005–0.2μm[145]) whose distribution in the lungs, unlike that of ^{129}Xe gas, is impacted by aerosol deposition mechanics. While Technegas behaves in a gas-like manner, permitting peripheral penetration and alveolar deposition,[70] it has been previously shown to aggregate at sites of severe obstruction leading to "hot-spots".[146] Shown in **Figure 3-1D**, we observed this effect in a 65-year-old male with severe COPD (FEV_1=28%$_{pred}$, FEV_1/FVC=31%). Bilateral hotspots are observed on Technegas SPECT in the left and right main bronchi. Greater ventilation is observed distal to the right main bronchi hotspot by ^{129}Xe MRI than Technegas SPECT. Second, the different acquisition conditions and spatial resolutions between modalities must be considered. Technegas SPECT is acquired during 15 minutes of tidal breathing, while ^{129}Xe MRI is acquired during a 10 second breath hold at functional residual capacity plus one liter. As a result, respiratory and cardiac motion have greater influence on ventilation assessed by SPECT, contributing to blurring and fewer counts at the lung borders. Additionally, lung inflation during imaging affects ventilation defects, with increased ventilation defects observed at lower levels of lung inflation.[147] As SPECT is on average acquired at a lower lung inflation (average over tidal volume) than ^{129}Xe MRI (functional residual capacity plus one liter), higher VDP is expected. Taken together, the aforementioned factors likely account for the higher VDP quantified by Technegas SPECT and the spatial discordances in focal ventilation defects that were observed upon visual inspection.

It is important to emphasize that this thesis did not intend to determine the optimal quantification approach for each modality, rather to determine if there was correlation and some equivalency between the two modalities using established quantification practices for each modality that are implemented in the literature. There are reasons why each modality may best be served by different segmentation methods, which is beyond the scope of this thesis. However, we

do note that for both modalities, the adaptive threshold method resulted in significantly higher VDPs compared to the k-means clustering method, irrespective of history of obstructive lung disease. In the subgroup of patients with no history of lung disease, the majority of whom had well-ventilated lungs by visual inspection, the VDPs determined using the k-means method were much closer to zero than the threshold method (Technegas SPECT: VDP_K=10.2% vs. VDP_T=22.2%; ^{129}Xe MRI: VDP_K=9.2% vs. VDP_T=19.7%), which better reflects what the images show (e.g., **Figure 3-2A**). It was also noticed that when the VDP was determined using the threshold method (but not the k-means method), the bias towards higher Technegas SPECT VDP_T increased with VDP_T, or greater airflow limitation (**Figure 3-2C**). This bias seems to be driven largely by a subset of patients with COPD in whom the Technegas SPECT VDP_T was considerably higher than the ^{129}Xe MRI VDP_T. Taken together, investigation of these cases reveals that the adaptive threshold classifies hypo-ventilated (or low ventilated) voxels as defect, leading to a significantly higher VDP_T, which can be misleading when interpreted in absolute terms. This effect, in combination with severe obstruction leading to "hot-spots," likely explains the exceptionally high Technegas SPECT VDP_T reported for two patients with COPD (62% and 84%).

Of note, a quantitative analysis to evaluate the spatial agreement of ventilation defects observed by Technegas SPECT and ^{129}Xe MRI was not performed. Such analysis is highly dependent on accurate registration and anatomical alignment of Technegas SPECT and ^{129}Xe MRI datasets, which was challenging due to differences in voxel size, acquisition conditions (tidal breathing vs. breath hold), and lung volume. To summarize, our observations indicate that, despite substantial differences between the imaging modalities, quantitative assessment of ventilation defects by Technegas SPECT and ^{129}Xe MRI is comparable.

4.2 Clinical Relevance of Pre-operative Ventilation Defect Burden

This is the first study to prospectively perform pre-operative ventilation imaging in lung cancer participants to evaluate the clinical relevance of the pre-operative ventilation defect burden. We observed that VDP was significantly higher in 41% of participants who had one or more complications during the 4-week post-operative period. Most notably, we established that VDP was a significant predictor of post-operative complications in multivariate regression models that included conventional demographic, co-morbidity, and surgical details used in risk stratification. Multivariate regression analyses were performed both within the overall evaluated cohort and specifically within a subgroup of participants who underwent minimally invasive lobectomy. Our rationale for conducting subgroup analysis was two-fold. Firstly, it aimed to mitigate variations in the extent of resection and surgical approaches. Secondly, this allowed for a comparative assessment of our results with previously established studies that specifically evaluated patients who underwent lobectomy. Based on current clinical guidelines, FEV_1 and DL_{CO} are used for risk stratification and selection of patients suitable for curative intent lung resection.[41] However, similar to our observations, previous studies have demonstrated conflicting results regarding the use of pre-operative PFTs as predictors of post-operative complications and lung function.[148-157] In a prospective observational study of 173 participants undergoing VATS lobectomy, Berry and colleagues reported that $FEV_1\%_{pred}$ and $DL_{CO}\%_{pred}$ were not significant independent risk factors for post-operative complications.[158] Likewise, Agostini and colleagues demonstrated in a prospective observational study involving 285 participants undergoing VATS lobectomy that $FEV_1\%_{pred}$ was not an independent predictor of post-operative complications.[159] It is important to note that pre-operative predictive FEV_1 and DL_{CO} have their limitations. As demonstrated by Varela and colleagues, the actual post-operative $FEV_1\%_{pred}$ in the immediate 1-6 days after

lobectomy was approximately 30% lower than the predicted FEV_1% and was not a predictor of complications.[159-161] This may have an impact on the clinical reliability of $ppoFEV_1$ when utilized in the selection of surgical candidates. Probable explanations for post-operative predicted values of FEV_1 and DL_{CO} not being predictors of complications may be attributed to two main factors. Firstly, the global PFT measurements cannot localize whether functional or non-functional lung segments are resected. Secondly, due to the lung volume reduction effect observed following surgery in participants with COPD, the predicted measurements of FEV_1 and DL_{CO} may be overestimated. In conjunction with PFT measurements, functional imaging can be utilized in pre-operative risk assessment and management to evaluate clinical and subclinical airway disease in the contralateral lung independent of tumor burden, as well as in the parts of the ipsilateral lung that are not involved with the tumor.

Previous studies have identified COPD as an independent risk factor for the development of post-operative complications.[162-164] In a prospective study of 343 patients with non-small cell lung cancer, Kim and colleagues observed that in patients with early stages of COPD, the odds of developing post-operative complications were found to be 3.42 times higher when compared to their non-COPD counterparts.[163] However, in this thesis, we did not observe such an association in the regression models. Several reasons may account for this discrepancy, including the variations in the definition of post-operative complications across different centers. Additionally, in this study, obstructive lung diseases (such as asthma and COPD) were grouped, potentially mitigating the specific signal related to COPD.

It is important to recognize that some participants with high pre-operative ventilation defect burden did not develop post-operative complications. For example, P106 had extensive ventilation abnormalities reflected by a high VDP, but a relatively unremarkable post-operative period with

no post-operative complications. The exact reasoning for this observation is not known, but VDP in some participants may be driven by slow-filling regions. Additionally, the location of resection in relation to ventilated and ventilated lung may play a role and requires further investigation.

Another important finding from this thesis is that greater pre-operative ventilation defect burden was associated with a longer post-operative length of hospital stay. Previously, in a large multi-center study of 4,979 patients who underwent lobectomy for primary lung cancer, age (OR= 1.30), male sex (OR=1.45), ASA score (OR=1.54), percentage predicted FEV_1 in 10% increments (OR=0.88), and smoking were (OR=0.88) identified as risk factors for a prolonged length of hospital stay. Although we were limited by the number of variables that were included in the model due to the relatively low sample size, it is encouraging that comparable results were observed in this thesis. More importantly, the findings of this thesis suggest that abnormal ventilation is relevant to post-operative outcomes, including complications and length of hospital stay.

4.3 Contributors to Ventilation Defects

Abnormal ventilation may be a modifiable risk factor for post-operative outcomes. In this context, it is important to understand potential contributors to ventilation defects. Based on previous research in asthma, ventilation defects have been shown to stem from intraluminal inflammation,[100,165] airway remodeling,[166] and mucus plugging.[167,168] In patients with COPD, ventilation defects have previously been associated with non-inflammatory structural abnormalities, such as airway wall remodeling, scarring, bronchiectasis, gas trapping and emphysema.[108] While it is conceivable that luminal obstruction due to inflammatory cells and/or mucus may contribute to ventilation defects in COPD, this has not yet been studied. We observed a high prevalence of pre-operative cellular inflammation in this cohort, which leads us to postulate that ventilation defects may be in part due to intraluminal inflammation in certain participants. For

example, in **Figure 3-2**, P47 had trivial neutrophilic inflammation, while P66 and P59 had mixed-granulocytic intraluminal inflammation, which may contribute to the observed ventilation defects. Previously, anti-eosinophilic therapies in patients with eosinophilic asthma have demonstrated the potential to resolve ventilation defects.[165] Additionally, inflammatory endotype-based treatment guided by sputum cell counts is used clinically to manage the inflammatory component of airways disease in patients with chronic bronchitis, COPD[132,169,170] and asthma.[171] Considering these findings, and our observations that 88% (7 of 8) of participants with asthma and 61% (14 of 23) of participants with COPD in whom sputum was collected had intraluminal inflammation, implementing a similar treatment strategy for patients that present with inflammation before resection to improve ventilation, may be of future interest.

Additional contributors to ventilation defects such as emphysema and mucus plugging were not evaluated in this thesis but need to be considered alongside intraluminal inflammation. In a prospective observational study, Capaldi et al. evaluated 32 participants with varying severity of COPD, where ventilation defects were found to be quantitatively and spatially related to both gas trapping and emphysema.[108] In this thesis, given the high prevalence of current and former smokers, and participants with reported history of COPD, it is likely that a subset of participants had emphysema. For instance, in P106, large ventilation defects on both lungs are observed despite the absence of intraluminal inflammation. In such cases, it becomes imperative to explore whether focal ventilation defects are due to emphysema or airways disease. Although emphysema is not modifiable, assessing this may be of clinical relevance, as the lung volume reduction effect secondary to anatomic lung resection may emerge as a beneficial strategy for improving post-operative lung function in individuals with COPD. Previous research has demonstrated that ventilation defects exhibit spatial correlations with both lobar and segmental mucus plugs. In a

prospective observational study involving 27 severe asthma patients, Svenningsen et al. established an association between whole-lung VDP and mucus plugs.[167] Furthermore, in a prospective analysis of 44 patients from the severe asthma research program cohort, Mummy et al. demonstrated the co-localization of segmental ventilation defects originating from segmental mucus plugs.[168] Building on this, identifying the mucus burden in patients scheduled to undergo lung cancer resection may be of importance to optimize pre-operative respiratory function. To our knowledge, although no direct treatment exists for reducing mucus plugging, pre-operative interventions such airway clearance techniques, or other respiratory therapies aimed at minimizing mucus accumulation can be explored. In short, VDP may serve as a comprehensive marker, encapsulating many underlying contributors to poor lung health and that have the potential to increase the likelihood of post-operative complications and prolonged hospital stays. Future research will aim to determine the specific pathologic contributors to ventilation defects observed prior to lung cancer resection, to better understand the extent to which ventilation may be modified or improved prior to lung cancer resection.

4.4 Implications for Clinical Use

The results of the thesis suggest that abnormal ventilation is prevalent prior to lung resection and is relevant to post-operative outcomes, including complications and length of hospital stay. In light of these observations, there may be opportunities to integrate pre-operative assessment of ventilation using imaging into the standard-of-care clinical workup of patients to improve patient outcomes. Specific roles may include risk assessment, risk modification, and treatment planning/guidance.

Regarding risk assessment, the inclusion of ventilation imaging may complement the evaluation of pre-operative respiratory function in conjunction with clinical PFT measurements.

Pre-operative ventilation imaging can be crucial in identifying individuals at a higher risk of complications after lung cancer resection, enabling closer monitoring of those at elevated risk for complications or longer hospital stays.

In the future, ventilation imaging can play a crucial role in risk modification by guiding efforts to preserve ventilated lung tissue, especially in patients with compromised lung function. This becomes pivotal in minimizing the removal of functional lung tissue during surgery, preserving post-operative respiratory function. For instance, in a patient with a low tumor burden scheduled for lobectomy, ventilation imaging can inform the decision-making process between sub-lobar and lobar resection, based on the presence of ventilated lung areas.

Moreover, ventilation imaging may prove valuable in planning and guiding treatment strategies by facilitating modifications in clinical care based on observed ventilation defects. This can ensure a targeted treatment approach, whether through surgery or alternative interventions such as chemotherapy or radiotherapy. For example, in the case of P59, who exhibited significant obstruction with an FEV_1/FVC of 35%, functional imaging provided insight, revealing a substantial central obstruction in the right bronchus and mostly non-ventilated right lung. Pneumonectomy of the left lung resulted in hypercapnic respiratory failure and death during the hospital stay. With pre-operative knowledge that the resected lung contributed significantly to the patient's respiratory function, surgery might not have been the optimal plan. Instead, a combination of chemotherapy, immunotherapy, or stereotactic body radiotherapy could have been considered. This underscores the importance of ventilation imaging in guiding treatment decisions and potentially avoiding adverse outcomes associated with surgical interventions.

4.5 Limitations

There are several limitations to this study that should be considered. First, this investigation was conducted as a single-center study with a relatively small sample size, which may influence the generalizability of the findings. Due to the low incidence of death, hospital readmissions, and individual complications, the sample size was insufficient to conduct a comprehensive analysis of the aforementioned outcomes. Nevertheless, it is worth emphasizing that, to the best of our knowledge, this study represents the largest prospective cohort study to utilize ventilation imaging to understand the prevalence and clinical relevance of abnormal ventilation in lung cancer patients prior to resection surgery. Second, our imaging assessment of lung function was limited to ventilation. With advanced pulmonary imaging, we now possess the capability to evaluate gas-exchange and perfusion. Detailed characterization of ventilation, gas-exchange and perfusion is crucial for a comprehensive assessment of respiratory function and may have additional value to treatment planning and risk stratification for post-operative complications. Third, co-registration of ventilation images to CT for co-localized assessment of lung structure such as tumor burden, emphysema, mucus plugging, and bronchiectasis was not performed. For example, tumor burden may have influenced segmentation of the thoracic cavity and VDP quantification. However, in our cohort, tumor size was not associated with whole-lung VDP, and ipsilateral and contralateral VDP were not different (**Figure 3-3**), suggesting this oversight has marginal impact on VDP quantification. These observations indicate that tumor burden did not significantly contribute to VDP assessed by either modality, which is not surprising given the small tumor burden in our cohort (Stage I in 76%, Stage II in 10% of participants). In addition, repeated ventilation imaging after bronchodilator administration to assess reversibility was not performed. We are unable to comment on the reversibility of ventilation defects observed, thus limiting the identification of

individuals who may benefit from bronchodilator therapy. Finally, the quantitative analysis of ventilation defect burden distilled regional and voxel-wise measurements of ventilation down to a single whole-lung value, in this case, the VDP. VDP is a binary whole-lung measurement that fails to characterize much of the information offered by ventilation imaging modalities. Co-registration of CT with ^{129}Xe MRI and Technegas SPECT was not performed to generate lobar or segmental VDP, which may be useful in determining the residual respiratory function following removal of the tumor burden parts of the lung.

Chapter 5: Conclusion and Future Directions

In summary, this is the first prospective study that aimed to identify the prevalence and clinical relevance of ventilation defect burden and its association with the clinical impact of post-operative complications in patients undergoing lung cancer resection. The results support the notion that ventilation defects are prevalent in patients scheduled to undergo lung cancer resection and are predictive of post-operative complications and length of hospital stay. The burden of ventilation defects quantified by Technegas SPECT and ^{129}Xe MRI was higher in participants that experienced post-operative complications and was a predictor of post-operative complications and length of hospital stay. The findings from this thesis suggest that the integration of ventilation imaging, using Technegas SPECT or ^{129}Xe MRI, has the potential to aid in pre-operative risk stratification and risk modification. In addition, since a subset of participants had intraluminal inflammation, investigating its potential contribution to ventilation defects will be the focus of future research. If confirmed, optimizing these parameters prior to lung resection could hold promise for improving post-operative outcomes. Lastly, the burden of ventilation defects quantified by Technegas SPECT and ^{129}Xe MRI were correlated. This observation indicates that, despite substantial differences between the imaging modalities, assessment of ventilation defects

using established quantification practices for Technegas SPECT and ^{129}Xe MRI are comparable, provided the same quantification approach is used. Therefore, the selection of ventilation imaging modality can be guided by local availability and regulatory approval, contraindications, and concern of radiation burden.

5.1 Future Work

The primary objective of this thesis was to determine the prevalence and clinical relevance of abnormal ventilation in lung cancer patients prior to resection. The observations from this proof-of-concept study lay the foundation for future research in the field. Based on our results, there may be considerable impact for imaging on surgical planning. A logical next step would be to investigate if pre-operative knowledge of regional ventilation influences the treatment plan, such as determining the extent of resection. To evaluate this, a retrospective review of the current dataset could be performed. Here, the surgeons would be provided with all pre-operative details, including ventilation information, while remaining blinded to post-operative patient outcomes. From here, the surgeons can, in conjunction with relevant pre-operative clinical work-up, determine whether knowledge of ventilation would impact the treatment decision-making process. For instance, in a case where the patient is scheduled for right upper lobectomy, awareness of complete lung ventilation might prompt a reconsideration of the extent of resection, potentially opting for a less invasive approach like segmentectomy. Or in a case where the patient is scheduled for a pneumonectomy and ventilation imaging indicates a substantial defect burden in the unaffected lung, particularly when the lung to be resected is a significant contributor to overall lung function, surgical candidacy may be reconsidered. In such instances, radiation therapy could be a beneficial alternative. If this retrospective analysis reveals that knowledge of regional ventilation defect burden influences surgical decision making, the next logical investigation would be conducting a

randomized controlled trial. This trial, mirroring the methodology employed in this thesis, would be designed to compare pre-operative planning with and without ventilation imaging. The key outcomes of this trial would be the occurrence of post-operative complications and the length of hospital stay between study arms.

Additional studies are needed to evaluate contributors to abnormal ventilation in this cohort to estimate the prevalence of modifiable ventilation defects. In chapter 2.3, a high prevalence of intraluminal inflammation was observed, but contributors such as mucus plugging, gas trapping, and emphysema warrant further investigation. Determining the modifiable and non-modifiable contributors will be important in identifying patients that may have a treatment response and will most benefit from treating the intraluminal inflammation. Should a high prevalence of modifiable risk factors be observed, evaluating whether the intervention to treat the modifiable defects translates into improved outcomes becomes the next critical step. If the results of the future investigations are positive, the integration of ventilation imaging into pre-operative assessments could become a valuable clinical tool for patients undergoing lung cancer resection. This has the potential to provide personalized patient care by identifying individuals who may benefit from targeted interventions, ultimately contributing to improved post-operative outcomes.

In this thesis, only ventilation imaging was investigated. However, both ventilation and perfusion are important for gas-exchange and maintaining adequate respiratory function. It is important to consider that although regions of the lung can be ventilated, there may be limited perfusion, leading to mismatched defects. Thus, it is pertinent to investigate the prevalence and clinical relevance of perfusion defects and ask the following research questions: What is the prevalence of ventilation and perfusion defects in patients scheduled to undergo lung cancer

resection? Does ventilation and perfusion defects predict the occurrence of post-operative complications following lung resection for lung cancer?

Clinically, perfusion SPECT is performed using ^{99m}Tc-macroaggregated albumin[172], while in MRI, the assessment of perfusion involves a novel method called dissolved phase imaging with ^{129}Xe.[13] This novel technique utilizes the advantage of xenon-129's ability to dissolve into the blood by attaching to red blood cells.[13] Dissolved phase imaging allows for the quantification of ventilation and/or perfusion defects in the lungs, and more importantly, identification of regions with mismatch defects.[13] Thus, it is important to investigate whether incorporating both ventilation and perfusion imaging into the standard clinical workup can provide comprehensive risk stratification for post-operative complications in lung cancer patients.

Chapter 6: References

1 Society, C. C. *Canadian Cancer Statistics 2021*, <https://cancer.ca/en/research/cancer-statistics/canadian-cancer-statistics> (2021).

2 Licker, M. J. *et al.* Operative mortality and respiratory complications after lung resection for cancer: impact of chronic obstructive pulmonary disease and time trends. *Ann Thorac Surg* **81**, 1830-1837 (2006). https://doi.org:10.1016/j.athoracsur.2005.11.048

3 Bernard, A. *et al.* Pneumonectomy for malignant disease: factors affecting early morbidity and mortality. *J Thorac Cardiovasc Surg* **121**, 1076-1082 (2001). https://doi.org:10.1067/mtc.2001.114350

4 Agostini, P. *et al.* Postoperative pulmonary complications following thoracic surgery: are there any modifiable risk factors? *Thorax* **65**, 815-818 (2010). https://doi.org:10.1136/thx.2009.123083

5 Stephan, F. *et al.* Pulmonary complications following lung resection: a comprehensive analysis of incidence and possible risk factors. *Chest* **118**, 1263-1270 (2000). https://doi.org:10.1378/chest.118.5.1263

6 Deslauriers, J., Ginsberg, R. J., Piantadosi, S. & Fournier, B. Prospective assessment of 30-day operative morbidity for surgical resections in lung cancer. *Chest* **106**, 329S-330S (1994). https://doi.org:10.1378/chest.106.6_supplement.329s

7 Lawrence, V. A., Cornell, J. E., Smetana, G. W. & American College of, P. Strategies to reduce postoperative pulmonary complications after noncardiothoracic surgery: systematic review for the American College of Physicians. *Ann Intern Med* **144**, 596-608 (2006). https://doi.org:10.7326/0003-4819-144-8-200604180-00011

8 Miskovic, A. & Lumb, A. B. Postoperative pulmonary complications. *Br J Anaesth* **118**, 317-334 (2017). https://doi.org:10.1093/bja/aex002

9 Lugg, S. T. *et al.* Long-term impact of developing a postoperative pulmonary complication after lung surgery. *Thorax* **71**, 171-176 (2016). https://doi.org:10.1136/thoraxjnl-2015-207697

10 Takenaka, T. *et al.* Does short-term cessation of smoking before lung resections reduce the risk of complications? *J Thorac Dis* **12**, 7127-7134 (2020). https://doi.org:10.21037/jtd-20-2574

11 Shigeeda, W. *et al.* Optimal period of smoking cessation to reduce the incidence of postoperative pulmonary complications in lung cancer. *Interdiscip Cardiovasc Thorac Surg* **36** (2023). https://doi.org:10.1093/icvts/ivad094

12 Nakagawa, M., Tanaka, H., Tsukuma, H. & Kishi, Y. Relationship between the duration of the preoperative smoke-free period and the incidence of postoperative pulmonary complications after pulmonary surgery. *Chest* **120**, 705-710 (2001). https://doi.org:10.1378/chest.120.3.705

13 Mugler, J. P., 3rd & Altes, T. A. Hyperpolarized 129Xe MRI of the human lung. *J Magn Reson Imaging* **37**, 313-331 (2013). https://doi.org:10.1002/jmri.23844

14 Kruger, S. J. *et al.* Functional imaging of the lungs with gas agents. *J Magn Reson Imaging* **43**, 295-315 (2016). https://doi.org:10.1002/jmri.25002

15 Pike, D., Kirby, M., Guo, F., McCormack, D. G. & Parraga, G. Ventilation heterogeneity in ex-smokers without airflow limitation. *Acad Radiol* **22**, 1068-1078 (2015). https://doi.org:10.1016/j.acra.2015.04.006

16 Sheikh, K. *et al.* Pulmonary ventilation defects in older never-smokers. *J Appl Physiol (1985)* **117**, 297-306 (2014). https://doi.org:10.1152/japplphysiol.00046.2014
17 Kirby, M. *et al.* Hyperpolarized 3He and 129Xe MR imaging in healthy volunteers and patients with chronic obstructive pulmonary disease. *Radiology* **265**, 600-610 (2012). https://doi.org:10.1148/RADIOL.12120485/-/DC1
18 Jögi, J., Ekberg, M., Jonson, B., Bozovic, G. & Bajc, M. Ventilation/perfusion SPECT in chronic obstructive pulmonary disease: an evaluation by reference to symptoms, spirometric lung function and emphysema, as assessed with HRCT. *European Journal of Nuclear Medicine and Molecular Imaging* **38**, 1344-1352 (2011). https://doi.org:10.1007/s00259-011-1757-5
19 Bajc, M. *et al.* Identifying the heterogeneity of COPD by V/P SPECT: a new tool for improving the diagnosis of parenchymal defects and grading the severity of small airways disease. *International Journal of Chronic Obstructive Pulmonary Disease* **Volume 12**, 1579-1587 (2017). https://doi.org:10.2147/copd.s131847
20 Mathew, L., Vandyk, J., Etemad-Rezai, R., Rodrigues, G. & Parraga, G. Hyperpolarized (3)He pulmonary functional magnetic resonance imaging prior to radiation therapy. *Med Phys* **39**, 4284-4290 (2012). https://doi.org:10.1118/1.4729713
21 Mathew, L. *et al.* Detection of longitudinal lung structural and functional changes after diagnosis of radiation-induced lung injury using hyperpolarized 3He magnetic resonance imaging. *Med Phys* **37**, 22-31 (2010). https://doi.org:10.1118/1.3263616
22 Ireland, R. H. *et al.* Detection of radiation-induced lung injury in non-small cell lung cancer patients using hyperpolarized helium-3 magnetic resonance imaging. *Radiother Oncol* **97**, 244-248 (2010). https://doi.org:10.1016/j.radonc.2010.07.013
23 Ireland, R. H. *et al.* Feasibility of image registration and intensity-modulated radiotherapy planning with hyperpolarized helium-3 magnetic resonance imaging for non-small-cell lung cancer. *Int J Radiat Oncol Biol Phys* **68**, 273-281 (2007). https://doi.org:10.1016/j.ijrobp.2006.12.068
24 Allen, A. M. *et al.* Can Hyperpolarized Helium MRI add to radiation planning and follow-up in lung cancer? *J Appl Clin Med Phys* **12**, 3357 (2011). https://doi.org:10.1120/jacmp.v12i2.3357
25 Pizzichini, E. *et al.* Indices of airway inflammation in induced sputum: reproducibility and validity of cell and fluid-phase measurements. *Am J Respir Crit Care Med* **154**, 308-317 (1996). https://doi.org:10.1164/ajrccm.154.2.8756799
26 West, J. B. & Luks, A. M. *West's Respiratory Physiology*. (Wolters Kluwer Health, 2020).
27 Clemente, C. D. *Anatomy: A Regional Atlas of the Human Body*. Vol. 6 (Lippincott Williams & Wilkins, 2010).
28 Chassagnon, G., Morel, B., Carpentier, E., Ducou Le Pointe, H. & Sirinelli, D. Tracheobronchial Branching Abnormalities: Lobe-based Classification Scheme. *Radiographics* **36**, 358-373 (2016). https://doi.org:10.1148/rg.2016150115
29 Ochs, M. *et al.* The number of alveoli in the human lung. *Am J Respir Crit Care Med* **169**, 120-124 (2004). https://doi.org:10.1164/rccm.200308-1107OC
30 Null, M., Arbor, T. C. & Agarwal, M. in *StatPearls* (2023).
31 Rusch, V. W. *et al.* The IASLC Lung Cancer Staging Project: A Proposal for a New International Lymph Node Map in the Forthcoming Seventh Edition of the TNM Classification for Lung Cancer. *Journal of Thoracic Oncology* **4**, 568-577 (2009). https://doi.org:10.1097/jto.0b013e3181a0d82e

32 Basumallik, N. & Agarwal, M. in *StatPearls* (2023).
33 De Groot, P. M., Wu, C. C., Carter, B. W. & Munden, R. F. The epidemiology of lung cancer. *Translational Lung Cancer Research* **7**, 220-233 (2018). https://doi.org:10.21037/tlcr.2018.05.06
34 Molina, J. R., Yang, P., Cassivi, S. D., Schild, S. E. & Adjei, A. A. Non-small cell lung cancer: epidemiology, risk factors, treatment, and survivorship. *Mayo Clin Proc* **83**, 584-594 (2008). https://doi.org:10.4065/83.5.584
35 Dubin, S. & Griffin, D. Lung Cancer in Non-Smokers. *Mo Med* **117**, 375-379 (2020).
36 Sabbula, B. R., Gasalberti, D. P. & Anjum, F. in *StatPearls* (2024).
37 Dela Cruz, C. S., Tanoue, L. T. & Matthay, R. A. Lung Cancer: Epidemiology, Etiology, and Prevention. *Clinics in Chest Medicine* **32**, 605-644 (2011). https://doi.org:10.1016/j.ccm.2011.09.001
38 Rudin, C. M., Brambilla, E., Faivre-Finn, C. & Sage, J. Small-cell lung cancer. *Nat Rev Dis Primers* **7**, 3 (2021). https://doi.org:10.1038/s41572-020-00235-0
39 Daabiss, M. American Society of Anaesthesiologists physical status classification. *Indian J Anaesth* **55**, 111-115 (2011). https://doi.org:10.4103/0019-5049.79879
40 Doyle, D. J., Hendrix, J. M. & Garmon, E. H. in *StatPearls* (2023).
41 British Thoracic, S., Society of Cardiothoracic Surgeons of Great, B. & Ireland Working, P. BTS guidelines: guidelines on the selection of patients with lung cancer for surgery. *Thorax* **56**, 89-108 (2001). https://doi.org:10.1136/thorax.56.2.89
42 Brunelli, A. *et al.* ERS/ESTS clinical guidelines on fitness for radical therapy in lung cancer patients (surgery and chemo-radiotherapy). *Eur Respir J* **34**, 17-41 (2009). https://doi.org:10.1183/09031936.00184308
43 Culver, B. H. *et al.* Recommendations for a Standardized Pulmonary Function Report. An Official American Thoracic Society Technical Statement. *Am J Respir Crit Care Med* **196**, 1463-1472 (2017). https://doi.org:10.1164/rccm.201710-1981ST
44 Detterbeck, F. C. The eighth edition TNM stage classification for lung cancer: What does it mean on main street? *J Thorac Cardiovasc Surg* **155**, 356-359 (2018). https://doi.org:10.1016/j.jtcvs.2017.08.138
45 Edge, S. B. & Compton, C. C. The American Joint Committee on Cancer: the 7th edition of the AJCC cancer staging manual and the future of TNM. *Ann Surg Oncol* **17**, 1471-1474 (2010). https://doi.org:10.1245/s10434-010-0985-4
46 Birchard, K. R. Transthoracic needle biopsy. *Semin Intervent Radiol* **28**, 87-97 (2011). https://doi.org:10.1055/s-0031-1273943
47 Gomez, M. & Silvestri, G. A. Endobronchial ultrasound for the diagnosis and staging of lung cancer. *Proc Am Thorac Soc* **6**, 180-186 (2009). https://doi.org:10.1513/pats.200808-081LC
48 Brenner, D. J. & Hall, E. J. Computed tomography--an increasing source of radiation exposure. *N Engl J Med* **357**, 2277-2284 (2007). https://doi.org:10.1056/NEJMra072149
49 Joarde, R. & Crundwell, N. 3-13 (Springer London, 2009).
50 Hounsfield, G. N. Computerized transverse axial scanning (tomography). 1. Description of system. *Br J Radiol* **46**, 1016-1022 (1973). https://doi.org:10.1259/0007-1285-46-552-1016
51 Ueda, K. *et al.* Computed tomography-diagnosed emphysema, not airway obstruction, is associated with the prognostic outcome of early-stage lung cancer. *Clin Cancer Res* **12**, 6730-6736 (2006). https://doi.org:10.1158/1078-0432.CCR-06-1196

52 Shin, S. *et al.* Joint effect of airflow limitation and emphysema on postoperative outcomes in early-stage nonsmall cell lung cancer. *European Respiratory Journal* **48**, 1743-1750 (2016). https://doi.org:10.1183/13993003.01148-2016
53 Almuhaideb, A., Papathanasiou, N. & Bomanji, J. 18F-FDG PET/CT imaging in oncology. *Ann Saudi Med* **31**, 3-13 (2011). https://doi.org:10.4103/0256-4947.75771
54 Bendixen, M., Kronborg, C., Jorgensen, O. D., Andersen, C. & Licht, P. B. Cost-utility analysis of minimally invasive surgery for lung cancer: a randomized controlled trial. *Eur J Cardiothorac Surg* **56**, 754-761 (2019). https://doi.org:10.1093/ejcts/ezz064
55 Falcoz, P. E. *et al.* Video-assisted thoracoscopic surgery versus open lobectomy for primary non-small-cell lung cancer: a propensity-matched analysis of outcome from the European Society of Thoracic Surgeon database. *Eur J Cardiothorac Surg* **49**, 602-609 (2016). https://doi.org:10.1093/ejcts/ezv154
56 Paul, S. *et al.* Outcomes after lobectomy using thoracoscopy vs thoracotomy: a comparative effectiveness analysis utilizing the Nationwide Inpatient Sample database. *Eur J Cardiothorac Surg* **43**, 813-817 (2013). https://doi.org:10.1093/ejcts/ezs428
57 Laursen, L. O. *et al.* Video-assisted thoracoscopic surgery lobectomy for lung cancer is associated with a lower 30-day morbidity compared with lobectomy by thoracotomy. *Eur J Cardiothorac Surg* **49**, 870-875 (2016). https://doi.org:10.1093/ejcts/ezv205
58 Paul, S., Isaacs, A. J., Treasure, T., Altorki, N. K. & Sedrakyan, A. Long term survival with thoracoscopic versus open lobectomy: propensity matched comparative analysis using SEER-Medicare database. *BMJ* **349**, g5575 (2014). https://doi.org:10.1136/bmj.g5575
59 Villamizar, N. R. *et al.* Thoracoscopic lobectomy is associated with lower morbidity compared with thoracotomy. *J Thorac Cardiovasc Surg* **138**, 419-425 (2009). https://doi.org:10.1016/j.jtcvs.2009.04.026
60 Aiolfi, A. *et al.* Pulmonary lobectomy for cancer: Systematic review and network meta-analysis comparing open, video-assisted thoracic surgery, and robotic approach. *Surgery* **169**, 436-446 (2021). https://doi.org:10.1016/j.surg.2020.09.010
61 Asamura, H., Aokage, K. & Yotsukura, M. Wedge Resection Versus Anatomic Resection: Extent of Surgical Resection for Stage I and II Lung Cancer. *American Society of Clinical Oncology Educational Book*, 426-433 (2017). https://doi.org:10.1200/edbk_179730
62 Broaddus, V. C. *et al. Murray & Nadel's textbook of respiratory medicine*. Seventh edition. edn, (Elsevier, 2022).
63 Seely, A. J. E. *et al.* Systematic Classification of Morbidity and Mortality After Thoracic Surgery. *The Annals of Thoracic Surgery* **90**, 936-942 (2010). https://doi.org:10.1016/j.athoracsur.2010.05.014
64 Ivanovic, J. *et al.* Evaluating the reliability and reproducibility of the Ottawa Thoracic Morbidity and Mortality classification system. *Ann Thorac Surg* **91**, 387-393 (2011). https://doi.org:10.1016/j.athoracsur.2010.10.035
65 Bajc, M. *et al.* Identifying the heterogeneity of COPD by V/P SPECT: a new tool for improving the diagnosis of parenchymal defects and grading the severity of small airways disease. *International journal of chronic obstructive pulmonary disease* **12**, 1579-1587 (2017). https://doi.org:10.2147/COPD.S131847
66 Farrow, C. E. *et al.* Peripheral ventilation heterogeneity determines the extent of bronchoconstriction in asthma. *Journal of Applied Physiology* **123**, 1188-1194 (2017). https://doi.org:10.1152/JAPPLPHYSIOL.00640.2016

67 Sharma, M. *et al.* Quantification of pulmonary functional MRI: state-of-the-art and emerging image processing methods and measurements. *Phys Med Biol* **67** (2022). https://doi.org:10.1088/1361-6560/ac9510
68 Ohno, Y. *et al.* Overview of MRI for pulmonary functional imaging. *Br J Radiol* **95**, 20201053 (2022). https://doi.org:10.1259/bjr.20201053
69 Roach, P. J., Schembri, G. P. & Bailey, D. L. V/Q scanning using SPECT and SPECT/CT. *J Nucl Med* **54**, 1588-1596 (2013). https://doi.org:10.2967/jnumed.113.124602
70 Bajc, M. *et al.* EANM guideline for ventilation/perfusion single-photon emission computed tomography (SPECT) for diagnosis of pulmonary embolism and beyond. *European Journal of Nuclear Medicine and Molecular Imaging* **46**, 2429-2451 (2019). https://doi.org:10.1007/s00259-019-04450-0
71 Genseke, P. *et al.* Pre-operative quantification of pulmonary function using hybrid-SPECT/low-dose-CT: A pilot study. *Lung Cancer* **118**, 155-160 (2018). https://doi.org:10.1016/j.lungcan.2018.02.010
72 Munawar, I. *et al.* Intensity modulated radiotherapy of non-small-cell lung cancer incorporating SPECT ventilation imaging. *Medical Physics* **37**, 1863-1872 (2010). https://doi.org:10.1118/1.3358128
73 Yuan, S. *et al.* Semiquantification and Classification of Local Pulmonary Function by V/Q Single Photon Emission Computed Tomography in Patients with Non-small Cell Lung Cancer: Potential Indication for Radiotherapy Planning. *Journal of Thoracic Oncology* **6**, 71-78 (2011). https://doi.org:10.1097/jto.0b013e3181f77b40
74 (!!! INVALID CITATION !!! 72).
75 Farrow, C. E. *et al.* Airway closure on imaging relates to airway hyperresponsiveness and peripheral airway disease in asthma. *Journal of Applied Physiology* **113**, 958-966 (2012). https://doi.org:10.1152/JAPPLPHYSIOL.01618.2011/ASSET/IMAGES/LARGE/ZDG01812029600 07.JPEG
76 Norberg, P. *et al.* Quantitative lung SPECT applied on simulated early COPD and humans with advanced COPD. *EJNMMI Res* **3**, 28 (2013). https://doi.org:10.1186/2191-219X-3-28
77 Bajc, M. *et al.* Grading obstructive lung disease using tomographic pulmonary scintigraphy in patients with chronic obstructive pulmonary disease (COPD) and long-term smokers. *Ann Nucl Med* **29**, 91-99 (2015). https://doi.org:10.1007/s12149-014-0913-y
78 Suga, K., Iwanaga, H., Tokuda, O., Okada, M. & Matsunaga, N. Intrabullous ventilation in pulmonary emphysema: assessment with dynamic xenon-133 gas SPECT. *Nucl Med Commun* **33**, 371-378 (2012). https://doi.org:10.1097/MNM.0b013e32834f264c
79 Venegas, J. G. *et al.* Self-organized patchiness in asthma as a prelude to catastrophic shifts. *Nature* **434**, 777-782 (2005). https://doi.org:10.1038/nature03490
80 Le Roux, P.-Y. *et al.* Gallium-68 perfusion positron emission tomography/computed tomography to assess pulmonary function in lung cancer patients undergoing surgery. *Cancer Imaging* **16** (2016). https://doi.org:10.1186/s40644-016-0081-5
81 Le Roux, P. Y., Hicks, R. J., Siva, S. & Hofman, M. S. PET/CT Lung Ventilation and Perfusion Scanning using Galligas and Gallium-68-MAA. *Semin Nucl Med* **49**, 71-81 (2019). https://doi.org:10.1053/j.semnuclmed.2018.10.013
82 Bergin, C. J., Glover, G. M. & Pauly, J. Magnetic resonance imaging of lung parenchyma. *J Thorac Imaging* **8**, 12-17 (1993).

83 Bergin, C. J., Noll, D. C., Pauly, J. M., Glover, G. H. & Macovski, A. MR imaging of lung parenchyma: a solution to susceptibility. *Radiology* **183**, 673-676 (1992). https://doi.org:10.1148/radiology.183.3.1584917

84 Bergin, C. J., Pauly, J. M. & Macovski, A. Lung parenchyma: projection reconstruction MR imaging. *Radiology* **179**, 777-781 (1991). https://doi.org:10.1148/radiology.179.3.2027991

85 Edelman, R. R., Hatabu, H., Tadamura, E., Li, W. & Prasad, P. V. Noninvasive assessment of regional ventilation in the human lung using oxygen-enhanced magnetic resonance imaging. *Nat Med* **2**, 1236-1239 (1996). https://doi.org:10.1038/nm1196-1236

86 Bauman, G. *et al.* Non-contrast-enhanced perfusion and ventilation assessment of the human lung by means of fourier decomposition in proton MRI. *Magn Reson Med* **62**, 656-664 (2009). https://doi.org:10.1002/mrm.22031

87 Albert, M. S. *et al.* Biological magnetic resonance imaging using laser-polarized 129Xe. *Nature* **370**, 199-201 (1994). https://doi.org:10.1038/370199a0

88 Kern, A. L. & Vogel-Claussen, J. Hyperpolarized gas MRI in pulmonology. *Br J Radiol* **91**, 20170647 (2018). https://doi.org:10.1259/bjr.20170647

89 Cho, A. Physics. Helium-3 shortage could put freeze on low-temperature research. *Science* **326**, 778-779 (2009). https://doi.org:10.1126/science.326_778

90 Kirby, M. *et al.* Hyperpolarized 3He Magnetic Resonance Functional Imaging Semiautomated Segmentation. *Academic Radiology* **19**, 141-152 (2012). https://doi.org:10.1016/J.ACRA.2011.10.007

91 He, M. *et al.* Extending semiautomatic ventilation defect analysis for hyperpolarized (129)Xe ventilation MRI. *Acad Radiol* **21**, 1530-1541 (2014). https://doi.org:10.1016/j.acra.2014.07.017

92 Tustison, N. J. *et al.* Ventilation-based segmentation of the lungs using hyperpolarized (3)He MRI. *J Magn Reson Imaging* **34**, 831-841 (2011). https://doi.org:10.1002/jmri.22738

93 Tzeng, Y. S., Lutchen, K. & Albert, M. The difference in ventilation heterogeneity between asthmatic and healthy subjects quantified using hyperpolarized 3He MRI. *Journal of Applied Physiology* **106**, 813-822 (2009). https://doi.org:10.1152/JAPPLPHYSIOL.01133.2007/ASSET/IMAGES/LARGE/ZDG0020983430007.JPEG

94 De Lange, E. E. *et al.* Evaluation of asthma with hyperpolarized helium-3 MRI: correlation with clinical severity and spirometry. *Chest* **130**, 1055-1062 (2006). https://doi.org:10.1378/CHEST.130.4.1055

95 Altes, T. A. *et al.* Hyperpolarized 3He MR lung ventilation imaging in asthmatics: preliminary findings. *J Magn Reson Imaging* **13**, 378-384 (2001). https://doi.org:10.1002/jmri.1054

96 de Lange, E. E. *et al.* Changes in regional airflow obstruction over time in the lungs of patients with asthma: evaluation with 3He MR imaging. *Radiology* **250**, 567-575 (2009). https://doi.org:10.1148/radiol.2502080188

97 Svenningsen, S. *et al.* Pulmonary functional magnetic resonance imaging: asthma temporal-spatial maps. *Acad Radiol* **21**, 1402-1410 (2014). https://doi.org:10.1016/j.acra.2014.08.002

98 de Lange, E. E. *et al.* The variability of regional airflow obstruction within the lungs of patients with asthma: assessment with hyperpolarized helium-3 magnetic resonance

imaging. *J Allergy Clin Immunol* **119**, 1072-1078 (2007). https://doi.org:10.1016/j.jaci.2006.12.659

99 Eddy, R. L., Svenningsen, S., Licskai, C., McCormack, D. G. & Parraga, G. Hyperpolarized Helium 3 MRI in Mild-to-Moderate Asthma: Prediction of Postbronchodilator Reversibility. *Radiology* **293**, 212-220 (2019). https://doi.org:10.1148/radiol.2019190420

100 Svenningsen, S. *et al.* What are ventilation defects in asthma? *Thorax* **69**, 63-71 (2014). https://doi.org:10.1136/thoraxjnl-2013-203711

101 de Lange, E. E. *et al.* Evaluation of asthma with hyperpolarized helium-3 MRI: correlation with clinical severity and spirometry. *Chest* **130**, 1055-1062 (2006). https://doi.org:10.1378/chest.130.4.1055

102 Fain, S. B. *et al.* Evaluation of structure-function relationships in asthma using multidetector CT and hyperpolarized He-3 MRI. *Acad Radiol* **15**, 753-762 (2008). https://doi.org:10.1016/j.acra.2007.10.019

103 Tgavalekos, N. T. *et al.* Relationship between airway narrowing, patchy ventilation and lung mechanics in asthmatics. *Eur Respir J* **29**, 1174-1181 (2007). https://doi.org:10.1183/09031936.00113606

104 Zha, W. *et al.* Regional Heterogeneity of Lobar Ventilation in Asthma Using Hyperpolarized Helium-3 MRI. *Acad Radiol* **25**, 169-178 (2018). https://doi.org:10.1016/j.acra.2017.09.014

105 Mummy, D. G. *et al.* Ventilation defects on hyperpolarized helium-3 MRI in asthma are predictive of 2-year exacerbation frequency. *J Allergy Clin Immunol* **146**, 831-839 e836 (2020). https://doi.org:10.1016/j.jaci.2020.02.029

106 Svenningsen, S., Nair, P., Guo, F., McCormack, D. G. & Parraga, G. Is ventilation heterogeneity related to asthma control? *Eur Respir J* **48**, 370-379 (2016). https://doi.org:10.1183/13993003.00393-2016

107 Mummy, D. G. *et al.* Ventilation defect percent in helium-3 magnetic resonance imaging as a biomarker of severe outcomes in asthma. *J Allergy Clin Immunol* **141**, 1140-1141 e1144 (2018). https://doi.org:10.1016/j.jaci.2017.10.016

108 Capaldi, D. P. *et al.* Pulmonary Imaging Biomarkers of Gas Trapping and Emphysema in COPD: (3)He MR Imaging and CT Parametric Response Maps. *Radiology* **279**, 597-608 (2016). https://doi.org:10.1148/radiol.2015151484

109 Mathew, L. *et al.* Hyperpolarized 3He magnetic resonance imaging of chronic obstructive pulmonary disease: reproducibility at 3.0 tesla. *Acad Radiol* **15**, 1298-1311 (2008). https://doi.org:10.1016/j.acra.2008.04.019

110 Pike, D. *et al.* Regional Heterogeneity of Chronic Obstructive Pulmonary Disease Phenotypes: Pulmonary (3)He Magnetic Resonance Imaging and Computed Tomography. *COPD* **13**, 601-609 (2016). https://doi.org:10.3109/15412555.2015.1123682

111 Virgincar, R. S. *et al.* Quantitative analysis of hyperpolarized 129Xe ventilation imaging in healthy volunteers and subjects with chronic obstructive pulmonary disease. *NMR Biomed* **26**, 424-435 (2013). https://doi.org:10.1002/nbm.2880

112 Kirby, M. *et al.* Pulmonary ventilation visualized using hyperpolarized helium-3 and xenon-129 magnetic resonance imaging: differences in COPD and relationship to emphysema. *J Appl Physiol (1985)* **114**, 707-715 (2013). https://doi.org:10.1152/japplphysiol.01206.2012

113 Kirby, M. *et al.* COPD: Do Imaging Measurements of Emphysema and Airway Disease Explain Symptoms and Exercise Capacity? *Radiology* **277**, 872-880 (2015). https://doi.org:10.1148/radiol.2015150037

114 Kirby, M., Pike, D., Coxson, H. O., McCormack, D. G. & Parraga, G. Hyperpolarized (3)He ventilation defects used to predict pulmonary exacerbations in mild to moderate chronic obstructive pulmonary disease. *Radiology* **273**, 887-896 (2014). https://doi.org:10.1148/radiol.14140161

115 Kirby, M. *et al.* On the role of abnormal DL(CO) in ex-smokers without airflow limitation: symptoms, exercise capacity and hyperpolarised helium-3 MRI. *Thorax* **68**, 752-759 (2013). https://doi.org:10.1136/thoraxjnl-2012-203108

116 Woodhouse, N. *et al.* Combined helium-3/proton magnetic resonance imaging measurement of ventilated lung volumes in smokers compared to never-smokers. *J Magn Reson Imaging* **21**, 365-369 (2005). https://doi.org:10.1002/jmri.20290

117 Fain, S. B. *et al.* Early emphysematous changes in asymptomatic smokers: detection with 3He MR imaging. *Radiology* **239**, 875-883 (2006). https://doi.org:10.1148/radiol.2393050111

118 Hamedani, H. *et al.* Alterations of regional alveolar oxygen tension in asymptomatic current smokers: assessment with hyperpolarized (3)He MR imaging. *Radiology* **274**, 585-596 (2015). https://doi.org:10.1148/radiol.14132809

119 Guenther, D. *et al.* (3)He MRI in healthy volunteers: preliminary correlation with smoking history and lung volumes. *NMR Biomed* **13**, 182-189 (2000). https://doi.org:10.1002/1099-1492(200006)13:4<182::aid-nbm642>3.0.co;2-n

120 Sheikh, K. *et al.* Magnetic resonance imaging biomarkers of chronic obstructive pulmonary disease prior to radiation therapy for non-small cell lung cancer. *Eur J Radiol Open* **2**, 81-89 (2015). https://doi.org:10.1016/j.ejro.2015.05.003

121 Yaremko, B. P. *et al.* Functional Lung Avoidance for Individualized Radiation Therapy: Results of a Double-Masked, Randomized Controlled Trial. *Int J Radiat Oncol Biol Phys* **113**, 1072-1084 (2022). https://doi.org:10.1016/j.ijrobp.2022.04.047

122 Ding, Y. *et al.* A pilot study of function-based radiation therapy planning for lung cancer using hyperpolarized xenon-129 ventilation MRI. *J Appl Clin Med Phys* **23**, e13502 (2022). https://doi.org:10.1002/acm2.13502

123 Stavngaard, T. *et al.* Hyperpolarised 3He MRI and 81mKr SPECT in chronic obstructive pulmonary disease. *European Journal of Nuclear Medicine and Molecular Imaging* **32**, 448-457 (2005). https://doi.org:10.1007/S00259-004-1691-X

124 Doganay, O. *et al.* Time-series hyperpolarized xenon-129 MRI of lobar lung ventilation of COPD in comparison to V/Q-SPECT/CT and CT. *European Radiology* **29**, 4058-4058 (2019). https://doi.org:10.1007/S00330-018-5888-Y

125 Kim, M., Doganay, O., Matin, T., Povey, T. & Gleeson, F. Comparison of the thoracic CT-based computational model with hyperpolarized Xenon-129 MRI and SPECT images to assess pulmonary ventilation in COPD patients. *European Respiratory Journal* **54**, OA1931-OA1931 (2019). https://doi.org:10.1183/13993003.CONGRESS-2019.OA1931

126 Tan, W. C. *et al.* Findings on Thoracic Computed Tomography Scans and Respiratory Outcomes in Persons with and without Chronic Obstructive Pulmonary Disease: A Population-Based Cohort Study. *PLoS One* **11**, e0166745 (2016). https://doi.org:10.1371/journal.pone.0166745

127 Mineo, T. C., Schillaci, O., Pompeo, E., Mineo, D. & Simonetti, G. Usefulness of lung perfusion scintigraphy before lung cancer resection in patients with ventilatory obstruction. *Ann Thorac Surg* **82**, 1828-1834 (2006). https://doi.org:10.1016/j.athoracsur.2006.05.041
128 Kawai, H. *et al.* Prediction of pulmonary function after major lung resection using lung perfusion scintigraphy with single-photon emission computed tomography/computed tomography. *Fujita Med J* **6**, 37-48 (2020). https://doi.org:10.20407/fmj.2019-012
129 Arnon-Sheleg, E., Haberfeld, O., Kremer, R., Keidar, Z. & Weiler-Sagie, M. Head-to-Head Prospective Comparison of Quantitative Lung Scintigraphy and Segment Counting in Predicting Pulmonary Function in Lung Cancer Patients Undergoing Video-Assisted Thoracoscopic Lobectomy. *J Nucl Med* **61**, 981-989 (2020). https://doi.org:10.2967/jnumed.119.234526
130 Wu, M. T. *et al.* Prediction of postoperative lung function in patients with lung cancer: comparison of quantitative CT with perfusion scintigraphy. *AJR Am J Roentgenol* **178**, 667-672 (2002). https://doi.org:10.2214/ajr.178.3.1780667
131 D'Silva, L. *et al.* Heterogeneity of bronchitis in airway diseases in tertiary care clinical practice. *Can Respir J* **18**, 144-148 (2011). https://doi.org:10.1155/2011/430317
132 Leigh, R. *et al.* Stable COPD: predicting benefit from high-dose inhaled corticosteroid treatment. *Eur Respir J* **27**, 964-971 (2006). https://doi.org:10.1183/09031936.06.00072105
133 Stanescu, D. *et al.* Airways obstruction, chronic expectoration, and rapid decline of FEV1 in smokers are associated with increased levels of sputum neutrophils. *Thorax* **51**, 267-271 (1996). https://doi.org:10.1136/thx.51.3.267
134 Dippolito, R. *et al.* Eosinophils in induced sputum from asymptomatic smokers with normal lung function. *Respir Med* **95**, 969-974 (2001). https://doi.org:10.1053/rmed.2001.1191
135 Niedbalski, P. J. *et al.* Protocols for multi-site trials using hyperpolarized ^{129}Xe MRI for imaging of ventilation, alveolar-airspace size, and gas exchange: A position paper from the ^{129}Xe MRI clinical trial. *Magnetic Resonance in Medicine* **86**, 2966-2986 (2021). https://doi.org:10.1002/mrm.28985
136 Charlson, M. E., Pompei, P., Ales, K. L. & MacKenzie, C. R. A new method of classifying prognostic comorbidity in longitudinal studies: development and validation. *J Chronic Dis* **40**, 373-383 (1987). https://doi.org:10.1016/0021-9681(87)90171-8
137 Graham, B. L. *et al.* 2017 ERS/ATS standards for single-breath carbon monoxide uptake in the lung. *Eur Respir J* **49** (2017). https://doi.org:10.1183/13993003.00016-2016
138 Graham, B. L. *et al.* Standardization of Spirometry 2019 Update. An Official American Thoracic Society and European Respiratory Society Technical Statement. *Am J Respir Crit Care Med* **200**, e70-e88 (2019). https://doi.org:10.1164/rccm.201908-1590ST
139 Nair, P. & Hargreave, F. E. Measuring bronchitis in airway diseases: clinical implementation and application: Airway hyperresponsiveness in asthma: its measurement and clinical significance. *Chest* **138**, 38S-43S (2010). https://doi.org:10.1378/chest.10-0094
140 Svenningsen, S. *et al.* Reproducibility of Hyperpolarized 129Xe MRI Ventilation Defect Percent in Severe Asthma to Evaluate Clinical Trial Feasibility. *Academic Radiology* **28**, 817-826 (2021). https://doi.org:10.1016/j.acra.2020.04.025

141 He, M. *et al.* Dose and pulse sequence considerations for hyperpolarized (129)Xe ventilation MRI. *Magn Reson Imaging* **33**, 877-885 (2015). https://doi.org:10.1016/j.mri.2015.04.005
142 McIntosh, M. J. *et al.* (129)Xe MRI Ventilation Defects in Asthma: What is the Upper Limit of Normal and Minimal Clinically Important Difference? *Acad Radiol* **30**, 3114-3123 (2023). https://doi.org:10.1016/j.acra.2023.03.010
143 Kirby, M. *et al.* Hyperpolarized 3He and 129Xe MR imaging in healthy volunteers and patients with chronic obstructive pulmonary disease. *Radiology* **265**, 600-610 (2012). https://doi.org:10.1148/radiol.12120485
144 Eddy, R. L. *et al.* Pulmonary MRI and Cluster Analysis Help Identify Novel Asthma Phenotypes. *Journal of Magnetic Resonance Imaging* **56**, 1475-1486 (2022). https://doi.org:10.1002/jmri.28152
145 Lemb, M., Oei, T. H., Eifert, H. & Gunther, B. Technegas: a study of particle structure, size and distribution. *Eur J Nucl Med* **20**, 576-579 (1993). https://doi.org:10.1007/BF00176550
146 De Nijs, R. *et al.* Comparison of 81mKrypton and 99mTc-Technegas for ventilation single-photon emission computed tomography in severe chronic obstructive pulmonary disease. *Nuclear Medicine Communications* **42**, 160-160 (2021). https://doi.org:10.1097/MNM.0000000000001314
147 Hughes, P. J. C. *et al.* Assessment of the influence of lung inflation state on the quantitative parameters derived from hyperpolarized gas lung ventilation MRI in healthy volunteers. *J Appl Physiol (1985)* **126**, 183-192 (2019). https://doi.org:10.1152/japplphysiol.00464.2018
148 Pierce, R. J., Copland, J. M., Sharpe, K. & Barter, C. E. Preoperative risk evaluation for lung cancer resection: predicted postoperative product as a predictor of surgical mortality. *Am J Respir Crit Care Med* **150**, 947-955 (1994). https://doi.org:10.1164/ajrccm.150.4.7921468
149 Nakahara, K. *et al.* A method for predicting postoperative lung function and its relation to postoperative complications in patients with lung cancer. *Ann Thorac Surg* **39**, 260-265 (1985). https://doi.org:10.1016/s0003-4975(10)62591-x
150 Markos, J. *et al.* Preoperative assessment as a predictor of mortality and morbidity after lung resection. *Am Rev Respir Dis* **139**, 902-910 (1989). https://doi.org:10.1164/ajrccm/139.4.902
151 Korst, R. J. *et al.* Lobectomy improves ventilatory function in selected patients with severe COPD. *Ann Thorac Surg* **66**, 898-902 (1998). https://doi.org:10.1016/s0003-4975(98)00697-3
152 Kearney, D. J., Lee, T. H., Reilly, J. J., DeCamp, M. M. & Sugarbaker, D. J. Assessment of operative risk in patients undergoing lung resection. Importance of predicted pulmonary function. *Chest* **105**, 753-759 (1994). https://doi.org:10.1378/chest.105.3.753
153 Edwards, J. G., Duthie, D. J. & Waller, D. A. Lobar volume reduction surgery: a method of increasing the lung cancer resection rate in patients with emphysema. *Thorax* **56**, 791-795 (2001). https://doi.org:10.1136/thorax.56.10.791
154 Carretta, A. *et al.* Improvement of pulmonary function after lobectomy for non-small cell lung cancer in emphysematous patients. *Eur J Cardiothorac Surg* **15**, 602-607 (1999). https://doi.org:10.1016/s1010-7940(99)00062-7

155 Brunelli, A. *et al.* Evaluation of expiratory volume, diffusion capacity, and exercise tolerance following major lung resection: a prospective follow-up analysis. *Chest* **131**, 141-147 (2007). https://doi.org:10.1378/chest.06-1345
156 Brunelli, A. *et al.* Predictors of early morbidity after major lung resection in patients with and without airflow limitation. *Ann Thorac Surg* **74**, 999-1003 (2002). https://doi.org:10.1016/s0003-4975(02)03852-3
157 Bolliger, C. T. *et al.* Exercise capacity as a predictor of postoperative complications in lung resection candidates. *Am J Respir Crit Care Med* **151**, 1472-1480 (1995). https://doi.org:10.1164/ajrccm.151.5.7735602
158 Berry, M. F. *et al.* Pulmonary function tests do not predict pulmonary complications after thoracoscopic lobectomy. *Ann Thorac Surg* **89**, 1044-1051; discussion 1051-1042 (2010). https://doi.org:10.1016/j.athoracsur.2009.12.065
159 Agostini, P. J. *et al.* Risk factors and short-term outcomes of postoperative pulmonary complications after VATS lobectomy. *J Cardiothorac Surg* **13**, 28 (2018). https://doi.org:10.1186/s13019-018-0717-6
160 Varela, G. *et al.* Measured FEV1 in the first postoperative day, and not ppoFEV1, is the best predictor of cardio-respiratory morbidity after lung resection. *Eur J Cardiothorac Surg* **31**, 518-521 (2007). https://doi.org:10.1016/j.ejcts.2006.11.036
161 Varela, G. *et al.* Predicted versus observed FEV1 in the immediate postoperative period after pulmonary lobectomy. *Eur J Cardiothorac Surg* **30**, 644-648 (2006). https://doi.org:10.1016/j.ejcts.2006.07.001
162 Smetana, G. W., Lawrence, V. A., Cornell, J. E. & American College of, P. Preoperative pulmonary risk stratification for noncardiothoracic surgery: systematic review for the American College of Physicians. *Ann Intern Med* **144**, 581-595 (2006). https://doi.org:10.7326/0003-4819-144-8-200604180-00009
163 Kim, E. S. *et al.* Prevalence of and risk factors for postoperative pulmonary complications after lung cancer surgery in patients with early-stage COPD. *Int J Chron Obstruct Pulmon Dis* **11**, 1317-1326 (2016). https://doi.org:10.2147/COPD.S105206
164 Gupta, H. *et al.* Impact of COPD on postoperative outcomes: results from a national database. *Chest* **143**, 1599-1606 (2013). https://doi.org:10.1378/chest.12-1499
165 Svenningsen, S. *et al.* Sputum Eosinophilia and Magnetic Resonance Imaging Ventilation Heterogeneity in Severe Asthma. *Am J Respir Crit Care Med* **197**, 876-884 (2018). https://doi.org:10.1164/rccm.201709-1948OC
166 Eddy, R. L. *et al.* Is Computed Tomography Airway Count Related to Asthma Severity and Airway Structure and Function? *Am J Respir Crit Care Med* **201**, 923-933 (2020). https://doi.org:10.1164/rccm.201908-1552OC
167 Svenningsen, S. *et al.* CT and Functional MRI to Evaluate Airway Mucus in Severe Asthma. *Chest* **155**, 1178-1189 (2019). https://doi.org:10.1016/j.chest.2019.02.403
168 Mummy, D. G. *et al.* Mucus Plugs in Asthma at CT Associated with Regional Ventilation Defects at (3)He MRI. *Radiology* **303**, 184-190 (2022). https://doi.org:10.1148/radiol.2021204616
169 Siva, R. *et al.* Eosinophilic airway inflammation and exacerbations of COPD: a randomised controlled trial. *Eur Respir J* **29**, 906-913 (2007). https://doi.org:10.1183/09031936.00146306

170 McDonald, V. M., Higgins, I., Wood, L. G. & Gibson, P. G. Multidimensional assessment and tailored interventions for COPD: respiratory utopia or common sense? *Thorax* **68**, 691-694 (2013). https://doi.org:10.1136/thoraxjnl-2012-202646

171 Aziz-Ur-Rehman, A., Dasgupta, A., Kjarsgaard, M., Hargreave, F. E. & Nair, P. Sputum cell counts to manage prednisone-dependent asthma: effects on FEV(1) and eosinophilic exacerbations. *Allergy Asthma Clin Immunol* **13**, 17 (2017). https://doi.org:10.1186/s13223-017-0190-0

172 Mirza, H. & Hashmi, M. F. Lung Ventilation Perfusion Scan (VQ Scan). *StatPearls* (2021).

Chapter 7: Appendix

7.1 Post-operative complication, Ipsilateral lung

Table 7-1 Binary logistic regression analysis for predictors of post-operative complications

Predictor Variables	Odds Ratio	95% CI	p-value
Model 1: Abnormal ventilation assessed by Technegas SPECT VDP			
Technegas SPECT VDP_{IL}, %	1.05	0.9-1.10	**0.09**
Segmentectomy†	10.38	1.42-76.0	0.02
Pack-year smoking history	1.02	1.00-1.04	0.07
Type of surgery‡	0.32	0.06-1.74	0.2
Model 2: Abnormal ventilation assessed by ^{129}Xe MRI VDP			
^{129}Xe MRI VDP_{IL}, %	1.13	1.04-1.23	0.004
Type of surgery‡	0.09	0.011-0.68	0.02
Segmentectomy†	16.08	1.63-158.73	0.02
Lobectomy†	6.84	1.08-43.25	0.04
Pack-year smoking history	1.02	1.00-1.05	0.05
$DL_{CO}\%_{pred}$	1.02	1.00-1.05	0.07

Predictor variables in the models included age, pack-year smoking history, Charlson Comorbidities Index, $FEV_1\%_{pred}$, $DL_{CO}\%_{pred}$, history of obstructive lung disease, type of surgery, extent of resection, Technegas SPECT VDP_{IL} and ^{129}Xe MRI VDP_{IL}.
†Compared to wedge resection. ‡Minimally invasive surgery compared to open thoracotomy. VDP_{IL}=ipsilateral lung ventilation defect percent; FEV_1=forced expiratory volume in one second; DL_{CO}=diffusion capacity for carbon monoxide.

7.2 Post-operative complication, contralateral lung

Table 7-2 Binary logistic regression analysis for predictors of post-operative complications

Predictor Variables	Odds Ratio	95% CI	p-value
Model 1: Abnormal ventilation assessed by Technegas SPECT VDP			
Technegas SPECT $VDPC_{CL}$, %	1.11	1.04-1.19	0.003
Segmentectomy†	18.91	2.08-171.82	0.009
Type of surgery‡	0.19	0.034-1.09	0.06
Pack-year smoking history	1.02	1.00-1.04	0.08
$DL_{CO}\%_{pred}$	1.02	1.00-1.04	0.1
Model 2: Abnormal ventilation assessed by ^{129}Xe MRI VDP			
^{129}Xe MRI VDP_{CL}, %	1.09	1.02-1.17	0.01
Type of surgery‡	0.11	0.18-0.73	0.02
Segmentectomy†	9.52	1.12-81.27	0.04
Lobectomy†	5.12	0.96-27.38	0.06
Pack-year smoking history	1.02	1.00-1.04	0.09
$FEV_1\%_{pred}$	1.02	0.99-1.05	0.15

Predictor variables in the models included age, pack-year smoking history, Charlson Comorbidities Index, $FEV_1\%_{pred}$, $DL_{CO}\%_{pred}$, history of obstructive lung disease, type of surgery, extent of resection, Technegas SPECT VDP_{CL} and ^{129}Xe MRI VDP_{CL}.
†Compared to wedge resection. ‡Minimally invasive surgery compared to open thoracotomy. VDP_{CL}=contralateral lung ventilation defect percent; FEV_1=forced expiratory volume in one second; DL_{CO}=diffusion capacity for carbon monoxide.

7.3 Length of hospital stay, ipsilateral lung

Table 7-3 Multivariate regression analysis for predictors of post-operative length of hospital stay

Predictor Variables	Unstandardized β	Standardized β	95% CI	p-value
MODEL 1: Anormal ventilation assessed by Technegas SPECT VDP (R^2=0.32, adjusted R^2=0.28, p<0.001)				
Technegas SPECT VDP_{IL}, %	0.14	0.38	0.06-0.22	**<0.001**
$DL_{CO}\%_{pred}$	-0.03	-0.21	-0.065-(-0.004)	**0.03**
Lobectomy†	2.29	0.25	0.33-4.25	**0.02**
Pneumonectomy‡	4.34	0.15	-1.29-9.97	0.13
Segmentectomy§	2.05	0.15	-0.87-4.97	0.17
MODEL 2: Abnormal ventilation assessed by ^{129}Xe MRI VDP (R^2=0.43, adjusted R^2=0.40, p<0.001)				
^{129}Xe MRI VDP_{IL}, %	0.26	0.60	0.19-0.33	**<0.001**
Pneumonectomy‡	6.73	0.24	2-11.45	**0.006**
Lobectomy†	2.59	0.28	0.76-4.42	**0.006**
Segmentectomy§	2.57	0.18	-0.09-5.23	0.058

Predictor variables in the model included age, pack-year smoking history, Charlson Comorbidities Index, $FEV_1\%_{pred}$, $DL_{CO}\%_{pred}$, history of obstructive lung disease, type of surgery, extent of resection, Technegas SPECT VDP_{IL} and ^{129}Xe MRI VDP_{IL}.
†‡§Compared to wedge resection. VDP_{IL}=ipsilateral lung ventilation defect percent; DL_{CO}=diffusion capacity for carbon monoxide.

7.4 Length of hospital stay, contralateral lung

Table 7-4 Multivariate regression analysis for predictors of post-operative length of hospital stay

Predictor Variables	Unstandardized β	Standardized β	95% CI	p-value
MODEL 1: Anormal ventilation assessed by Technegas SPECT VDP (R^2=0.32, adjusted R^2=0.28, p<0.001)				
Technegas SPECT VDP_{CL}, %	0.12	0.38	0.055-0.19	**<0.001**
$DL_{CO}\%_{pred}$	-0.03	-0.21	-0.06-(-0.002)	**0.04**
Lobectomy†	2.37	0.26	0.40-4.33	**0.02**
Pneumonectomy‡	4.82	0.17	-0.70-10.34	0.09
Segmentectomy§	2.05	0.15	-0.87-4.97	0.17
MODEL 2: Abnormal ventilation assessed by ^{129}Xe MRI VDP (R^2=0.29, adjusted R^2=0.26, p<0.001)				
^{129}Xe MRI VDP_{CL}, %	0.14	0.37	0.55-0.23	**0.002**
Lobectomy†	1.60	0.17	-0.069-3.28	0.06
$DL_{CO}\%_{pred}$	-0.03	-0.17	-0.06-0.005	0.09
Pneumonectomy§	4.68	0.17	-0.77-10.13	0.09

Predictor variables in the model included age, pack-year smoking history, Charlson Comorbidities Index, $FEV_1\%_{pred}$, $DL_{CO}\%_{pred}$, history of obstructive lung disease, type of surgery, extent of resection, Technegas SPECT VDP_{CL} and ^{129}Xe MRI VDP_{IL}.
†‡§Compared to wedge resection. VDP_{CL}=contralateral lung ventilation defect percent; DL_{CO}=diffusion capacity for carbon monoxide.

7.5 Subgroup analysis: Post-operative complication, ipsilateral lung

Table 7-5 Binary logistic regression analysis for predictors of post-operative complications in participants who underwent minimally invasive lobectomy

Predictor Variables	Odds Ratio	95% CI	p-value
Model 1: Abnormal ventilation assessed by Technegas SPECT VDP			
Technegas SPECT VDP_{IL}, %	1.07	0.99-1.16	0.09
Obstructive respiratory disease	2.25	0.77-6.58	0.14
Model 2: Abnormal ventilation assessed by ^{129}Xe MRI VDP			
^{129}Xe MRI VDP_{IL}, %	1.12	1.03-1.22	**0.008**

Predictor variables in the model included age, pack-year smoking history, Charlson Comorbidities Index, $FEV_1\%_{pred}$, $DL_{CO}\%_{pred}$, history of obstructive lung disease, Technegas SPECT VDP_{IL} and ^{129}Xe MRI VDP_{IL}. VDP_{IL}=ipsilateral lung ventilation defect percent.

7.6 Subgroup analysis: Post-operative complication, contralateral lung

Table 7-6 Binary logistic regression analysis for predictors of post-operative complications in participants who underwent minimally invasive lobectomy

Predictor Variables	Odds Ratio	95% CI	p-value
Model 1: Abnormal ventilation assessed by Technegas SPECT VDP			
Technegas SPECT VDP_{CL}, %	1.18	1.07-1.31	**0.001**
Model 2: Abnormal ventilation assessed by ^{129}Xe MRI VDP			
^{129}Xe MRI VDP_{CL}, %	1.10	1.02-1.19	**0.02**

Predictor variables in the model included age, pack-year smoking history, Charlson Comorbidities Index, $FEV_1\%_{pred}$, $DL_{CO}\%_{pred}$, history of obstructive lung disease, Technegas SPECT VDP_{CL} and ^{129}Xe MRI VDP_{CL}. VDP_{CL}=contralateral lung ventilation defect percent.

7.7 Subgroup analysis: Length of hospital stay, ipsilateral lung

Table 7-7 Multivariate regression analysis for predictors of post-operative length of hospital stay in in participants who underwent minimally invasive lobectomy

Predictor Variables	Unstandardized β	Standardized β	95% CI	p-value
MODEL 1: Anormal ventilation assessed by Technegas SPECT VDP (R^2=0.36, adjusted R^2=0.33, p<0.001)				
Technegas SPECT VDP_{IL}, %	0.18	0.34	0.064-0.30	**0.003**
$DL_{CO}\%_{pred}$	-0.05	-0.26	-0.087-(-0.008)	**0.02**
$FEV_1\%_{pred}$	-0.04	-0.19	-0.09-0.008	0.10
MODEL 2: Abnormal ventilation assessed by ^{129}Xe MRI VDP (R^2=0.52, adjusted R^2=0.51, p<0.001)				
^{129}Xe MRI VDP_{IL}, %	0.37	0.72	0.28-0.45	**<0.001**

Predictor variables in the model included age, pack-year smoking history, Charlson Comorbidities Index, $FEV_1\%_{pred}$, $DL_{CO}\%_{pred}$, history of obstructive lung disease, Technegas SPECT VDP_{IL} and ^{129}Xe MRI VDP_{IL}. VDP_{IL}=ipsilateral lung ventilation defect percent; DL_{CO}=diffusion capacity for carbon monoxide. FEV_1=forced expiratory volume in one second.

7.8 Subgroup analysis: Length of hospital stay, contralateral lung

Table 7-8 Multivariate regression analysis for predictors of post-operative length of hospital stay in in participants who underwent minimally invasive lobectomy

Predictor Variables	Unstandardized β	Standardized β	95% CI	p-value
MODEL 1: Anormal ventilation assessed by Technegas SPECT VDP (R^2=0.43, adjusted R^2=0.39, p<0.001)				
Technegas SPECT VDP_{CL}, %	0.25	0.47	0.13-0.36	**<0.001**
$DL_{CO}\%_{pred}$	-0.04	-0.25	-0.09-(-0.004)	**0.03**
$FEV_1\%_{pred}$	0.04	-0.20	-0.09-0.002	0.06
Pack-year smoking history	-0.03	-0.14	-0.06-0.12	0.2
MODEL 2: Abnormal ventilation assessed by ^{129}Xe MRI VDP (R^2=0.38, adjusted R^2=0.35, p<0.001)				
^{129}Xe MRI VDP_{CL}, %	0.33	0.55	0.18-0.47	**<0.001**
$DL_{CO}\%_{pred}$	-0.04	-0.22	-0.08-0.003	0.07
Pack-year smoking history	-0.03	-0.19	-0.07-0.007	0.11

Predictor variables in the model included age, pack-year smoking history, Charlson Comorbidities Index, $FEV_1\%_{pred}$, $DL_{CO}\%_{pred}$, history of obstructive lung disease, Technegas SPECT VDP_{CL} and ^{129}Xe MRI VDP_{CL}. VDP_{CL}=contralaeral lung ventilation defect percent; DL_{CO}=diffusion capacity for carbon monoxide. FEV_1=forced expiratory volume in one second.